

# Evaluating the feasibility of shared mooring systems on a combined solar and wind farm array

MSc Thesis

Camiel Schreuder

WFA-3

# Evaluating the feasibility of shared mooring systems on a combined solar and wind farm array

MSc Thesis

by

Camiel Schreuder

<u>Student Name</u>	<u>Student Number</u>
Camiel Schreuder	4496787

Supervisor: Dr. O. Colomé Gené  
Company Supervisors: Ir. A. Haenen & Ir. R. van Driel  
Faculty: Faculty of Offshore & Dredging Engineering, Delft

# Preface

This thesis marks the end of my career as a student at the Delft University of Technology. As the world is in the midst of the energy transition, the goal of my thesis was to look into innovations in the offshore industry that could pave the way for clean, cost-effective energy. Additionally, I wanted to step out of my comfort zone and use this final opportunity to improve my programming skills in preparation for my engineering career. Although this came with the necessary struggles, I must say that I have learned a lot over the past ten months, both personally and professionally. From making decisions based on the limited information available to jumping the hurdle and asking for help when stuck, it all helped me become a better engineer.

First, I want to thank my supervisors, Oriol, Anner, and Robert, for their help and feedback during these last ten months. Second, I want to thank my friend Marijn for his programming wizardry and patience, which helped me get through the last few weeks of finalising my model. Third, a big thanks to the people at Mocean, who provided great sparring partners when having coding, OrcaFlex, or physics problems. Lastly, a big thanks to my girlfriend, family, and friends for providing support during these final stages of my study.

*Camiel Schreuder  
Delft, August 2023*

# Abstract

The demand for clean energy has led to potential cost-effective solutions for the offshore industry. One of these solutions is shared mooring systems, where floating offshore structures for renewable energy are coupled to each other. While this approach saves mooring lines and anchors, it introduces new dynamic loading compared to conventional mooring systems. This study focuses on the feasibility of using a shared mooring system to combine floating offshore wind and floating solar support structures in different configurations in a farm layout.

This research uses the Voltorn US-S platform to model the floating wind turbines and recreates the Tractebel Seavolt concept for the modelling of the floating solar arrays. Six configurations are simulated, undergoing irregular waves under various wave headings, load cases, and line materials. The configurations involve two wind turbines with one or more solar arrays in between them. A Quasi-dynamic model is used to identify critical cases. These cases are re-evaluated using OrcaFlex. The assessment of these configurations is done based on two Key Performance Indicators, related to line tensions and the floating support structures' displacements. During the process, polyester lines are chosen due to their favourable characteristics.

The four configurations that met the Key Performance Indicators are compared to a base case of a single turbine regarding its displacements and anchored line tensions. Effective utilisation of the shared lines and limited displacements lead to a preference for the configuration with three solar arrays. Additionally, the anchored line tensions of the turbine in this configuration increase the least compared to other configurations.

In summary, using a shared mooring system to combine both floating offshore wind structures and floating solar structures in a farm layout is feasible. Further research should be done on other configurations and the impact of these mooring systems on the Levelized Cost Of Energy. Additionally, wind and current loading should be incorporated in future studies.

# Contents

<b>Preface</b>	<b>i</b>
<b>Summary</b>	<b>ii</b>
<b>1 Introduction</b>	<b>1</b>
1.1 Problem statement . . . . .	1
1.2 Research objective . . . . .	3
<b>2 Background</b>	<b>5</b>
2.1 Mooring types . . . . .	5
2.2 Anchors . . . . .	8
2.3 Line types . . . . .	9
<b>3 Theory</b>	<b>12</b>
3.1 Mooring theory . . . . .	12
3.2 Mooring Modelling Fidelities . . . . .	13
3.3 Environmental loading . . . . .	16
3.4 Descriptions of waves . . . . .	16
3.5 Equations of Motion . . . . .	18
3.6 Wave loading . . . . .	19
<b>4 Case study</b>	<b>21</b>
4.1 Floating wind structure . . . . .	21
4.2 Floating solar structure . . . . .	23
4.3 Configurations . . . . .	24
<b>5 Method</b>	<b>26</b>
5.1 Quasi-dynamic Model . . . . .	26
5.2 Floater modelling . . . . .	28
5.3 Static mooring response . . . . .	29
<b>6 Verification and comparison with OrcaFlex</b>	<b>33</b>
6.1 Verification of the static mooring response . . . . .	33
6.2 Sanity check RAOs solar floaters . . . . .	35
6.3 Comparison of the model to OrcaFlex . . . . .	40
6.4 JONSWAP spectrum . . . . .	48
6.5 Assessment of limitations . . . . .	49
6.6 Conclusions . . . . .	51
<b>7 Results</b>	<b>53</b>
7.1 Key Performance Indicators . . . . .	53
7.2 Static results . . . . .	54
7.3 Dynamic Results . . . . .	55
7.4 Identification of critical cases (Quasi-dynamic Model) . . . . .	56
7.5 Evaluating the critical cases (OrcaFlex) . . . . .	57
7.6 Feasibility of the configurations . . . . .	59
7.7 Comparison with the base case . . . . .	59
<b>8 Discussion</b>	<b>62</b>
8.1 Limitations of the research . . . . .	63
<b>9 Conclusions</b>	<b>66</b>
<b>10 Recommendations</b>	<b>68</b>

---

<b>Bibliography</b>	<b>69</b>
<b>A Sanity checks</b>	<b>73</b>
<b>B Static results</b>	<b>78</b>
<b>C Quasi-Dynamic model results</b>	<b>80</b>
<b>D Orcaflex results</b>	<b>86</b>
<b>E Basecase comparisons</b>	<b>94</b>

# Nomenclature

<i>CAD</i>	Computer-Aided Design
<i>CALM</i>	Catenary Anchor Leg Mooring
<i>CFD</i>	Computational Fluid Dynamics
<i>DEA</i>	Drag Embedded Anchor
<i>EoM</i>	Equations of Motion
<i>HMPE</i>	High-Modulus Poly-Ethylene
<i>IRF</i>	Impulse Response Function
<i>JONSWAP</i>	JOint North Sea Wave Project
<i>LCOE</i>	Levelized Cost Of Energy
<i>MBL</i>	Mimimum Breaking Load
<i>MSL</i>	Mean Sea Level
<i>O&amp;G</i>	Oil & Gas
<i>PV</i>	Photovoltaics
<i>RAO</i>	Response Amplitude Operator
<i>ROV</i>	Remotely Operated underwater Vehicle
<i>SALM</i>	Single Anchor Leg Mooring
<i>SM</i>	Spread Mooring
<i>SPM</i>	Single Point Mooring
<i>TD</i>	Time Domain
<i>TLP</i>	Tension Leg Platform
<i>WEC</i>	Wave Energy Converter

# List of Figures

1.1	Example of a shared mooring system (depicted by the blue line)	2
1.2	Shared mooring layouts considered	2
1.3	The combined wind and solar farm from López et al.	3
1.4	Graphical representation of the research questions and research plan: Dark green represents the research question, light green the subquestions, and blue the means to answer these questions.	4
2.1	Left: Catenary system, Right: Taut leg system	5
2.2	Catenary, taut and TLP system	6
2.3	Turret configuration for a SPM system	6
2.4	Multiple mooring line configurations	7
2.5	The EcoTLP concept	8
2.6	Various anchor types	8
2.7	DEA from Delmar systems	9
2.8	Installation of suction and driven piles	9
2.9	Different chain diameters with their corresponding MBL for different chain grades	10
2.10	Different types of wire rope	10
2.11	Example of a stress-strain curve	10
2.12	Composition of a polyester rope	11
3.1	Small element of a mooring line	12
3.2	Quasi-static modeling vs dynamic modeling	14
3.3	Representation of the lumped-mass method	15
3.4	Environmental loads on a FOWT	16
3.5	Representation of a linear wave	17
3.6	Example of a JONSWAP spectrum	18
3.7	Vessel motions in six DOF	18
4.1	The UMaine VoltturnUS-S reference semi-submersible platform	21
4.2	Dimensions of the VoltturnUS semi-submersible	22
4.3	The Seavolt concept on which the model is based	23
4.4	Configuration 1 side view	24
4.5	Configuration 2.1 side view	25
4.6	Configuration 2.5 side view	25
4.7	Top views of each configuration	25
5.1	Overview of the quasi-dynamic model	27
5.2	Meshed structure using GMSH, viewed in OrcaWave	29
5.3	Setup of shared mooring system in Python	30
5.4	Flow of the static mooring force calculation	30
5.5	Comparison of JONSWAP spectra	31
5.6	Time series of a JONSWAP spectrum	31
6.1	Verification of quasi-static model in OrcaFlex	34
6.2	Different line segment lengths in OrcaFlex	35
6.3	Convergence of RAOs at 0° wave heading	36
6.4	Convergence of RAOs at 30° wave heading	37
6.5	Convergence of RAOs at 45° wave heading	37
6.6	Convergence of RAOs at 90° wave heading	37

6.7	Maximum wave loading occurring at the wavelength $\lambda$ equal to distances of the columns	38
6.8	Geometry and RAO of a single floater	38
6.9	Geometry and RAO of the 4 floaters	39
6.10	Geometry and RAO of the 16 floaters	39
6.11	Displacements considering only first-order wave loading	41
6.12	Line 1 tensions, considering only first-order wave loading	42
6.13	Line 2 tensions, considering only first-order wave loading	43
6.14	Displacements including wave drift	44
6.15	Line 1 tensions including wave drift	45
6.16	Line 2 tensions including wave drift	46
6.17	Displacements considering only first-order wave loading	47
6.18	Shared line tensions, considering only first-order wave loading	48
6.19	JONSWAP time series with $H_s = 3, T_p = 8$	49
6.20	Mean and maximum displacements	50
6.21	Mean and maximum tensions anchored lines	51
6.22	Mean and maximum tensions shared lines	51
7.1	Workflow of the assessment of configurations	53
7.2	Conventions used for fairlead positions	54
7.4	Displacements and tensions configuration 1	56
7.5	Displacements and tensions configuration 2.1	57
7.6	KPI 1 check of configuration 1	58
7.7	KPI 2 check of configuration 1	58
7.8	Maximum displacements compared to basecase	59
7.9	Maximum displacements compared to basecase	60
8.1	Alternative configurations	64
A.1	Line 2 tensions, considering only first order wave loading	73
A.2	Displacements including drift	74
A.3	Line 1 tensions including drift	75
A.4	Line 2 tensions including drift	76
A.5	Shared line tensions including drift	77
C.1	Displacements of configuration 1	80
C.2	Shared line tensions configuration 1	80
C.3	Displacements of configuration 2.1	81
C.4	Shared line tensions configuration 2.1	81
C.5	Displacements of configuration 2.2	82
C.6	Shared line tensions configuration 2.2	82
C.7	Displacements of configuration 2.3	83
C.8	Shared line tensions configuration 2.3	83
C.9	Displacements of configuration 2.4	84
C.10	Shared line tensions configuration 2.4	84
C.11	Displacements of configuration 2.5	85
C.12	Shared line tensions configuration 2.5	85
D.1	Displacement check configuration 2.1	88
D.2	Tension check configuration 2.1	88
D.3	Displacement check configuration 2.2	89
D.4	Tension check configuration 2.2	89
D.5	Displacement check configuration 2.3	89
D.6	Tension check configuration 2.3	90
D.7	Displacement check configuration 2.4	90
D.8	Tension check configuration 2.4	91
D.9	Displacement check configuration 2.5	91
D.10	Tension check configuration 2.5	92

---

D.11 Displacement check configuration 2.1 . . . . .	92
D.12 Tension check configuration 2.1 . . . . .	93
D.13 Displacement check configuration 2.3 . . . . .	93
D.14 Tension check configuration 2.3 . . . . .	93
E.1 Turbine displacements . . . . .	94
E.2 Anchor 1 tensions . . . . .	95
E.3 Anchor 2 tensions . . . . .	95
E.4 Anchor 3 tensions . . . . .	96

# 1

## Introduction

In the past few years, the offshore industry has been in the process of substantial development. The global demand for renewable energy has been steadily increasing, leading to more offshore projects being developed [29]. The construction of offshore wind farms worldwide has been increasing, accompanied by advancements in floating structures for wind energy [30]. Additionally, alternative renewables such as wave, tidal, and solar energy technologies have undergone increasing research.

In addition to other renewable energy resources, offshore wind is regarded as the foundation for harnessing clean energy from the offshore environment. Recently, the Dutch government stated that it aims to have 3 GW of floating solar installed in the North Sea by 2030 [8], which emphasizes the increasing urgency for research into sustainable solutions to address the demand for clean energy.

In the last decades, large wind farms have been built to produce renewable energy at scale. These are mostly based on a bottom-founded structure. However, as shallow water is scarce, floating wind provides a solution, as these structures can be installed in deeper waters. Currently, there are three commercial floating wind farms in operation, although not on the same scale as bottom-fixed wind [11, 24]. In the case of wave, tidal and solar energy, these renewables have not been deployed at a large scale yet. There are many concepts in development with several parties having upcoming pilot projects in the following years [1, 15, 22].

### 1.1. Problem statement

Mooring systems play a crucial role in keeping floating renewable installations in their desired positions by using mooring lines hooked up to anchors at the seabed, counteracting the effects of environmental loads exposed to the structure. However, compared to traditional offshore structures like oil rigs, renewable mooring solutions face unique challenges due to the sheer number of structures in the water. Moreover, floating wind poses additional aerodynamical loads that are not present in traditional structures. Nevertheless, the risk associated with mooring line failure is generally lower for floating wind, as the structures are typically unmanned and do not hold explosive hydrocarbons. Overall, the current knowledge based on the Oil & Gas industry can be applied to the development of the next generation of floating structures, although careful and different engineering designs and decisions are required.

According to Ramachandran et al. [45], efficiency optimization in the manufacturing, installation, and commissioning of floating wind turbines offers opportunities for the offshore wind industry to become a more competitive option in terms of Levelized Cost of Energy (LCOE). Additionally, standardization and mass production of the same type of wind turbines can contribute to making it more cost-competitive.

One of the main contributors to the capital costs of a floating wind turbine is its mooring system [29, 35]. With deeper waters, more line length is demanded for the stationkeeping ability which introduces higher costs. Proposed solutions are the option of shared anchoring and/or shared mooring systems, of which shared anchoring has already been deployed in the Hywind Tampen wind farm [11]. Sharing

the anchors between turbines would lead to fewer anchors installed, which cuts the overall costs of material and installation. Shared mooring systems work by interconnecting the adjacent turbines to each other, leading to the installation of fewer anchors and mooring lines to the seabed. Also, fewer geotechnical surveys of the seabed would be required due to fewer anchor placements. This could all reduce (installation) costs and reduce environmental impact on the seabed [45].

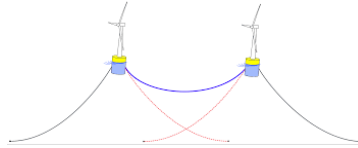


**Figure 1.1:** Example of a shared mooring system (depicted by the blue line)

One of the disadvantages of linking the turbines to one another is the more complex dynamics, which can result in higher loads on the mooring lines. Moreover, the case of a line failure could lead to the cascading event of more turbines drifting away, increasing the risk of collisions. Furthermore, displacements of wind turbines increase due to the lower stiffness of the mooring system.

#### Literature on shared mooring systems

Shared mooring is currently in the early stages of development. Currently, there have been no applications in the offshore industry, although some research has been done by Goldschmidt and Muskulus [31] and Connolly and Hall [26], who analyzed the dynamic behaviour and the cost-saving potential of the configurations considered in their research.

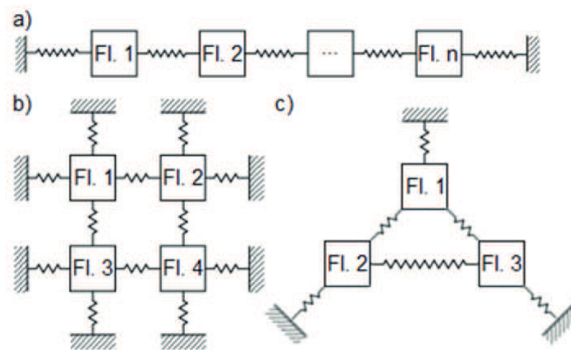


**Figure 1.2:** Shared mooring layouts considered by Goldschmidt and Muskulus [31]

Continuing research of Hall [32, 48] focuses on additional configurations and optimisation of the layouts considered in an attempt to further reduce costs. In the research of Zhang and Liu [49], displacement of the floaters was observed to increase when more turbines with shared lines were introduced to a system.

From this literature review can be concluded that shared mooring has a cost-saving potential in certain configurations, but further research into the dynamics and layouts is required. Some studies rely on Quasi-static models, which only take into account the mean forces applied on structures to assess the tensions on the mooring lines using the catenary equation. The catenary equation, however, provides only the static restoring force of a mooring line. Other studies use a fully lumped mass approach to assess the tensions. Although this approach is more accurate since it considers the dynamics of the mooring lines, it comes at the expense of computational power. A Quasi-dynamic model, which is a dynamic time-domain model using the static response of a mooring line, would be a mid-fidelity solution to this problem, providing a more computationally efficient model while also taking into account the dynamic behaviour of the structures considered.

### Combination of renewables

One of the challenges that come with the rise of renewables is their intermittent nature and the space they require [27]. Some research has addressed these challenges by combining multiple renewables in an offshore farm, as doing so could diversify the energy mix and improve the area's use efficiency [14, 41]. An example of such a layout can be found in Figure 1.3. For solar in particular, it is expected that irradiance at sea is higher due to the reflection of sunlight on the sea, and that efficiency will be higher due to the cooling effect of the sea [14]. Additionally, infrastructure could be shared which could lower costs. Some preliminary studies regarding offshore solar and Wave Energy Converters (WEC) in combination with wind have been performed. However, due to their high costs, these innovative technologies are not expected to compete with offshore wind until 2050, but they may provide a solution to the problems mentioned above and may therefore be commercialised sooner [14].

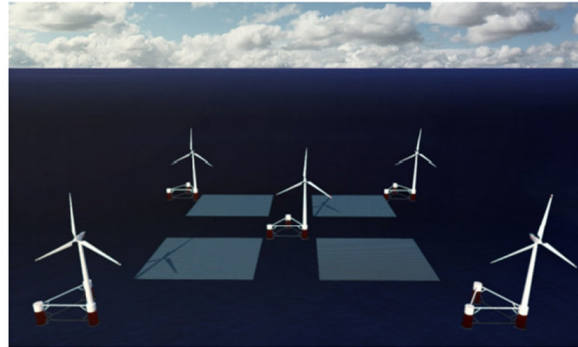


Figure 1.3: The combined wind and solar farm from López et al. [41]

## 1.2. Research objective

The objective of this research is to assess the feasibility of using a shared mooring system, combining offshore Photovoltaics (PV) energy within a floating wind farm in deep water. The combination of these two topics is not present in the reviewed literature and would therefore be a contribution to the existing knowledge. It could be a cost-effective solution by reducing the amount of line material and anchors, while efficiently utilising the available space and reducing the intermittency problem.

The following research question has been defined to reach this objective:

*"What is the feasibility of using a **shared mooring system** within a hybrid renewable farm, combining **floating wind and floating solar**?"*

To answer this main question, the following subquestions have been defined:

1. *What are the existing methods of modelling shared mooring systems of floating wind farms?*
2. *Which factors are important for modelling a shared mooring system for a floating wind farm?*
3. *What is a computationally efficient and feasible way of modelling a (preliminary) design of a floating wind farm in combination with floating PV?*
4. *Is a shared mooring system feasible for hybrid renewable energy farms? If so, in which configurations?*

Below, a graphical representation of the research done is given:

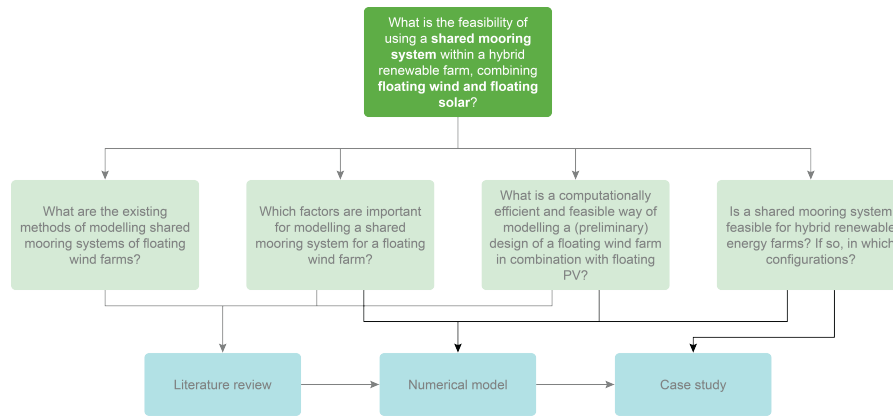


**Figure 1.4:** Graphical representation of the research questions and research plan: Dark green represents the research question, light green the subquestions, and blue the means to answer these questions.

### 1.2.1. Report outline

This thesis starts with an introduction to offshore mooring in Chapter 2, after which the theory used can be found in Chapter 3. The structures and configurations considered to evaluate the feasibility of the shared mooring systems in this thesis are elaborated on in Chapter 4. The methodology and the model used is explained in 5. The results found using the methodology and model are presented in Chapter 7, after which these are discussed in Chapter 8. Final conclusions are made in Chapter 9. Suggestions for future research are made in Chapter 10.

# 2

## Background

This chapter provides a brief summary of the different aspects of mooring. It aims to give insight into the parameters that affect a mooring system, such as the different mooring configuration types, line materials and anchors. Mooring systems are designed to keep a floating structure in its intended position under the influence of environmental loading, providing a limitation of its (second-order) motions. Although most of the knowledge and current mooring systems are based on the O&G industry, this thesis will focus on mooring systems in offshore wind and other renewables.

### 2.1. Mooring types

Mooring systems are generally divided into two categories; catenary and taut systems. A depiction of these two systems can be found in Figure 2.1.

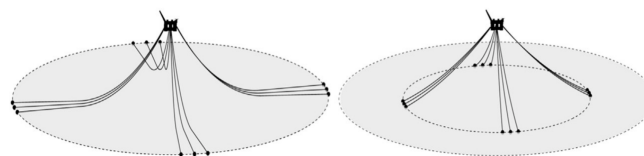


Figure 2.1: Left: Catenary system, Right: Taut leg system. [42]

#### Catenary systems

A catenary system allows the chain or rope to sag in a curve between two anchor points. This shape allows for the own weight of the line (which partially rests on the seabed) to be used as an added mooring stiffness of the line in case of floater displacement. In case the floater is displaced by a force, the lower part of the line will be lifted from the seabed, increasing the restoring force due to its own weight. One of the benefits of the catenary line is that the costs of these systems are relatively low in depths of up to 500 metres. Additionally, it is a simpler concept and easier to install and maintain. However, due to the anchors usually only being able to resist horizontal forcing, sufficient space is to be reserved for the line lying on the seabed. This causes the footprint of a catenary shape to be larger than a taut system [4]. Moreover, the catenary mooring system can lead to greater platform motions due to its relatively lower mooring stiffness.

#### Taut systems

The taut leg system has no line lying on the seabed and relies on the elasticity of the mooring line as the restoring force in case of displacement of the floater. This provides a smaller footprint compared to the catenary shape. However, this system also introduces larger tensions on the mooring line and anchors, as the anchors now also have to account for vertical forcing. Additionally, the taut system allows the use of less conventional materials, such as polyester fibres or wire instead of chains. Due to its larger stiffness capabilities, the taut system also makes deeper waters accessible and provides

a better station-keeping ability. Taut systems are generally more cost-effective at greater water depths due to material costs; the systems are however generally more costly than catenary systems in terms of their engineering, installation, and maintenance [4, 42].

A variant of the taut system is the Tension Leg Platform (TLP), which relies on a buoyant structure that is held in place by vertically tensioned tendons, or tethers of steel or synthetic fibres. The tension of the tendons or risers keeps the system in its place, providing excellent heave stability. It also requires a smaller footprint for the system to be installed. The differences between the systems can be found below in Figure 2.2:

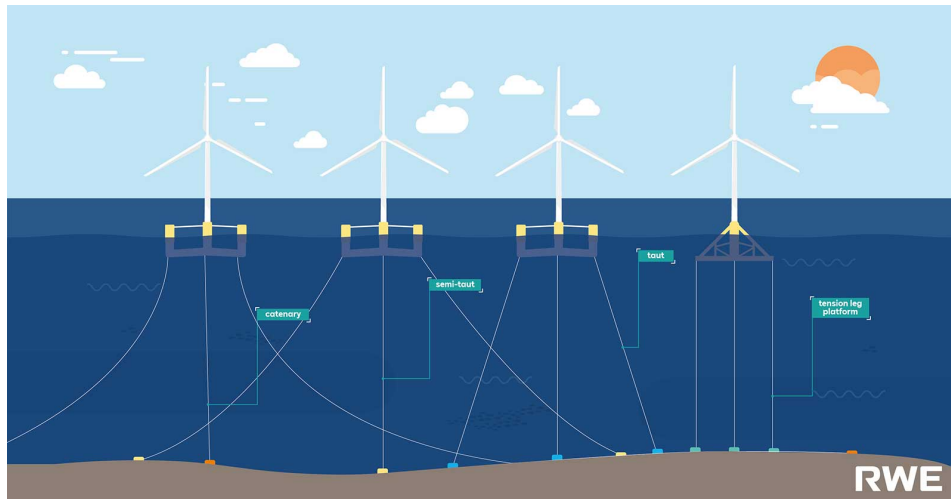


Figure 2.2: Catenary, taut and TLP system [9]

Apart from the choice of the shape of the system, mooring systems can either be configured as a spread mooring (SM) system or a single point (SPM) system. An SM system allows for the mooring lines to be attached to various positions of the floater, while an SPM system connects one or more lines to the centre of rotation of the floater (usually in a turret configuration, see Figure 2.3 which allows the floater to weathervane).

SM systems have enhanced stationkeeping capabilities over an SPM due to the multiple mooring lines carrying the loads, reducing the systems' motion. Additionally, it provides redundancy in the case of a mooring line failure. SM systems do however provide higher costs due to more necessary equipment, increasing costs in terms of installation and maintenance with it. SPM systems have the benefit of simplified installations. Since fewer anchors and lines are generally needed, costs will be reduced. These systems do however provide less precise stationkeeping, as they rely on a single anchor point. This also means that in case of line failure, the system has a higher risk of colliding with other systems.



Figure 2.3: Turret configuration for a SPM system [16]

### 2.1.1. Configurations

Multiple configurations are possible within the systems depicted above, as can be seen in Figure 2.4:

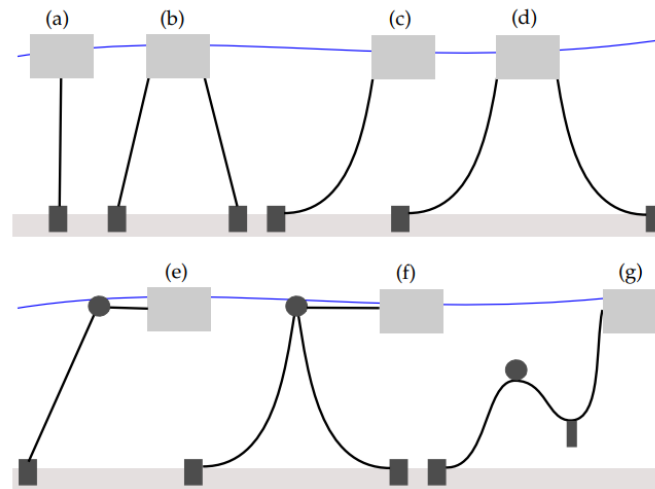


Figure 2.4: Multiple mooring line configurations [28]

Where the configurations are as follows:

- (a) Taut
- (b) Taut spread
- (c) Catenary
- (d) Catenary spread
- (e) Single Anchor Leg Mooring (SALM)
- (f) Catenary Anchor Leg Mooring (CALM)
- (g) Lazy-S

Where (e), (f), and (g) are the more exotic configurations. The SALM, CALM and lazy-s configurations are systems used in O&G operations for offloading oil and other hydrocarbons, as well as a temporary mooring for vessels by using buoyant elements (depicted by the circles) and clump weights (squares) to reach a desired mooring stiffness.

### 2.1.2. Use in renewables

The development of mooring systems for renewables, in particular offshore wind, is currently in its early stages. Although the O&G industry can provide knowledge, additional research is necessary to reduce costs, due to differences in scale, size, and nature of renewables. All three commercial floating wind farms (Kincardine, Hywind, and Windfloat Atlantic) are installed with a spread catenary mooring system. Windfloat Atlantic uses fibre line segments as its main component of the mooring line, whereas the other two use chain segments [11, 12, 24]. Other types of mooring systems exist for floating wind. One of them is the EcoTLP, which is a TLP concept currently in development for deep water conditions [7].



Figure 2.5: The EcoTLP concept [7]

## 2.2. Anchors

Depending on the mooring configuration, water depth, seabed conditions and required capacity, various anchor types have been developed over time. An overview can be seen below in Figure 2.6. Currently, all operational commercial floating wind farms make use of catenary systems. Since in that case, the Drag embedded anchor (DEA) is a logical and cost-effective choice, this system is therefore used by Kincardine and WindFloat Atlantic [12, 24]. The Hywind Scotland Farm uses suction piles [11] due to its shared anchoring, which requires anchors to resist loading from multiple directions.

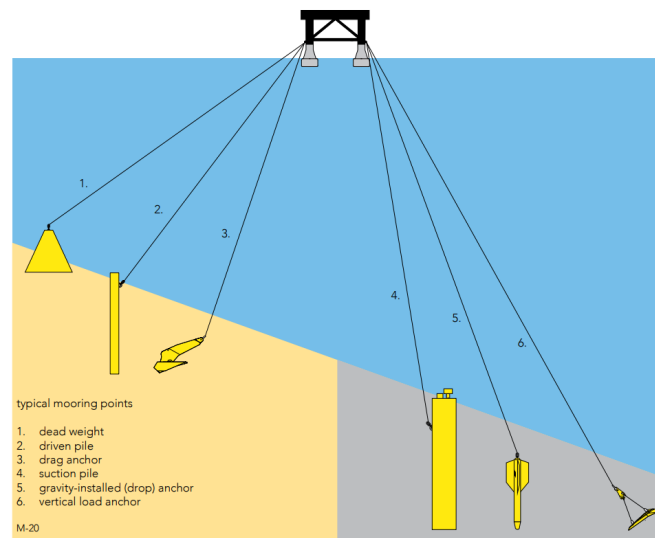


Figure 2.6: Various anchor types [46]

### Drag embedded anchor

The drag-embedded anchor (DEA) is currently one of the most used types of anchoring due to its simple installation, costs, and performance [42]. It consists of a bearing plate (fluke) attached to a shank that is connected to the mooring line. Because of the angle of the fluke, soil failure occurs by dragging the anchor through the soil, ensuring self-embedment. The DEA was initially designed for temporary moorings, but has since been improved and is now often used for permanent mooring. One of the downsides however is that a DEA does not have a large vertical capacity in comparison to its horizontal capacity, although this is dependent on the soil type and penetration depth of the anchor. It is mostly only suitable in combination with a catenary mooring system, and the positioning accuracy during installation of the system is relatively low compared to suction and driven piles. It is however fairly easy to install and has a large holding capacity in comparison to its weight.



Figure 2.7: DEA from Delmar systems [21]

### Suction pile

Similar to a driven pile, the suction pile is a hollow cylinder. The difference is that the top end of the cylinder is closed off by an end-cap and their wall thicknesses are typically lower since there is no hammering required. It can therefore also be installed in deeper waters as opposed to driven piles, as hammer equipment cannot reach ultradeep waters. Installation begins by self-penetration of the pile due to its weight, with up to 60% of its length embedded [2]. After a succession of self-penetration, water is pumped out of the top end of the pile by a Remotely Operated Underwater Vehicle (ROV) to create suction to finalize the embedment of the pile into the soil.



(a) A suction pile being installed [23]



(b) A driven pile being installed [6]

Figure 2.8: Installation of suction and driven piles

## 2.3. Line types

The industry currently uses a wide range of line types for mooring structures, employing both traditional and more modern options. Materials are selected based on their strength, cost, and durability since they must be able to withstand environmental conditions throughout their lifespan.

### Chain

Chains have been the most used type of line in the offshore industry. These lines consist of heavy-duty shackles made of high-strength steel links. Sorted in chain grades (from R3 to R5), they all have different strengths and thus Minimum Breaking Loads (MBLs). An overview of chain diameter vs their MBLs can be found in Figure 2.9. Chains can be manufactured with studs inserted between the links, which increases their weight and hydrodynamic drag but also makes them less prone to fatigue. Studless chains are currently mostly used in deep water moorings.

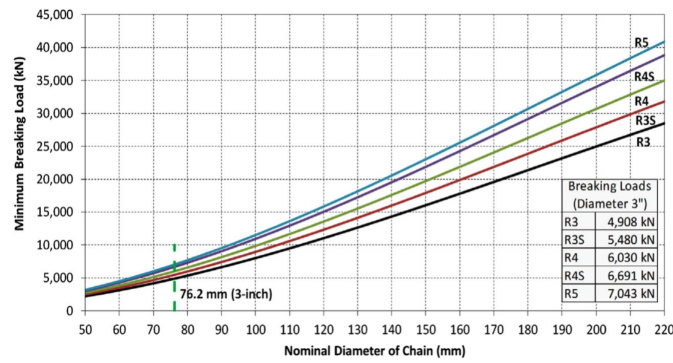


Figure 2.9: Different chain diameters with their corresponding MBL for different chain grades [42]

### Wire rope

In deeper waters, the use of chains becomes less feasible due to their weight per meter. An alternative for these conditions is to use wire rope, since it is lighter and more elastic than chains. Wire rope comes in several types, ranging from six to eight-strands to spiral strands, see Figure 2.10. Spiral strand is usually used for permanent mooring, and therefore also has a sheathed option to prevent corrosion.

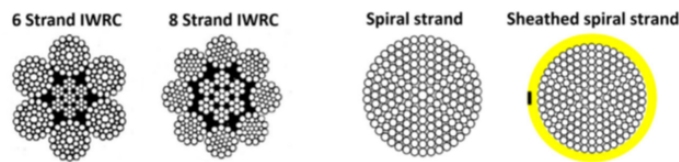


Figure 2.10: Different types of wire rope [42]

### Synthetic rope

An even more lightweight and commonly used option is synthetic mooring line. The most common synthetic line is polyester rope, however, numerous alternatives such as nylon, high-modulus polyethylene (HMPE), and Aramid (used in Kevlar) exist for mooring systems. Synthetics have become the most used line for taut systems in deep and ultradeep waters. These materials provide higher strength than steel and are more fatigue resistant against load cycles. They do however degrade more over time and are influenced by temperature, which poses maintenance challenges over its lifetime. Additionally, unlike wire rope and chain, synthetic ropes exhibit nonlinear stress-strain properties, which depend on time, tension and temperature. The line will, after pre-tensioning, be longer than the fabricated length. Moreover, after the first high-tension load such as in extreme weather, it will elongate even more. This will have to be taken into account during the engineering phase of a design.

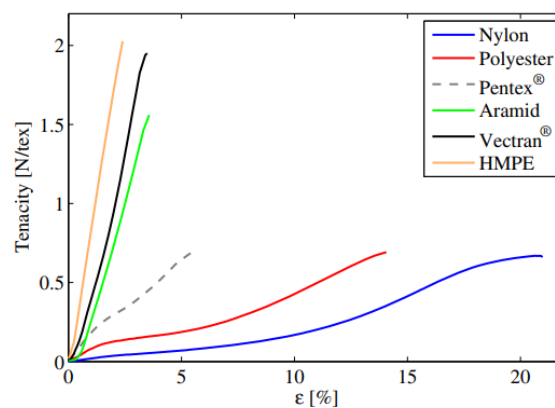


Figure 2.11: Example of a stress-strain curve, taken from Weller et al. [47]



**Figure 2.12:** Composition of a polyester rope

# 3

## Theory

Floating offshore structures are subjected to extreme environmental loading, such as wind, currents and in particular, waves. This necessitates an accurate description of the motions and loadings on such a structure for a reliable design. Design restrictions, in particular for floating wind turbines, are the maximum nacelle accelerations of the turbine itself, the minimum bending radius of the power cable, as well as the MBL of the mooring lines. This chapter provides an overview of the applied theory in this thesis, first describing mooring theory, after which an overview of the environmental loading is given.

### 3.1. Mooring theory

Before conducting an extensive analysis of the mooring system of a floating structure, accurate modelling of the mooring lines and the entire system is essential to achieve a realistic representation. The foundational approach to mooring line modelling relies on the catenary equation; however, more advanced numerical methods are also being used nowadays in the industry. Below, an overview of different mooring modelling methods is given, alongside an explanation of catenary theory.

#### 3.1.1. Analytic catenary equation

The analytic catenary equation is a static approach for solving the tensions and shape of the mooring line. Considering a small element of a mooring line in a 2-D plane as shown in Figure 3.1, with  $V$  being the vertical (z-axis) external force component, and  $H$  being the horizontal (x-axis) force component of the external force of the mooring line at the fairlead.  $W$  is defined as the weight in water,  $s$  the (unstretched) Lagrangian coordinate and  $T$  the tension in the mooring line [36].

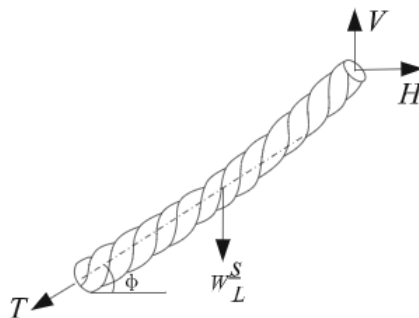


Figure 3.1: Small element of a mooring line as found in Jiang et al. [36]

To find the shape and restoring forces for the line, the horizontal and vertical forces will have to be in equilibrium with the line tension [36]:

$$T \frac{dx}{dp} = H \quad (3.1a)$$

$$T \frac{dz}{dp} = V - W \frac{s}{L} \quad (3.1b)$$

Where  $p$  is the stretched coordinate and  $T$  is defined by Hooke's Law, using the elastic stiffness of the material and its deformation:

$$T = EA \left( \frac{dp}{ds} - 1 \right) \quad (3.2)$$

Using the rewriting found in Jiang et al. [36] for  $x$  and  $z$ , the equations for finding the catenary shape can be found:

$$x(s) = \frac{Hs}{EA} + \frac{HL}{W} \left[ \operatorname{asinh} \left( \frac{V}{H} \right) - \operatorname{asinh} \left( \frac{V - W \frac{s}{L}}{H} \right) \right] \quad (3.3)$$

$$z(s) = \frac{Ws}{EA} \left( \frac{s}{2L} - \frac{V}{W} \right) - \frac{HL}{W} \left[ \sqrt{1 + \left( \frac{V}{H} \right)^2} - \sqrt{1 + \left( \frac{V - W \frac{s}{L}}{H} \right)^2} \right] \quad (3.4)$$

With  $s$  being the instantaneous position within the coordinate system,  $L$  the total length of the mooring line, and  $EA$  the axial stiffness of the material. The first part of the right side of Equation 3.3 and Equation 3.4 represents the elastic stretching of the mooring line, while the second part describes the parabolic shape of the mooring line caused by its own weight.

Given the total line length and its boundary positions relative to the origin, this leads to the final horizontal distance  $l$  and vertical distance  $h$ :

$$l = \frac{HL}{EA} + \frac{HL}{W} \left[ \operatorname{asinh} \left( \frac{V}{H} \right) - \operatorname{asinh} \left( \frac{V - W}{H} \right) \right] \quad (3.5)$$

$$h = \frac{WL}{EA} \left( \frac{1}{2L} - \frac{V}{W} \right) - \frac{HL}{W} \left[ \sqrt{1 + \left( \frac{V}{H} \right)^2} - \sqrt{1 + \left( \frac{V - W}{H} \right)^2} \right] \quad (3.6)$$

As can be seen from Equation 3.5 and 3.6, the horizontal and vertical distance are dependent on the horizontal and vertical forcing, with the vertical forcing assumed equal to zero. If one wants to know the distances from anchor point to fairlead point of the floater, the horizontal restoring force can be found using a numerical iteration process with initial guesses for the suspended length  $L$  and restoring force  $F_{hor}$  using the equations above:

$$x_{susp} = \frac{F_{hor} L_{susp}}{EA} + \frac{F_{hor} L_{susp}}{W} \left[ \operatorname{asinh} \left( \frac{F_{vert}}{F_{hor}} \right) - \operatorname{asinh} \left( \frac{F_{vert} - W}{F_{hor}} \right) \right] \quad (3.7)$$

$$z_{anch-fairlead} = \frac{W L_{susp}}{EA} \left( \frac{1}{2L_{susp}} - \frac{F_{vert}}{W} \right) - \frac{F_{hor} L_{susp}}{W} \left[ \sqrt{1 + \left( \frac{F_{vert}}{F_{hor}} \right)^2} - \sqrt{1 + \left( \frac{F_{vert} - W}{F_{hor}} \right)^2} \right] \quad (3.8)$$

For the total horizontal distance from the anchor point to fairlead, the following is used:

$$x_{total} = L_{total} - L_{susp} + x_{susp} \quad (3.9)$$

### Suspended (shared) line

A shared line, fully suspended from the seabed, can be modelled with the same catenary equation as from above by coupling two catenary-shaped mooring lines at their lowest points (normally the anchor points), with one of the catenary shapes mirrored over the  $x$ -axis. The shared line has a simplified calculation, as it can be assumed that  $L_{total} = L_{susp}$  for each part of the line, leaving only one unknown ( $F_{hor}$ ) left to be solved.

## 3.2. Mooring Modelling Fidelities

Below an overview of different modeling techniques for mooring design is given. Although different definitions are given in the literature for modelling techniques, for example, described by Davidson and Ringwood [28] and Lehmann [39], the definition of each modelling technique in this report is taken from Bureau Veritas [13] and OrcaFlex [17].

### 3.2.1. Static approach

The static analysis represents the simplest form of modelling a mooring line. By assuming static equilibrium between the mean environmental loading (static loading) and the total restoring mooring force, a relation between the displacement of the structure and the mooring force can be found. Static load restoring curves are calculated using the catenary equation. This modelling approach is nowadays barely used in the offshore industry, as more sophisticated software is available that captures dynamic forcing. Nevertheless, static analysis still finds its utility in the initial phases of a design.

### 3.2.2. Quasi-static approach

As defined by Lehmann [39], the Quasi-static approach takes the dynamic wave loads into account by offsetting the floater by a distance defined by a statistical analysis of the wave motions.

The method still relies on a certain mean displacement based on the static equilibrium, however, an extra displacement is added which is derived from the Response Amplitude Operator (RAO), determined by the sea state and the response function of the floater [39]. This method still ignores all dynamic effects. The Quasi-static approach is also rarely used for the final design in the offshore industry, but can again be used in the preliminary stages.

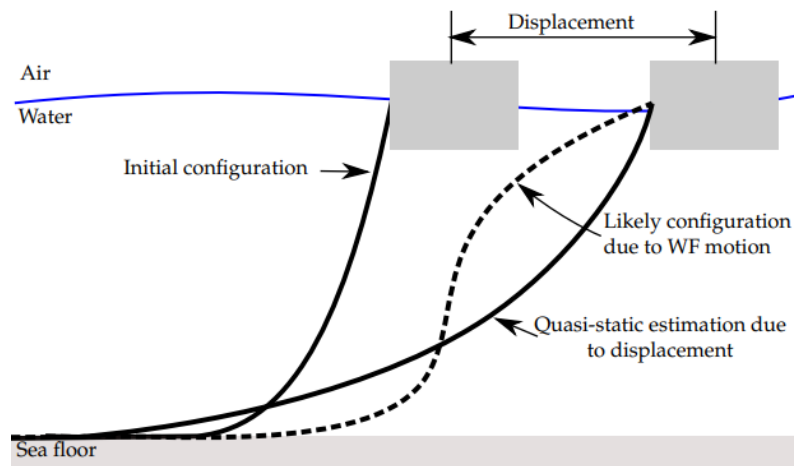


Figure 3.2: Quasi-static modeling vs dynamic modeling [28]

### 3.2.3. Quasi-dynamic approach

The Quasi-dynamic approach involves a time-domain (TD) simulation of the mooring system under environmental loads. It models the mooring lines as non-linear massless springs, modelling the tensions as derived from the static catenary equations from the static approach. It is assumed that there is no overlap between low-frequency components and wave frequencies when calculating wave loading and can therefore be evaluated separately and summed at each time step.

The dynamics of the floater are evaluated at each time step using the equations of motion to evaluate the position of the floater. The tensions in the mooring lines are then assessed using the static catenary responses. The benefit of this method is that the static responses can be pre-calculated, saving computing power.

For this approach, it is assumed that the mooring system is not in resonance with the wave frequency and that out-of horizontal-plane low-frequency motions are negligible. Moreover, it is assumed that horizontal and wave frequency phenomena do not coincide. According to Lehmann [39], this assumption is reasonable if the resonance period of the mooring system in surge, sway and yaw is greater than 5 times the zero-up crossing period of the wave.

### 3.2.4. Dynamic approach

The full dynamic approach for modelling mooring lines is considered to be the most accurate in the industry due to the fact that it entails all dynamic effects, including nonlinearities. A full dynamic approach has different methods of modelling the mooring line:

1. Lumped mass method
2. Finite Element Method
3. Finite Difference Method

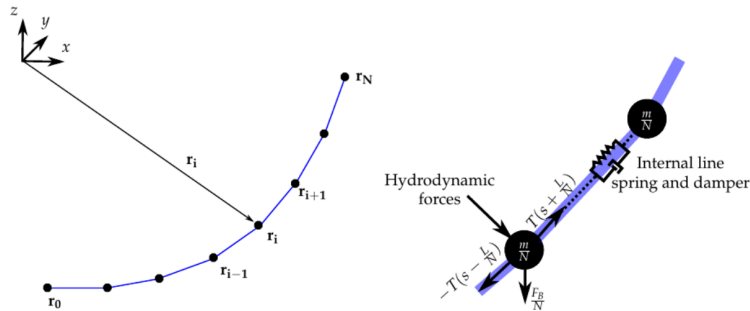


**Figure 3.3:** Representation of the lumped-mass method as found in Davidson and Ringwood [28]

Due to the high number of degrees of freedom in the simulation, this modelling approach comes at a high computational cost. It is currently the most used standard within the offshore industry. Additionally, there is the option of a coupled and uncoupled analysis. Nowadays, a coupled analysis is considered to be a necessity in terms of the complexity of the systems.

#### Coupled analysis

A coupled analysis allows for the mooring system to not only apply a restoring force on the floater but also to apply damping and inertia loads. There is, so to say, a direct coupling between the vessel's motions and all dynamic loads of the mooring system. This coupling is nowadays mostly used in deep water mooring analysis, as the damping and inertia of the mooring system play a large role.

### 3.3. Environmental loading

A floating offshore structure, loaded by environmental forces such as waves, wind and current, demands an accurate enough description of its motions and loadings to design confidently. In particular, for a floating wind turbine, the design restrictions must be met for the electrical cable, which has a minimum bending radius and maximum nacelle accelerations. Knowing these restrictions and the met-ocean conditions on the intended location, a specific mooring system can be designed to meet these restrictions.

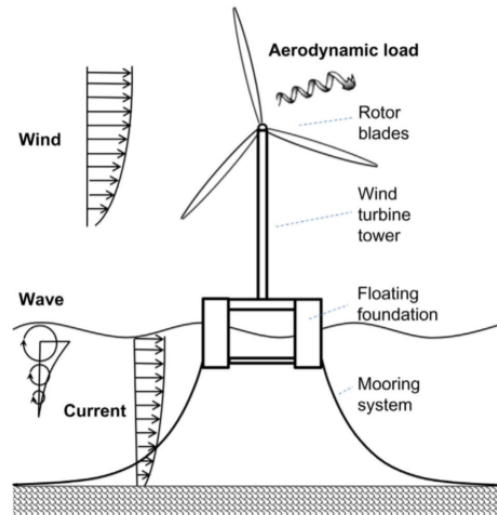


Figure 3.4: Environmental loads on a FOWT [42]

The environmental forces depicted in Figure 3.4 can be calculated in different ways, ranging from low accuracy and computational cost to high fidelity and time-consuming simulations. In this chapter, only waves are discussed, as these have the most significant impact on the loading of a floating structure.

### 3.4. Descriptions of waves

Waves are depicted as wind waves and swell. Wind waves are generated by wind blowing on the water surface, causing ripples which, over time and length (called fetch) can turn into large waves. As these waves are generated locally, they are also called local waves or sea waves [42]. If the wind blows for a long time, the waves can travel over a longer duration of time. These so-called swells can therefore travel to other local systems. The wavelengths of these swells are not significantly affected by the local winds.

Depending on the type of structure and the sea state, different wave theories can be used for describing waves. The most basic theory is the Linear (Airy) wave theory. However, also nonlinear waves such as Cynoidal, Stokes' second, third, and fifth order wave theories can be used. These all describe a regular wave; however, because of their non-linear nature, they cannot be applied in a spectrum. Therefore, the industry still relies heavily on linear wave theory, which is applicable in the case of deep water.

#### 3.4.1. Linear wave theory

Linear wave theory is a simplified method of describing waves, where the assumption has been made that waves are small and perform a sinusoidal motion. The height of the water surface (water elevation) can be described by the following:

$$\zeta = \zeta_a \cos(kx - \omega t) \quad (3.10)$$

Where  $\zeta$  is the elevation,  $\zeta_a$  is the amplitude of the wave,  $k$  is the wave number,  $x$  is the position where

the sea elevation is evaluated, and  $\omega$  is the wave frequency. The wave number  $k$  can be expressed as

$$k = \frac{2\pi}{\lambda} \quad (3.11)$$

Where  $\lambda$  is the wavelength, which for deep water is equal to:

$$\lambda = \frac{gT^2}{2\pi} \quad (3.12)$$

With  $T$  being the wave period, and  $g$  being the gravitational constant.  $\omega$  can be given by:

$$\omega = \frac{2\pi}{T} \quad (3.13)$$

The total wave height  $H$  can be expressed as  $H = 2 * \zeta_a$ . A depiction of this wave can be found in Figure 3.5.

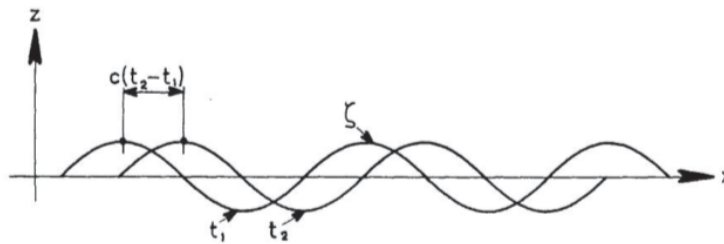


Figure 3.5: Representation of a linear wave

### 3.4.2. Wave spectra

In the offshore industry nowadays mostly irregular wave spectra are used for the determination of the environmental loading. One of the most used spectra is the JOint North Sea Wave Project spectrum, also known as JONSWAP. The JONSWAP spectrum is based on measurements of waves in the North Sea and gives a realistic representation of the distribution and wave energy across a spectrum of wave frequencies. It was originally derived from the Pierson-Moskowitz spectrum with an additional shaping factor, see Figure 3.6. The complete expression for the JONSWAP spectrum is [33]:

$$E_{JONSWAP}(f) = \alpha g^2 (2\pi)^{-4} f^{-5} \exp \left[ -\frac{5}{4} \left( \frac{f}{f_{peak}} \right)^{-4} \right] \gamma \exp \left[ -\frac{1}{2} \left( \frac{f/f_{peak} - 1}{\sigma} \right)^2 \right] \quad (3.14)$$

Where:

- $f$  is the wave frequency in [Hz]
- $\alpha$  is the spectral energy parameter
- $f_{peak}$  is the peak frequency
- $\gamma$  is the peak enhancement factor
- $\sigma$  represents the spectral width parameter

Usually,  $\gamma$  is taken with a value of 3.3 and  $\sigma$  as:

$$\sigma = 0.07 \text{ for } f \leq f_{peak}, \sigma = 0.09 \text{ for } f > f_{peak} \quad (3.15)$$

$\alpha$  is dependent on the conditions, however, Isherwood [34] found an equation for the estimation of this parameter.

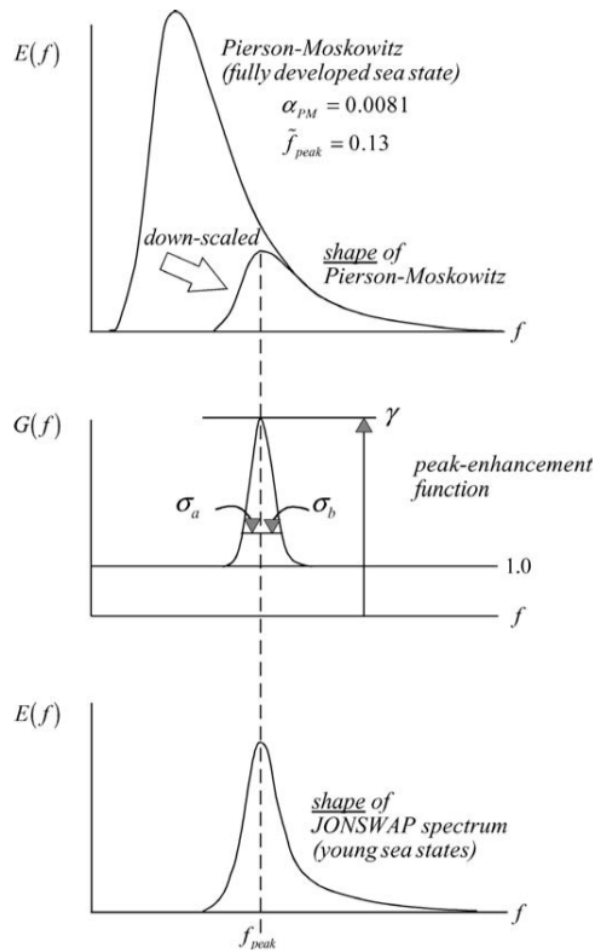


Figure 3.6: Example of a JONSWAP spectrum [33]

### 3.5. Equations of Motion

The influence of waves, wind, and current can be captured in the dynamics of rigid bodies by using the Equations of Motion (EoM) of the structure. A rigid body can move in six degrees of freedom, as depicted by Figure 3.7:

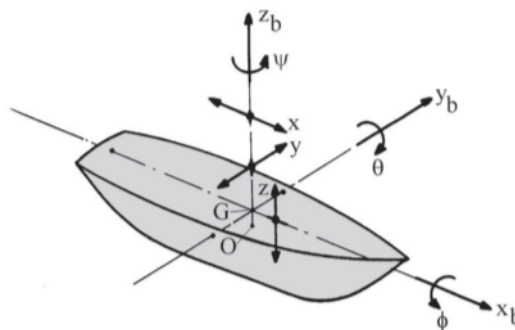


Figure 3.7: Vessel motions in six DOF [38]

Where the following definitions are given for each motion:

- Surge ( $x$ ), movement in the longitudinal direction
- Sway ( $y$ ), movement in the lateral direction
- Heave ( $z$ ), movement in the vertical direction
- Roll ( $\phi$ ), rotation along the longitudinal direction
- Pitch ( $\theta$ ), rotation along the lateral direction
- Yaw ( $\psi$ ), rotation around the vertical direction

As a rigid body can move in six degrees of freedom, the equations of motion are usually depicted in matrix form:

$$(M + A)\ddot{x}(t) + B\dot{x}(t) + Cx(t) = F_{ext}(t) \quad (3.16)$$

In hydrodynamics, the EoMs of a vessel or structure in waves have the following depictions:

- $M$  is the mass matrix of the structure
- $A$  is the added mass, which represents the inertia of the water displaced by the structure
- $B$  is the resistance of the structure to move in the water, also known as hydrodynamic damping
- $C$  represents the hydrostatic forces on the structure due to its weight
- $F_{ext}$  represents all external forces on the structure

The EoMs can be solved in both TD and FD, although in FD the system will have to be linearized.

### 3.6. Wave loading

The wave loading on a floating structure can be simulated with the use of various methods. Three methods are well-known and used in the industry:

- Morison's equation
- Diffraction-radiation theory
- Computational Fluid Dynamics

Morison's equation is used in the case of a slender (in comparison to the wavelength of the waves) structure, which is drag and inertia-dominated. If high accuracy is demanded (in the case of breaking waves for example), Computational Fluid Dynamics (CFD) come into play, with large computational cost as its main downside. It is however the most complete and accurate description of wave loading, as it employs the full viscous Navier-Stokes equation. For high-volume structures such as semi-submersibles, the hydrodynamic problem can be split into two problems, called the diffraction and radiation problem.

#### Diffraction

The diffraction force is the force that is exerted on a structure by the waves, assuming that the structure itself is fixed. The wave force  $F_w$  can be split in two different forces:

$$F_w = F_{FK} + F_D \quad (3.17)$$

Where  $F_{FK}$  is called the Froude-Krylov force, and  $F_D$  is called the diffraction force. The Froude-Krylov forces are the forces introduced by loading the structure with the waves. These waves are then diffracted, as the structure is impermeable, which introduces the diffraction force. Both are obtained by integrating the water pressure over the submerged surface of the structure.

#### Radiation

The radiation problem represents the structure moving with the frequency of the incoming wave field, assuming no waves are present. The moving of the structure introduces waves by itself and therefore produces the added mass, damping, and hydrostatic restoring coefficients.

The diffraction-radiation problem is solved by using Linear potential flow theory, which uses the simplified Navier-Stokes problem with a set of boundary conditions and assumptions to describe a velocity potential field ( $\Phi$ ). This velocity potential field can be used to solve the flow of a fluid in every direction. The calculation of the forces, moments, and hydrodynamic coefficients is often done by using the Boundary Element Method (BEM), which meshes the surface of the structure into panels (typically triangular or rectangular) to integrate the potentials over it, using Green's function [38].

### 3.6.1. Response Amplitude Operator

In the maritime and offshore industry, a vessel or structure's motion is usually depicted by the Response Amplitude Operator, also known as RAO. An RAO is a transfer function that describes the relation between a wave spectrum and the motion response to these waves:

$$RAO(\omega) = \frac{x_a(\omega)}{\zeta(\omega)} \quad (3.18)$$

Where  $x_a$  is the motion amplitude and  $\zeta$  is the wave elevation amplitude. It gives a convenient insight into how a vessel or structure behaves in the offshore environment. Integrating over a range of frequencies (spectrum) will give the full RAO, from which the response spectrum  $S_{xx}$  of a structure loaded by the wave spectrum  $S_{\zeta\zeta}$  is given:

$$S_{xx}(\omega) = |RAO|^2 \cdot S_{\zeta\zeta}(\omega) \quad (3.19)$$

RAOs are generally the resulting output of radiation-diffraction software tools.

### 3.6.2. Drift loads

The responses of a structure in waves consist of first, second-order, and higher-order wave forces. Above, a description of the first-order wave force is given by the diffraction-radiation theory. Higher-order terms are usually omitted, as these cause small loads on structures. The second-order wave force however does present a significant effect on the total loads on a structure, also known as drift loads. Drift loads are especially important for moored structures, as this drift will cause a displacement of the structure which the mooring system will have to oppose.

The second-order wave drift force consists of low-frequency components and high-frequency components. The low-frequency components contain the mean wave drift loads and frequency difference components. High-frequency components, also known as sum frequency loads, are mostly calculated in the case of stiff structures such as TLP designs.

The second-order wave drift force is a quadratic force dependent on the wave amplitudes of a pair of wave components. The contribution to the drift force is proportional to the frequency difference of these two wave components. If the wave components have the same frequency, it gives a constant contribution called the mean wave drift force. This mean wave drift gives a mean offset under a certain load. Wave components that differ from each other in terms of frequency give rise to low-frequency load contributions, which determine the slow drift motion of a structure. The wave components with low-frequency differences usually give the highest slow drift motion. The wave components with large frequency differences are usually less important.

There are two different methods for calculating the drift force, far field, and near field approach, described by Newman [43] and Pinkster et al. [44]. Far-field gives only mean wave drift force, the near-field approach also contains the frequency-difference components. These components are usually given in the Quadratic Transfer Function (QTF), which is calculated in diffraction-radiation potential software. For the calculation of the mean wave drift force, only the diagonal of the QTF is necessary.

### Conclusion

Based on the introduced theory and modelling methods, it was decided to design a Quasi-dynamic time domain model, making use of the static catenary equations to acquire the mooring forces in the system. For the modelling of the motions and loadings of the floating structures, the equations of motion will be solved using hydrodynamics, making use of linear wave theory. The model will be able to simulate irregular waving, from which the first-order wave forces and second-order mean wave drift forces will be calculated. Wind and current loading is left out of the model to keep the project within scope.

# 4

## Case study

This chapter describes the structures considered for this study, including the mooring line properties and configurations considered. The structures used are existing concepts, out of which the solar floater model was recreated due to no data being available.

### 4.1. Floating wind structure

The semi-submersible platform from the University of Maine, known as the UMaine VoltturnUS-S as found in Allen et al. [25], was used for the modelling of the floating wind turbines. A render of this floater is shown in Figure 4.1. The choice of this turbine and its semi-submersible platform was made based on its publicly available data and its potential to accurately represent the trend towards larger turbines in the offshore industry. Additionally, this turbine has been the subject of extensive research, providing benchmark data for future research.



**Figure 4.1:** The UMaine VoltturnUS-S reference semi-submersible platform [25]

The semi-submersible supporting the 15MW turbine consists of four columns: one central column and three radially spaced columns. Three catenary mooring lines are used to install the turbine at a depth of 200 metres. The platform is designed to have a 20-metre draft and a 15-metre column that is not submerged, resulting in 35-metre-long columns.

A general overview of the specifications of the turbine can be found in Table 4.1:

Property	Value	Unit
Turbine Rating	15	MW
Hub height	150	m
Length	90.1	m
Width	102.1	m
Height	290	m
Draft	20	m
Total mass	20,093,000	kg
Platform mass	17,839,000	kg
Tower mass	1,263,000	kg
RNA mass	991,000	kg
Water Depth	200	m

**Table 4.1:** System specifications taken from Allen et al. [25]

The dimensions of the wind turbine can be found below in Figure 4.2.

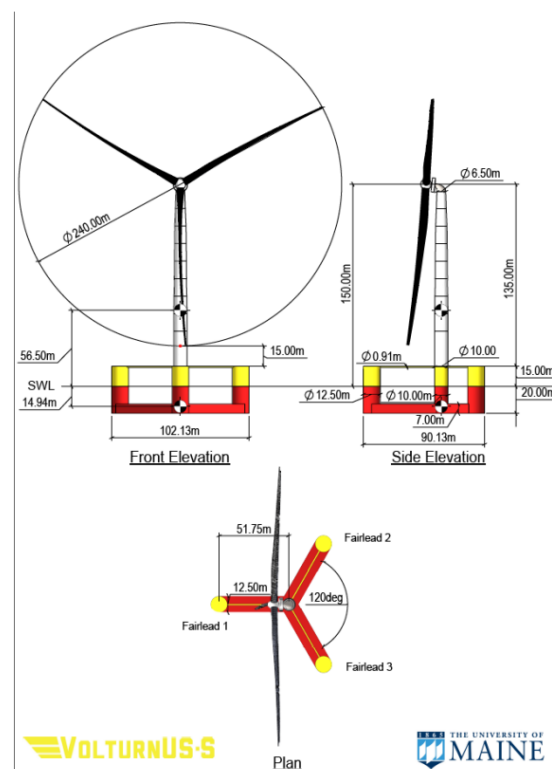


**Figure 4.2:** Dimensions of the VoltturnUS semi-submersible [25]

#### 4.1.1. Mooring system

The three catenary chain mooring lines are hooked up to the fairlead points of the platform. These fairlead points are placed at the outer ends of each one of the outer columns at 14 metres depth below Mean Sea Level (MSL). The lines are of a grade R3 studless chain with a nominal diameter of 0.185 m. Full properties of the mooring system can be found in Table 4.2

Property	Value	Unit
MBL	22,286	kN
Chain diameter	0.185	m
Mass per unit length	685	kg/m
Axial stiffness	3,270	MN
Line length	850	m
Fairlead pretension	2,437	kN
Anchor Depth	200	m
Fairlead depth	14	m
Anchor radial spacing	837.6	m
Fairlead radial spacing	58	m

**Table 4.2:** Mooring system properties, taken from Allen et al. [25]

## 4.2. Floating solar structure

For the modelling of the solar panels, no reference data was available of any existing concept. It was therefore chosen to recreate a model based on the Tractebel Seavolt concept. The Seavolt concept is a semi-submersible structure design, based on four equally spaced columns. The topside is covered with solar panels. The benefit of this concept is that the solar panels are far above sea level, protecting the panels from the harsh offshore environment.

Dimensions were drawn based on existing renders of the concept. The structure, depicted in Figure 4.3, consists of four floaters of equal diameter arranged in a square formation. The dimensions used for the modelling of the floater can be found in Table 4.3:



**Figure 4.3:** The Seavolt concept on which the model is based

Property	Value	Unit
Topside length	42	m
Column diameter	2.4	m
Spacing between columns	24	m
Height floater	17.5	m
Draft	6.5	m
Fairlead depth	6	m
Total mass	115,200	kg

**Table 4.3:** Dimensions of modeled structure

### 4.2.1. Mooring system

The mooring system of the floating solar system was designed from a derivative of the mooring system of the base case of the Voltorn US-S floater. Three options were considered; a regular catenary chain, a wire rope, and a polyester rope. The lines were scaled to a configuration of 16 connected floaters, in order to represent a large scale solar farm.

The catenary chain properties of the solar floater were determined by scaling the mass per unit length of the Umaine base case to the total mass of the floating solar array. As the mass of 16 floaters equals 1843.2 tonnes, this leads to a scaling of 1/10.92. Next, the mass per unit lengths were scaled accordingly to the number of lines attached to each floater. In the case of the solar floater, this led to a ratio of 3:4 turbine lines versus solar floater lines. For the wire and polyester rope configurations, the properties were scaled by 2x the MBL of the catenary chain as a conservative choice. An elaboration on the derivation of these properties can be found in Chapter 5. The properties found are depicted in Table 4.4.

Property	Chain		Wire		Polyester	
	Value	Unit	Value	Unit	Value	Unit
MBL	1,886	kN	4,053	kN	3,853	kN
Diameter	0.049	m	0.08	m	0.15	m
Mass per unit length	41.52	kg/m	22.24	kg/m	4.55	kg/m
Axial stiffness	205,000	kN	258,000	kN	24,520	kN

Table 4.4: Mooring properties catenary chain solar floater

### 4.3. Configurations

For this study, multiple arrangements of the floaters were considered. These arrangements were based on the study of Goldschmidt and Muskulus [31] and Connolly and Hall [26], and adjusted to allow the addition of the floating solar structures in between. The configurations used are described below, with top views of each configuration at the end of this section.

#### 4.3.1. Configuration 1

The first configuration consists of two turbines placed 1000 metres apart, interconnected with one solar floater array consisting of 16 floaters. Each turbine has two anchored lines and one shared line that connects them in order to give the turbines a larger mooring stiffness to limit displacements. It should, however, be noted that in this configuration, the turbines are approximately four turbine spacings apart. As this would introduce significant wake effects in downstream turbines, this configuration is impractical in reality. In the case of a smaller turbine, this configuration would be more realistic since the smaller rotor diameter would reduce the wake effects, allowing a smaller turbine spacing. Therefore, this configuration was researched nevertheless, to be able to have an indication of the behaviour of such a setup.

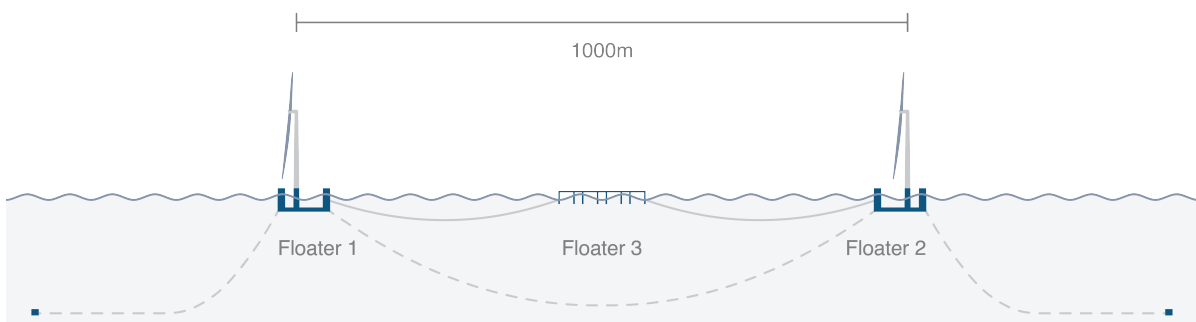


Figure 4.4: Configuration 1 side view

#### 4.3.2. Configuration 2.1-2.5

The second configuration of the model incorporates additional floating solar arrays within a turbine spacing of 2000 metres, equivalent to approximately eight rotor diameters. It was not considered economically viable to apply a shared mooring line between the two turbines, since that would require significantly longer lines compared to conventional mooring methods. Hence, the choice was made to conventionally moor the wind turbines, while only the solar floaters' mooring system would be using a

shared mooring system across the layout. The increased turbine spacing allows for the introduction of more solar floaters into the overall system. Multiple subconfigurations were taken into consideration in order to explore various possibilities, increasing the number of solar floaters to a maximum of five, as is depicted in Figure 4.5-4.6.

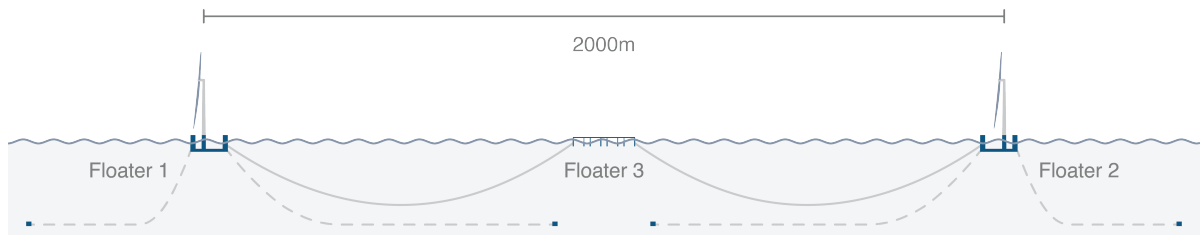


Figure 4.5: Configuration 2.1 side view

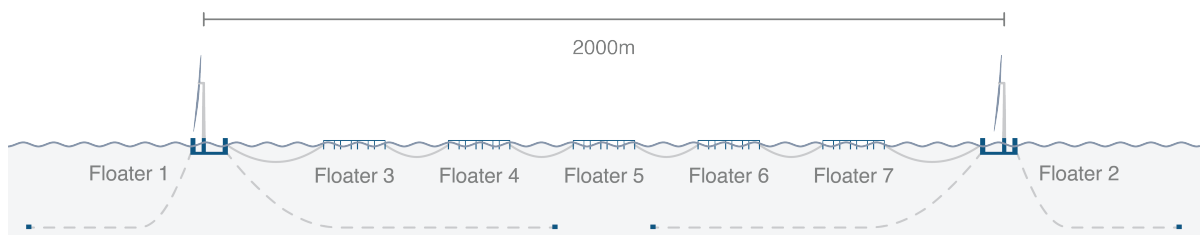
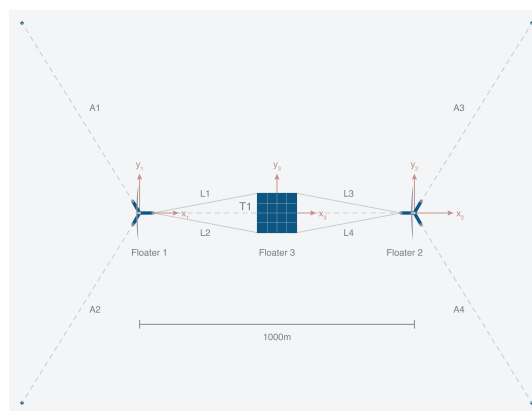
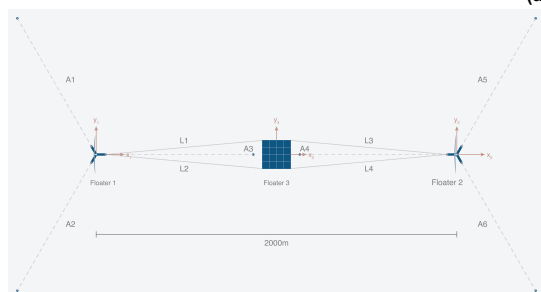


Figure 4.6: Configuration 2.5 side view

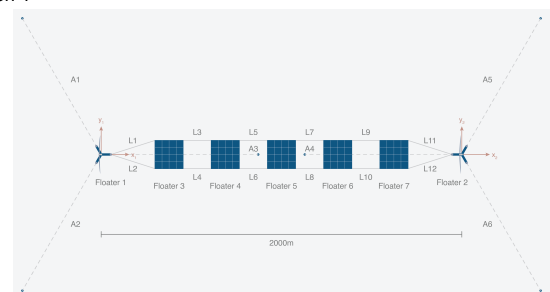
Top views



(a) Configuration 1



(b) Configuration 2.1



(c) Configuration 2.5

Figure 4.7: Top views of each configuration

# 5

## Method

This chapter describes the methodology used in this research. First, the Quasi-dynamic model is described, which was built to model the configurations found in Chapter 4. To acquire the hydrodynamic data required as input for the model, a diffraction analysis was done on both the turbine and the solar floater using OrcaWave, a widely used diffraction and radiation analysis software package developed by Orcina. By using the Python API of OrcaFlex, a software package used by the marine industry for dynamic analysis, the hydrodynamic data was imported into the model.

### 5.1. Quasi-dynamic Model

As was introduced in chapter 3, the Quasi-Dynamic model is a hydrodynamic time domain model which simulates the responses of floating structures and their mooring systems while disregarding the dynamics of the mooring lines. The mooring lines are considered as non-linear springs, which only induce the forces that are based on the static restoring force of the catenary equation. The dynamics of the floating structure are calculated using the EoMs. The model then acquires a time series of the motions and loadings on the floating structures considered next to the line tensions of each mooring line. A full description of the quasi-dynamic model can be found in the Bureau Veritas NR493 guidelines [3].

The model built can be represented by Figure 5.1, of which the orange boxes represent data from OrcaFlex/OrcaWave, the green parts are self-modelled inputs, and the yellow parts represent forcings. The designed model solves the Equation of Motion using the Runge-Kutta 45 method, which is an explicit time-domain solver giving two solutions in the order of 4 and 5. This allows varying step sizes, which makes it an accurate and computationally efficient method of solving the system [20].

The EoM that is solved in the model is equal to:

$$(M + A)\ddot{x}(t) + C\dot{x}(t) + Kx(t) = F_{wave}(t) + F_{mooring}(t) \quad (5.1)$$

Where  $F_{wave}$  is represented by both the 1st order and mean wave drift forces, and  $F_{mooring}$  is represented by the static restoring force of the mooring lines. The vector  $x$  represents all the DOF contained in the system in surge and sway.

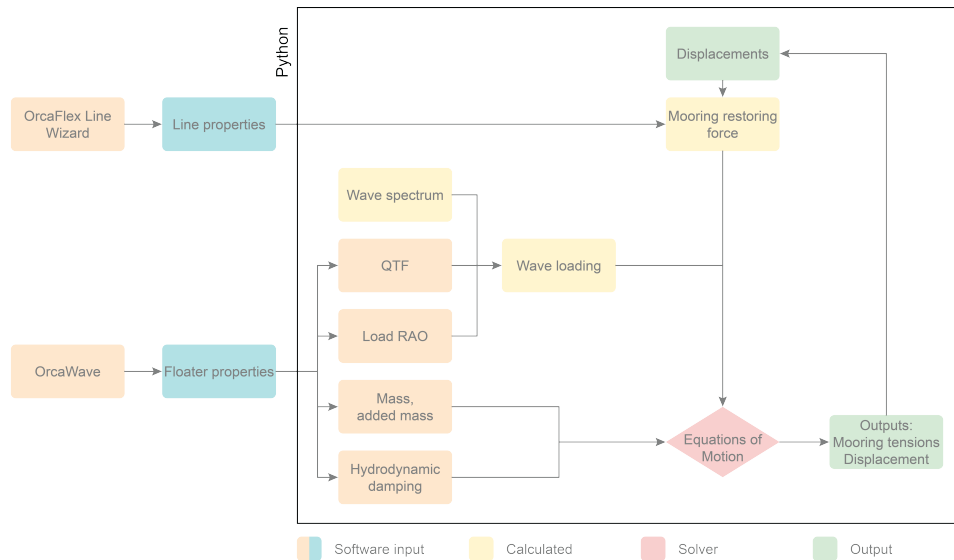


Figure 5.1: Overview of the quasi-dynamic model

### 5.1.1. Assumptions within the model

To stay within scope of the project, the Python model was built around some assumptions, which could lead to limitations of the model itself. These assumptions are listed below; some of them are explained below in more detail. The limitations due to the most important assumptions of the model are assessed in Chapter 6.

1. The static restoring force of the mooring lines
2. The mean wave drift forces
3. The constant added mass and damping for irregular waving
4. The linear axial stiffness of the mooring lines
5. A constant depth (no variation of the seabed) is assumed
6. The anchors were assumed to be static and rigid, neglecting the displacements and deflections of these anchors.
7. Potential seabed friction coming from the lines scraping the seabed is neglected.
8. No slacking of the mooring lines
9. Linear wave theory is used for the modelling of waves

#### Static restoring force

The implication of using the static restoring force is that the dynamic forcing of for example the wave loading and displacements of the floaters will not be fully coupled to the mooring lines. This could lead to an underestimation of the dynamic tensions in the mooring lines and therefore is considered a limitation. The quantification of this limitation is done in the verification in section 6.1.

#### Mean wave drift force

In conventional hydrodynamic models, the full QTF is utilized using Newman's approach or the fully calculated QTFs through diffraction analysis (see Chapter 3). However, in this project's scope, only the diagonal terms of the QTF, obtained from diffraction analysis, were taken into consideration. Consequently, only the mean wave drift force was considered to capture the second-order wave drift forces present in the environmental loading. Slow varying drift forces are therefore not captured in the model, which could lead to an underestimation of the dynamics. The impact of this assumption is assessed in section 6.5.

### Constant damping and added mass

Most hydrodynamic time-domain models incorporate frequency-dependent added mass and damping terms to capture the hydrodynamics of a structure, such as OrcaFlex. This is achieved using an Impulse Response Function (IRF), which is a function dependent on the hydrodynamic damping and added mass. This is applied on the EoM at each timestep by using a convolution integral to account for the past motion of the structure. To stay within scope, constant damping and added mass were chosen. These values were chosen at the frequency corresponding to the highest load RAO. The implications of this assumption is evaluated in section 6.5.

### Axial stiffness of the mooring lines

The values of the axial stiffnesses are based on the values from the line wizard of OrcaFlex and are assumed linear. The values of the chain, polyester and wireline types have been based on catalogue data [19]. For polyester rope in particular, it has been assumed the lines have been subjected to the following conditions to have more realistic data:

- pre-loading: The ropes are loaded to 50% of the MBL, after which they are untouched for 24 hours. This ensures consistent and repeatable elastic behaviour
- slow-varying loads, to account for second-order forces
- soaked lines, to account for the wet conditions

For the calculation of the average performance of the lines, stress-strain figures have been used, by taking the tangent of the stress-strain curve at 10% mean extension. An example of such a stress-strain curve can be found in the theory in Chapter 3. Although these values have been carefully determined, it is still an estimation of the real behaviour due to its linear approximations of the axial stiffness. The dynamics of the system could be different in reality, as it followed from Chapter 3 that synthetic lines exhibit nonlinear behaviour which is influenced by numerous factors. The limitation of this assumption was not assessed in this research to stay within scope.

## 5.2. Floater modelling

The solar concept (see Chapter 4) was modelled using multiple configurations. Options of one, four, and 16 floaters were considered for this study.

### Rigid assumption

The final design chosen has 16 solar floaters rigidly connected to represent a large solar farm. In reality, the concept would have hinging connections, allowing the floaters to move relatively to each other. This could have significant impact on the total response of such an array. However, the diffraction analysis used assumes an undisturbed wave for the assessment of the responses. This means that downwave floaters experience the same loading as the upwave floater, while in reality, the waves' energy would be dissipated through the field. Additionally, a hinging connection would introduce damping, dissipating responses into heat. The rigid assumption was, in this part of the process, considered a valid approach for modelling the displacements of the solar arrays, due to its overestimation of displacements of the total structure. For a more detailed approach however, this method is considered insufficient due to the neglecting of the aforementioned damping. Additionally, flexible structures could introduce different natural frequencies which could influence the behaviour of the systems.

### 5.2.1. Designing and meshing

The structure of the solar concept was modelled using Rhinoceros 3D [18], a commercial Computer-Aided Design (CAD) software package developed by Robert McNeel & Associates. The structure considered consists of four floaters of equal diameter. On top of the floater, a topside is placed for the solar panels to be installed. For this hydrodynamic study, only the four (cylindrical) floaters are modelled, as these are assumed to be the only parts of the structure to be in contact with the waves.

A diffraction analysis requires a meshed structure as input. The model from Rhino was therefore meshed in the open-source meshing program GMSH [10]. For the meshing of the model, a rule of thumb which is also considered in the guidelines of DNV[5] is used: A panel size is of a maximum of  $\frac{\lambda}{6}$ , where  $\lambda$  is the smallest wavelength analysed.

For larger structures, however, this would mean a large number of panels due to the sheer size of it, increasing computation time. To see if panel sizes could be made larger, a convergence study of the RAOs has been done in chapter 6. The meshed model of the single floater can be found below in Figure 5.2

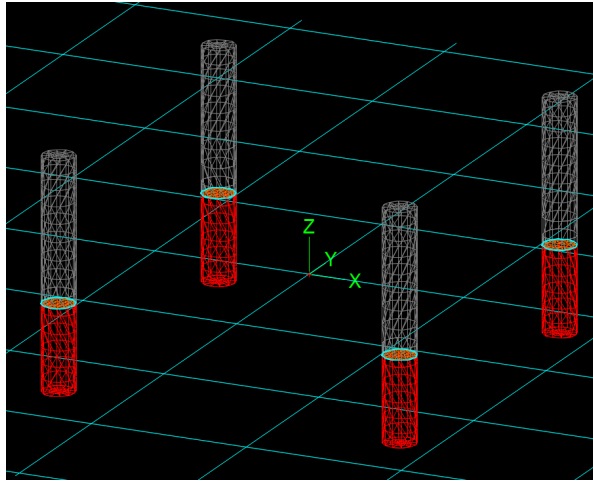


Figure 5.2: Meshed structure using GMSH, viewed in OrcaWave

### 5.2.2. Diffraction analysis

The diffraction analysis was done using OrcaWave. It calculates the loading and responses of a structure in waves using linear potential theory. It solves the diffraction and radiation potentials, giving the following outputs:

- Displacement and load RAOs
- Added mass
- Damping terms
- QTFs

For this study, OrcaWave was used to calculate the potential and source formulations only, meaning that only the diagonal terms of the QTF were determined. For the wave loading, wave periods of 2 to 50 seconds were considered.

The data obtained by OrcaWave is then used in Python using the OrcaFlex API, which is a tool, coupling OrcaFlex and Python for automation and batch running. The displacement RAOs were disregarded, as the actual displacements were solved using the Equations of Motion defined in the Quasi-Dynamic model. Load RAOs represent purely the Froude-Krylov and diffraction forcings from the diffraction analysis. The EoMs still need to be solved for the environmental loading present, and can therefore be used in the model with a variable mooring system, as there is no displacement solved yet.

### 5.2.3. Floating wind turbine model

The UMaine 15 MW reference turbine semi-submersible was used for modelling the floating wind turbine [25]. For the full system properties, see chapter 4. An existing model of the turbine was already available. The diffraction analysis was redone, however, accounting for the specific conditions for this study. The obtained data, just like the solar floaters, was imported into the model using the OrcaFlex API.

## 5.3. Static mooring response

The system modelled by the static model is shown below in Figure 5.3. From the use of the catenary equation (Equation 3.3) from Chapter 3, an initial guess of the shape of the catenary equation can be found using an estimation of the suspended length  $L_{susp}$  and the horizontal force  $F_{hor}$ . In the case of

the shared line, the suspended length is equal to the total length ( $L_{susp} = L_{total}$ ), which simplifies the system as only one variable is unknown ( $F_{hor}$ ). Using an optimizer in Python, the correct forcing and suspended length are found.

Note that from Figure 5.3, the shared line is modelled as two symmetric lines, coupled to each other at the midpoint between the two floaters.

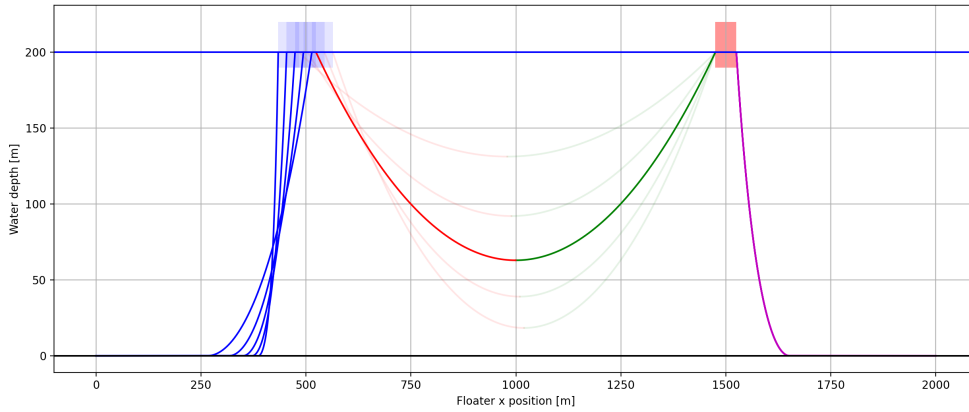


Figure 5.3: Setup of shared mooring system in Python

From the equations used, a force-displacement relation can be found for both anchor lines as the shared line for different displacements of the floater. This relation is used in the Quasi-Dynamic model to acquire the restoring forces on each floater to keep the structure in its intended position. An overview of the flow of the calculation of the mooring force can be found in Figure 5.4:

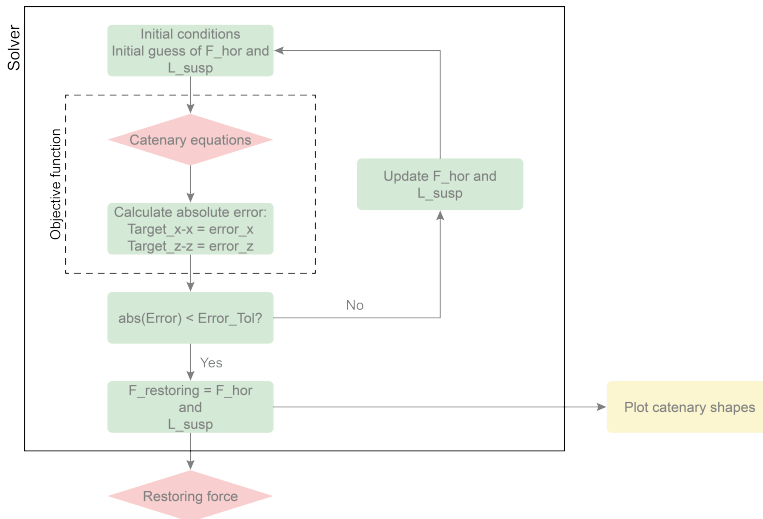
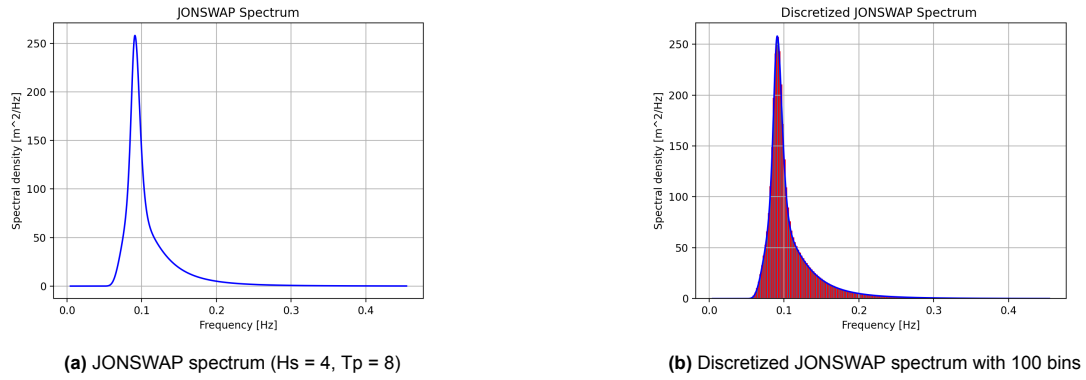


Figure 5.4: Flow of the static mooring force calculation

### 5.3.1. Wave loading

This study made use of both regular and irregular waves for the description of these waves. The modelling of these waves was conducted based on the theory presented in Chapter 3. For the irregular wave loading to be used in the time domain, a JONSWAP spectrum was used. This spectrum was first discretised in  $n$  amount of bins with a width of  $\Delta\omega$  (see Figure 5.5b).



**Figure 5.5:** Comparison of JONSWAP spectra

These bins represent a mean wave frequency with a certain amplitude and phase. The phases are computed randomly with a seed, while the amplitudes are computed by calculating the energy contained in the bin. The energy contained in a wave, according to Holthuijsen [33] can be expressed as:

$$E(\omega) = \frac{1}{\Delta\omega} \frac{1}{2} \zeta_\alpha^2 \quad (5.2)$$

Rewriting this equation results in the amplitude of the wave being:

$$\zeta_\alpha = \sqrt{2E(\omega)\Delta\omega} \quad (5.3)$$

Calculating these amplitudes for every bin results in  $n$  amount of wave components in the spectrum. This results in a time series by stacking these wave components on top of each other (see Figure 5.6).

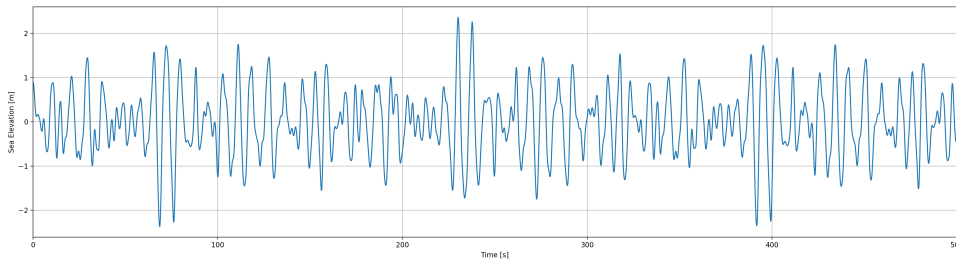


**Figure 5.6:** Time series of a JONSWAP spectrum

This irregular wave spectrum is then used in the quasi-dynamic model to calculate the first and second-order wave loading on each structure (see Chapter 3) by using the obtained load RAOs, QTFs, hydrodynamic damping, and added mass terms from OrcaWave.

### 5.3.2. Load cases

For the design of a mooring system for a FOWT, the same standard for mooring offshore oil & gas facilities can be used [42]. The only difference in terms of structure is that a FOWT is unmanned, and the effects of failure are less severe than with conventional oil rigs. Therefore, instead of using the 100-year return period for the environmental conditions, the 50-year return period can be used [42].

Two load cases were selected as those that were thought to have the greatest contribution to the loads on the floaters, representing a normal operating condition and a severe storm case in the North Sea. The load cases are partly derived from the study of Li et al. [40]. In the table below an overview of the load cases can be found:

	<b>Hs [m]</b>	<b>Tp [s]</b>
<b>Load Case I</b>	4	7
<b>Load Case II</b>	11	11

**Table 5.1:** Load cases as used in the simulations

# 6

## Verification and comparison with OrcaFlex

Before the results on the configurations defined in Chapter 4 could be generated, OrcaFlex was used to verify the model developed in Python. The goal of this chapter is to understand the capabilities and limits of the Quasi-dynamic model built. The verification and comparisons were conducted earlier in the research before the configurations were defined. The comparisons, therefore, have different mooring properties and layouts than the configurations defined in Chapter 4. The final comparison using the irregular waving is however using one of the configurations. The verification should, however, be independent of the layout.

### 6.1. Verification of the static mooring response

The layout as displayed in Figure 5.3 was applied to multiple scenarios with different water depths. Next, the results were compared to the model in OrcaFlex as verification of the static mooring response. To check the forcing, the left floater was displaced over the x position while the right floater remained in its static position. A 0.1-metre diameter chain with an axial stiffness of 854000 kN and submerged weight of 0.17292 kg/m was used throughout the verification process. The length of the shared line was set at 1000 metres. The line lengths of the anchored lines are displayed in the table below:

<b>Water depth [m]</b>	200	400	600	800
<b>Line length [m]</b>	600	750	900	1,050

**Table 6.1:** Line lengths over different water depths

#### 6.1.1. Sensitivity study over different water depths

Figure 6.1 illustrates the percentage errors of the restoring force for the different water depths, compared to OrcaFlex. The errors are displayed for a range of -40 to +40 metres offset about the static initial position. The results show a maximum difference of 1.52% between the OrcaFlex and Python models, which is deemed acceptable. The error was constant and near 0 for the shared line (red), indicating that the error is not significantly influenced by the shape of the catenary chain. Two notes can be taken from the error in the restoring force of the anchored lines:

1. As more line length is laying on the seabed (when the displacement of the left floater is negative), the error becomes larger.
2. A static position of the line (Anchored line 2) gives a small baseline error.

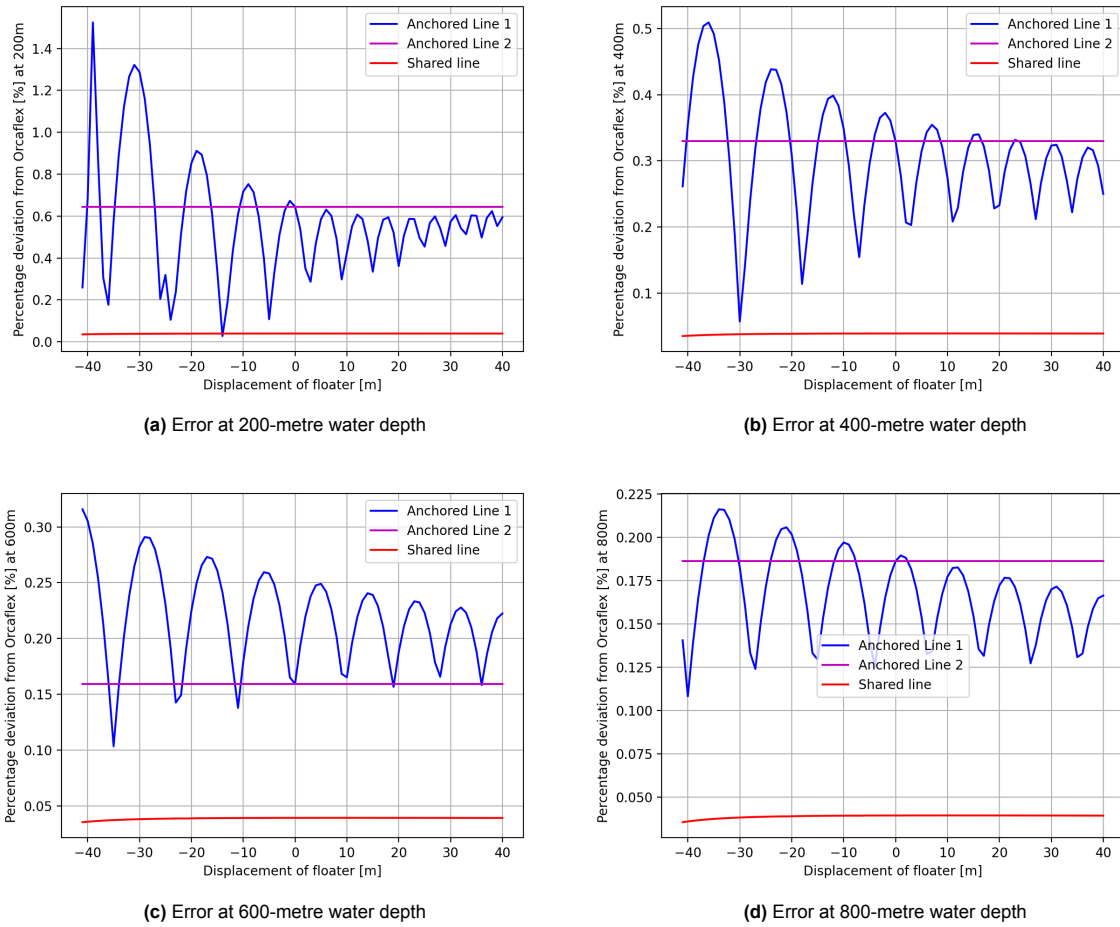


**Figure 6.1:** Verification of quasi-static model in OrcaFlex

As shown, the error with OrcaFlex is not constant. Rather, it fluctuates with the displacement of the floater, around 10 metres of displacement each. This was further researched by varying the segment lengths in OrcaFlex since the initial segment length within OrcaFlex was 10 metres. Figure 6.2 shows that the error can be smoothed out by reducing the segment length, increasing the total number of segments per line. Increasing the number of segments implicitly increases the resolution, increasing accuracy of the mooring line forces.

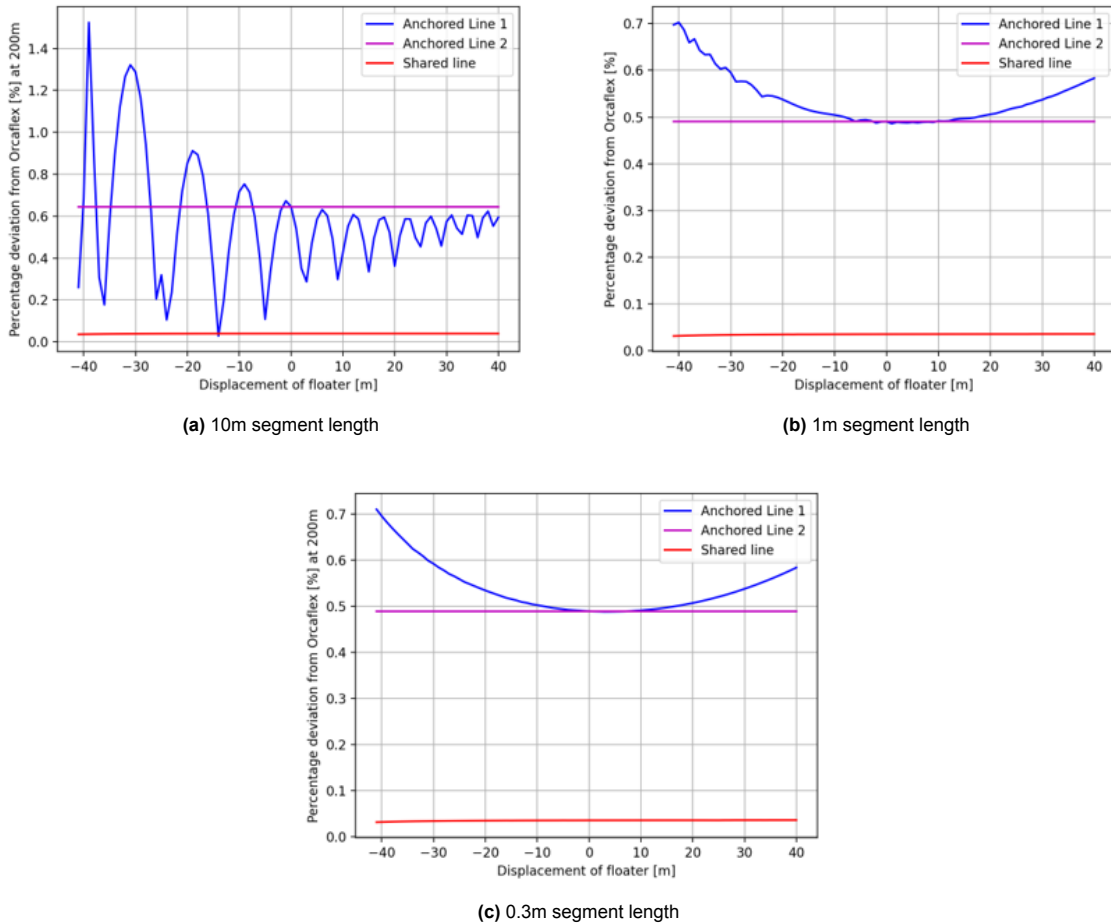


**Figure 6.2:** Different line segment lengths in OrcaFlex

Increasing the accuracy in OrcaFlex reduces the error in static response. As OrcaFlex has a maximum number of lumped masses per line, the most accurate state for the anchored had a 0.3 m segment length. This results in a maximum error of 0.7%.

The sensitivity study showed that increasing the number of segments, and therefore resolution, in OrcaFlex led to reduced differences. This indicates correct modelling of the static mooring line response.

## 6.2. Sanity check RAOs solar floaters

As no hydrodynamic data of a solar floater was available during the research, data was created (see chapter 5) using Rhino and the diffraction analysis software Orcawave. A sanity check was done on the RAOs of the model to check the correctness of these results. The checks that were done can be found below:

- Convergence study on panel sizes
- Interpretation of RAOs

### 6.2.1. Convergence study panel sizing

To check whether the results of the diffraction analysis performed in OrcaWave contained numerical errors, a convergence study on the panel sizes of the meshing was done on the single floater. The goal of this study was to see whether the accuracy of the RAOs would decline if panel sizes would increase. An increase in panel sizes (and therefore a decrease in number of panels) would lead to a decrease in computational cost, as fewer calculations have to be done on the total amount of panels.

The smallest wave period considered for this study was two seconds; this was considered conservative, as usually a marginal amount of spectral energy is left in these periods, which would lead to insignificant responses.

The panel sizes considered can be found in Table 6.2. As mentioned in Chapter 5, the industry standard is to use  $\lambda/6$  as the maximum panel size. A wave period of 2 seconds in deep water leads to a wavelength of  $\frac{gT^2}{2\pi} = 6.245$ , which leads to a panel size of 1040 mm. A smaller panel size of 750 mm was considered as a verification, to examine if results still deviated with an increase in accuracy. Increments of larger panel sizes were considered, up until 4000 mm.

The resulting RAOs of the floaters are shown in Figure 6.3-6.6 for surge, sway, and heave. Wave headings considered were  $0^\circ$ ,  $30^\circ$ ,  $45^\circ$ , and  $90^\circ$  degrees. As can be seen, overall there is not much deviation between the different RAOs. The only visible discrepancies can be found in the sway RAO at  $0^\circ$  and the surge RAO at  $90^\circ$ . The observed differences, however, are of such minor magnitude that these were considered negligible.

It could therefore be concluded that even the largest chosen panel size was sufficient for this study to work with, as the RAOs are sufficiently reminiscent of each other. This paved the way for a computationally efficient way to simulate the RAOs of larger configurations of solar floaters (4 and 16 floaters, as described in Chapter 5).

Panel size [mm]	No. of panels
750	6,188
1,250	2,973
2,000	1,263
4,000	1,002

**Table 6.2:** Different panel sizes and number of panels for a single floater.

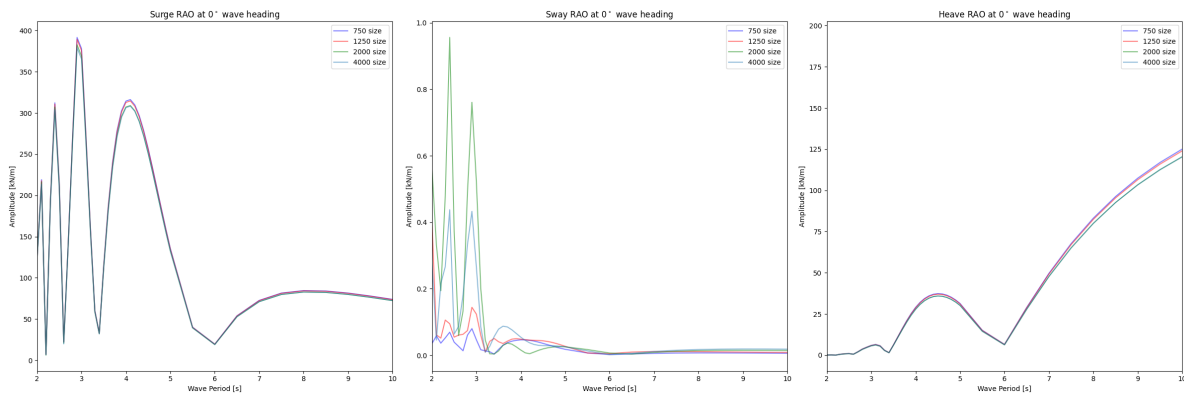


**Figure 6.3:** Convergence of RAOs at  $0^\circ$  wave heading

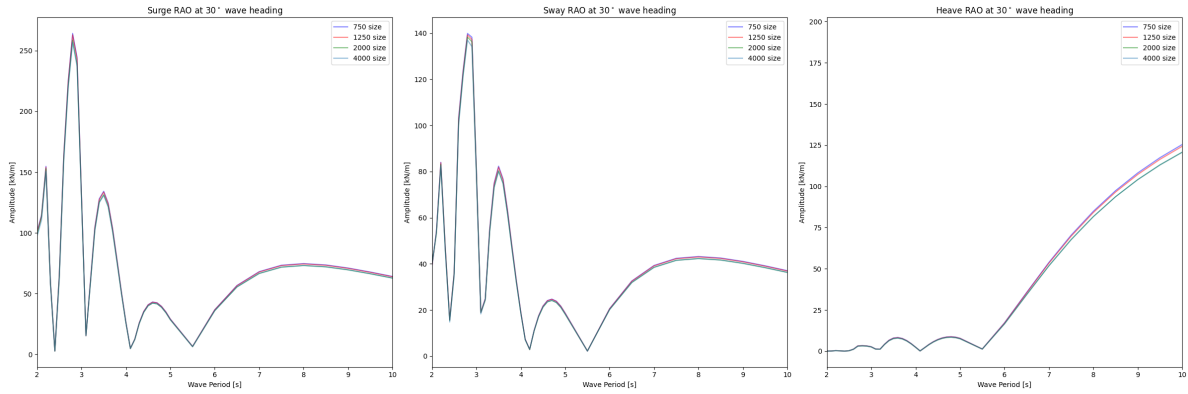


Figure 6.4: Convergence of RAOs at 30° wave heading

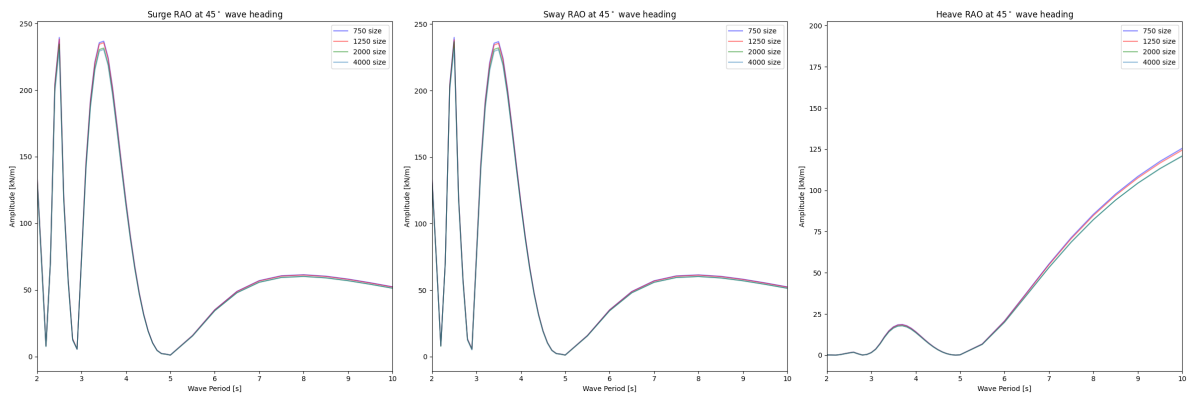


Figure 6.5: Convergence of RAOs at 45° wave heading

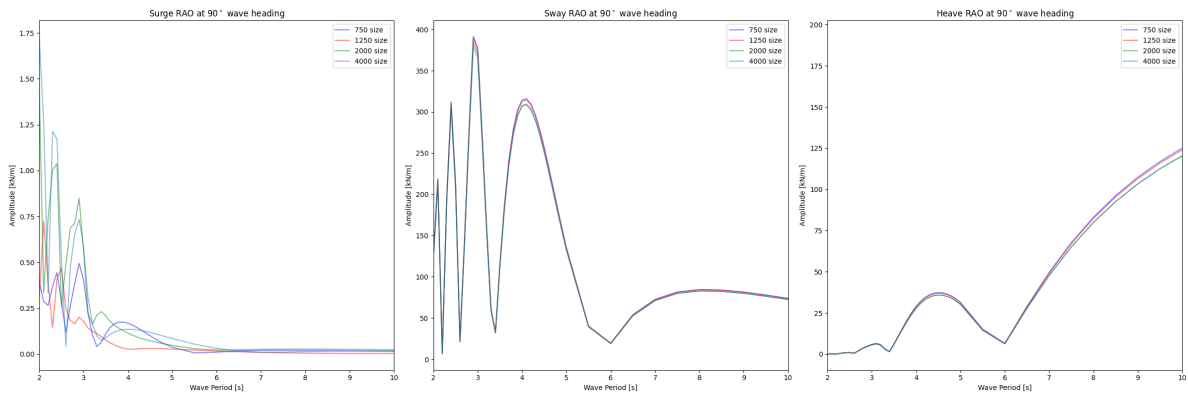
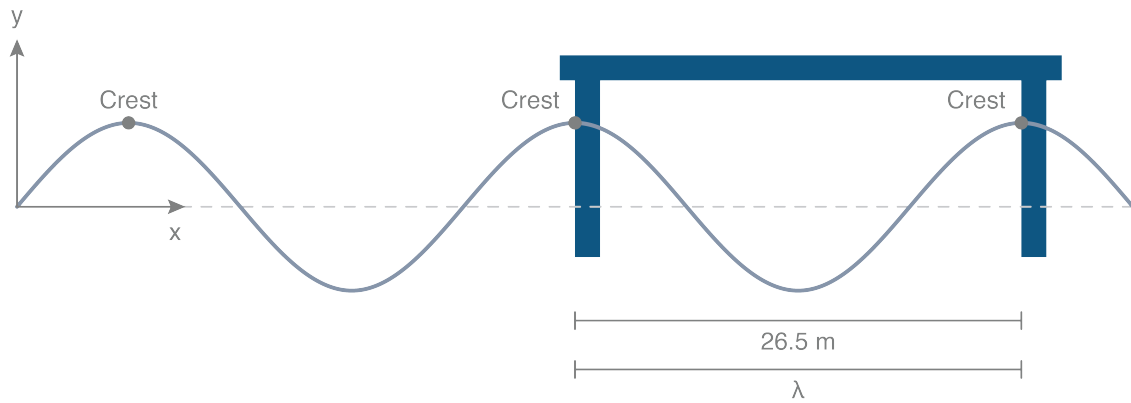


Figure 6.6: Convergence of RAOs at 90° wave heading

### 6.2.2. Interpretation of RAOs

The next step was to check whether the generated RAOs made sense. This was done by analyzing the peaks in the RAOs present. For this check, only the surge RAOs at 0° wave heading were considered. A maximum wave loading, and therefore a peak in an RAO, can be estimated by assuming that the maximum wave loading is reached when the wavelengths (or a fraction of these wavelengths) are equal to the front-to-front distance of the cylindrical columns of the solar structure. This is, in the case of a single solar floater, 26.5 metres. For example, the crest of a wave with a wavelength of 26.5 metres will hit the first column, while the second wave (26.5 metres further away) will hit the second column as well, inducing maximal loading on the structure. A visualisation is depicted in Figure 6.7:



**Figure 6.7:** Maximum wave loading occurring at the wavelength  $\lambda$  equal to distances of the columns

A visual representation of the geometries and the corresponding RAOs can be found in Figure 6.8-6.10. A table of the (fractioned) wavelengths and their corresponding wave periods can be found in Table 6.3-6.5. The highlighted wavelengths correspond to the original geometry of the floater, while the highlighted wave periods are corresponding to the peaks in the RAOs. For the configurations with multiple connected floaters, wave periods of the single floater are also taken as an explanation for the corresponding peaks in their RAOs.

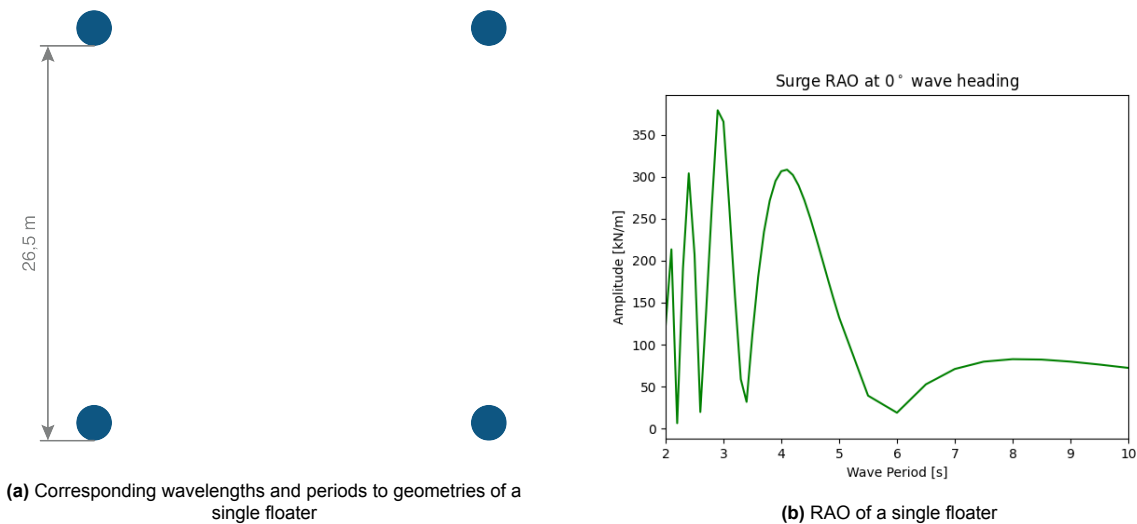


**Figure 6.8:** Geometry and RAO of a single floater

In the case of the single floater, multiple peaks are visible at wave periods equal to the fractions of the distances between the cylindrical columns. The largest peaks in the RAOs are therefore justified.

Fractions of wavelengths [m]	Wave period [s]
<b>26.50</b>	<b>4.12</b>
13.25	<b>2.91</b>
8.83	<b>2.38</b>
6.63	<b>2.06</b>

**Table 6.3:** Corresponding wavelengths and periods to geometries of a single floater

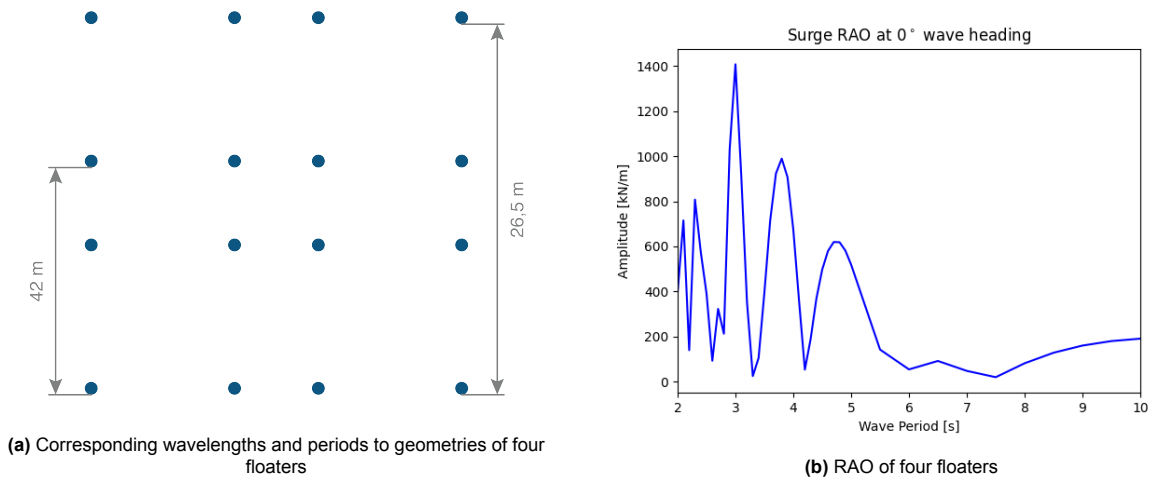


Figure 6.9: Geometry and RAO of the 4 floaters

In the case of 4 floaters coupled, the peaks visible in Figure 6.9 can also be explained by the corresponding geometries of the floaters. The same is true for the case of 16 floaters, which can be found below in Figure 6.10 and Table 6.5

Fractions of wavelengths [m]	Wave period [s]	Fractions of wavelengths [m]	Wave period [s]
42	5.19	68.50	6.62
21	3.67	34.25	4.68
14	2.99	22.83	3.82
10.5	2.59	17.13	3.31
8.4	2.32	13.7	2.96
7	2.12	11.42	2.70

Table 6.4: Corresponding wavelengths and periods to geometries of four floaters

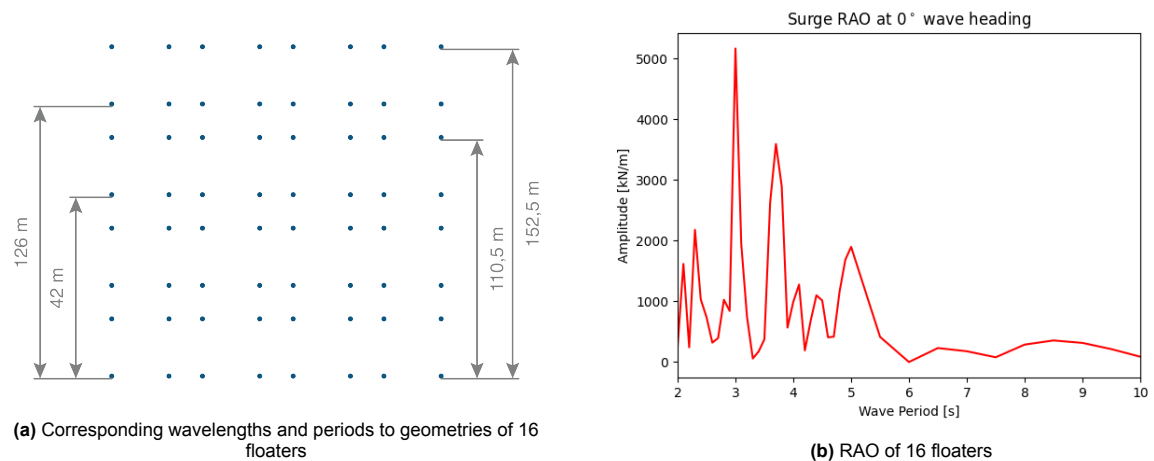


Figure 6.10: Geometry and RAO of the 16 floaters

Fractions of wave-lengths [m]	Wave period [s]	Fractions of wave-lengths	Wave period [s]	Fractions of wave-lengths [m]	Wave period [s]	Fractions of wave-lengths	Wave period [s]
<b>126</b>	8.98	<b>84</b>	7.33	<b>110.50</b>	8.41	<b>152.5</b>	9.88
63	6.35	42	5.19	55.25	5.95	76.25	6.99
42	5.19	28	4.23	36.83	4.86	50.83	5.71
31.5	4.49	21	<b>3.67</b>	27.63	4.21	38.13	<b>4.94</b>
25.2	4.02	16.8	3.28	22.10	<b>3.76</b>	30.5	<b>4.42</b>

**Table 6.5:** Corresponding wavelengths and periods to geometries of 16 floaters

From this sanity check can be concluded that the RAOs can be explained by looking at the geometries of the floaters. The RAOs can therefore be considered valid, and can be used for this thesis.

### 6.3. Comparison of the model to OrcaFlex

Before the model could be used for simulating the different configurations considered, it was first compared to OrcaFlex. First, the simple case of a single floating turbine moored to the seabed with two anchored lines (Line 1 and Line 2) is considered (reminiscent of Figure 5.3, but without the shared line). The second case considers two turbines with a shared line in between the turbines, where Line 1 is connected to floater 1 and Line 2 to floater 2.

The comparisons are considered with and without second-order wave drift to verify the implementation of this forcing. A  $0^\circ$  wave heading was considered. Therefore, only the surge direction is shown, as the sway directions were less relevant in this part of the research. Finally, considering irregular waving, one of the configurations defined in Chapter 4 was compared to OrcaFlex to assess the limitations of the final model.

1. Single floater only first-order wave loading
2. Single floater including 2nd order wave drift (QTFs)
3. Two wind turbines with only first-order wave loading
4. Two wind turbines including 2nd order wave drift
5. Assessment of limitations using irregular waving

As the introduction of wave drift did not produce any noticeable differences compared to the others, comparison 4 has been moved to Appendix A. For the linear waves, wave periods considered were in the range of 2 up to 50 seconds with a wave height of  $H = 3m$ . All regular wave cases consider the maximum and mean displacements and tensions of the turbines and their lines.

#### 6.3.1. Single floater, only first-order wave loading

For the single turbine, first, the wave loading is considered without wave drift to validate the implementation of the first-order wave loading.

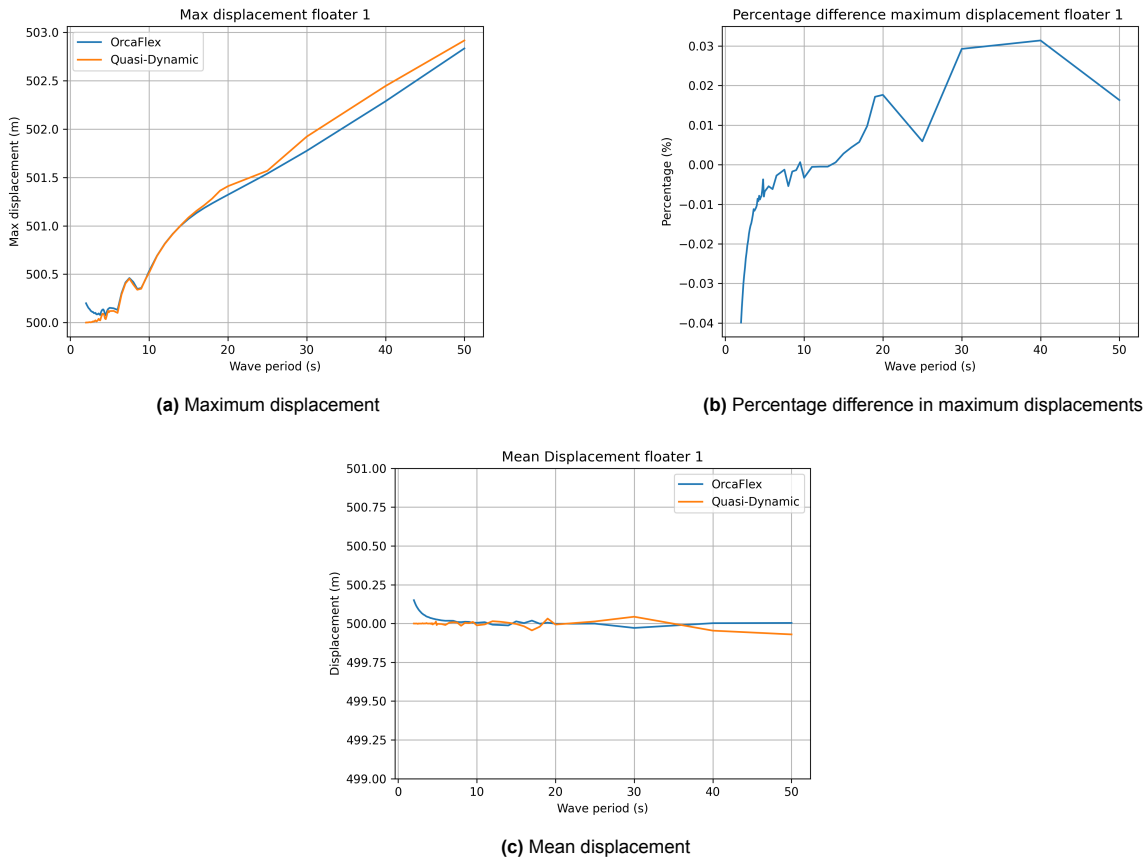


**Figure 6.11:** Displacements considering only first-order wave loading

As depicted in Figure 6.11, the maximum displacement differences are below 1%. Additionally, the mean displacements correspond quite well to the OrcaFlex results. In terms of tensions, which can be found in Figure 6.12, the maximum tensions do differ more. The maximum tensions are larger at resonance periods of the turbine, for example at the wave period of 7 seconds (where there is a peak in the RAO). This can be explained due to the implementation of the lines in the Quasi-dynamic model as opposed to the OrcaFlex model, as OrcaFlex takes into account line dynamics using its lumped mass method. This introduces extra dynamics in the tensions, and thus larger amplitudes.

Overall, the percentage difference of the maximum tensions is quite low (under 1%). The mean tensions are relatively similar as can be seen in the mean tension plot. This further confirms that the maxima differences are coming from the amplitudes instead of the means.

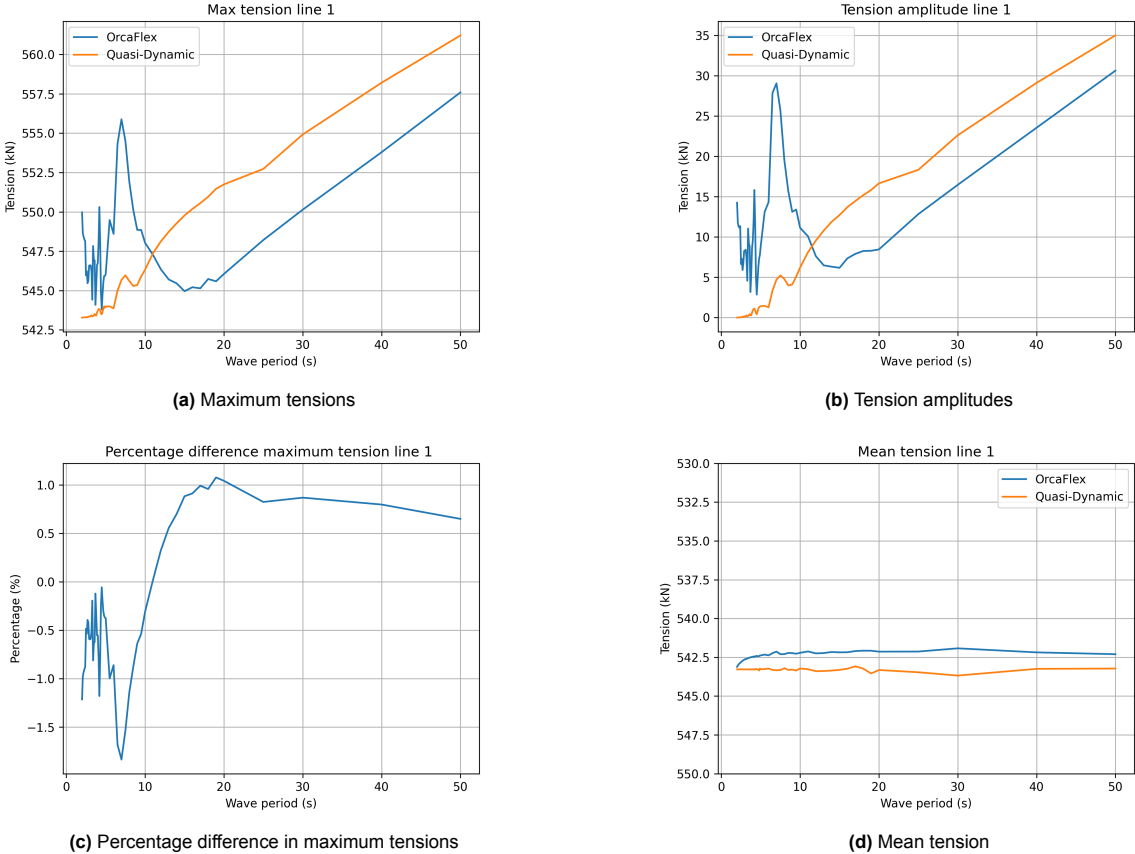
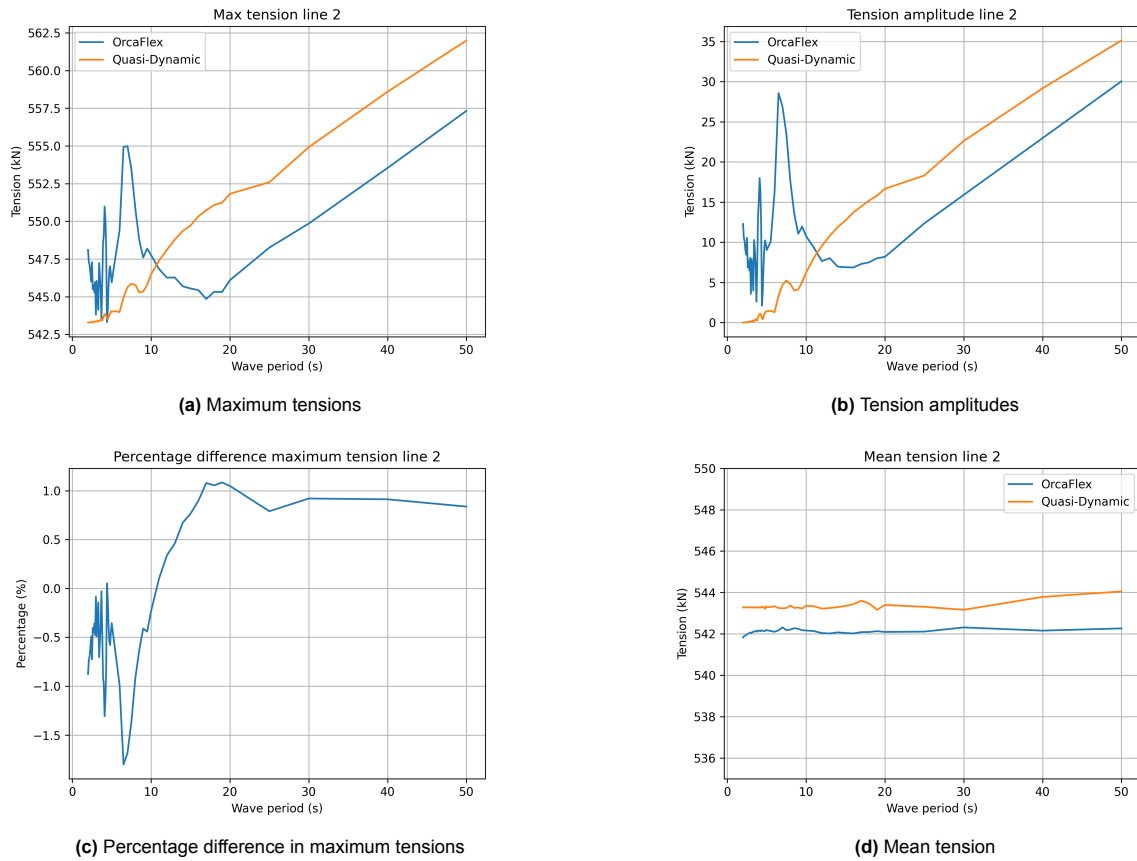


Figure 6.12: Line 1 tensions, considering only first-order wave loading

As for Line 2 (Figure 6.13), the same differences can be found in terms of maximum tensions.

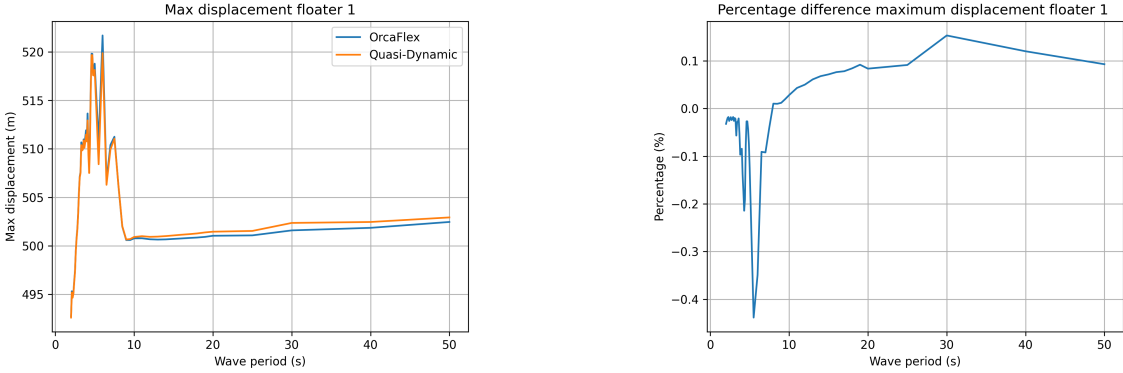


**Figure 6.13:** Line 2 tensions, considering only first-order wave loading

Overall, it can be concluded that the first-order wave loading and mooring line tensions for moored lines are implemented correctly, as the differences with OrcaFlex are negligible.

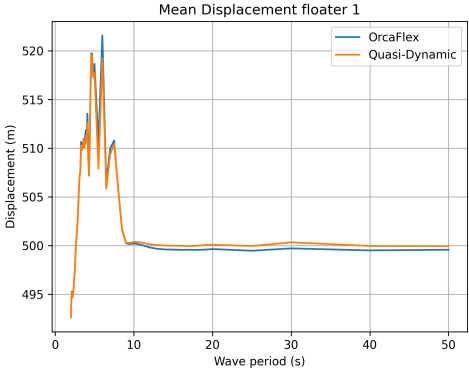
### 6.3.2. Single floater including wave drift

Considering next, the single floater including wave drift, the results can be found below in Figure 6.14- Figure 6.16.



(a) Maximum displacement

(b) Percentage difference in maximum displacements



(c) Mean displacement

Figure 6.14: Displacements including wave drift

As can be seen for the displacement, there is good agreement between the models. Only at a wave period of 7 seconds, the differences become larger, although negligible, which is again due to the larger response in first order wave loading present.

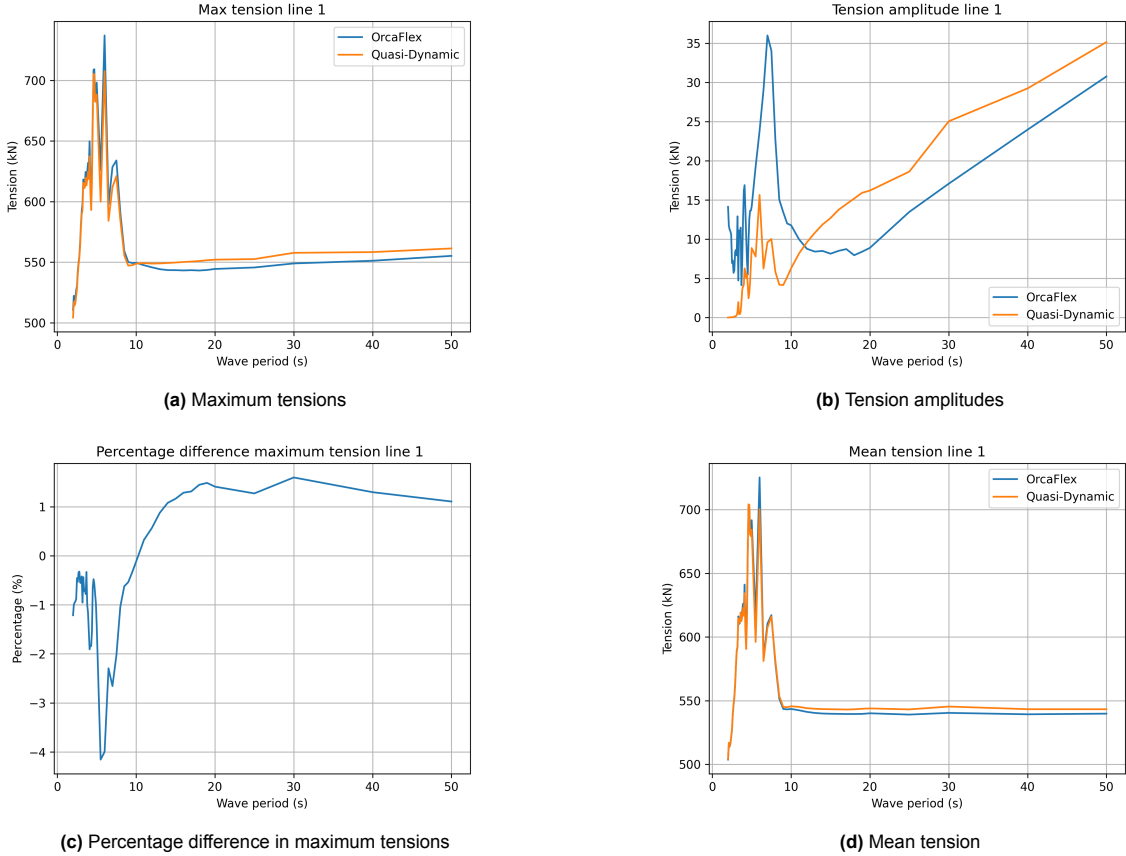


Figure 6.15: Line 1 tensions including wave drift

The differences in tension 1 are as well quite low, although the differences become larger with larger tensions, as the wave period of 7 seconds exhibits a difference of 4%. These are still quite low though and are deemed acceptable for the time being.

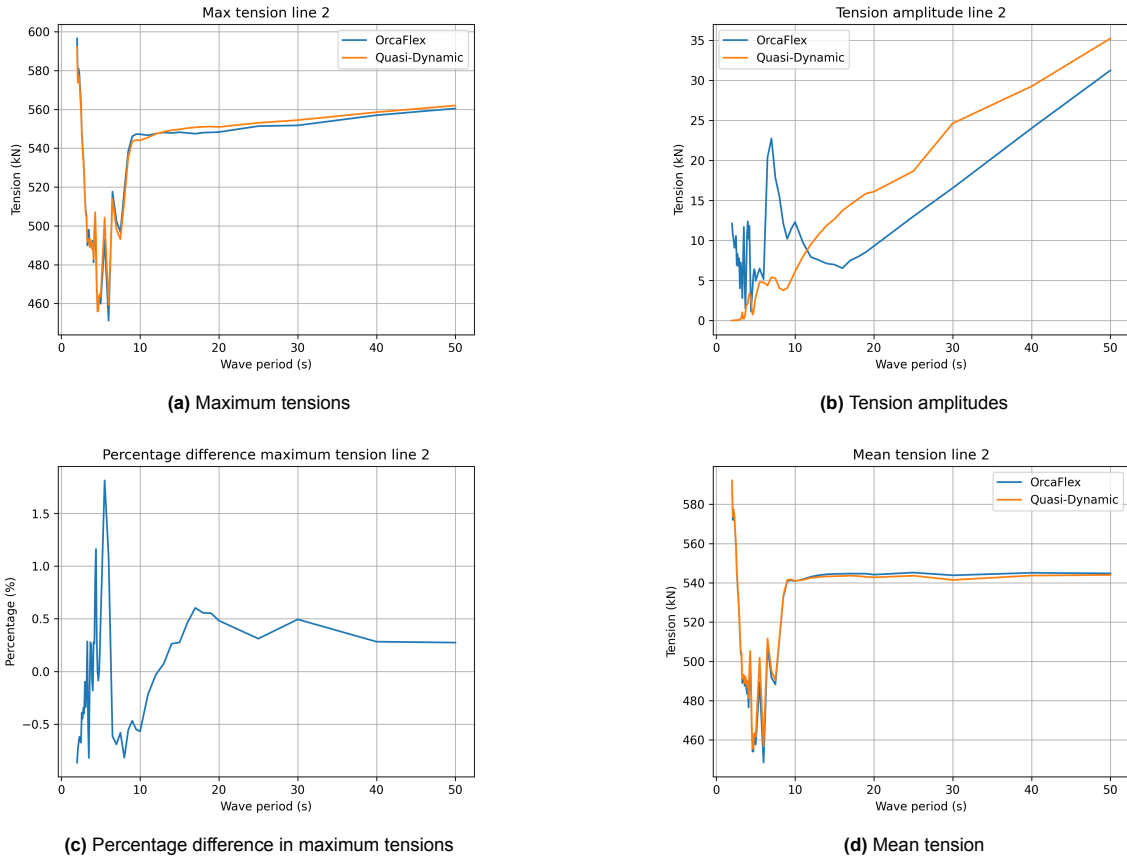


Figure 6.16: Line 2 tensions including wave drift

As for line 2, the differences between OrcaFlex and the Quasi-dynamic model are also under 2%. Again, these differences can be explained by the lack of the dynamics present in the Quasi-dynamic model.

### 6.3.3. Two floaters, first-order wave loading

For the case of two floaters with a shared line, the displacements and tensions of the lines can be found below. Overall, the Quasi-dynamic model is, just like the single floater, in agreement with the OrcaFlex results. The introduction of the shared line introduces the same dynamic discrepancies in terms of maximum tensions due to the static approach of the lines in the Quasi-dynamic approach. The tension plots of Line 1 and Line 2 can be found in Appendix A.

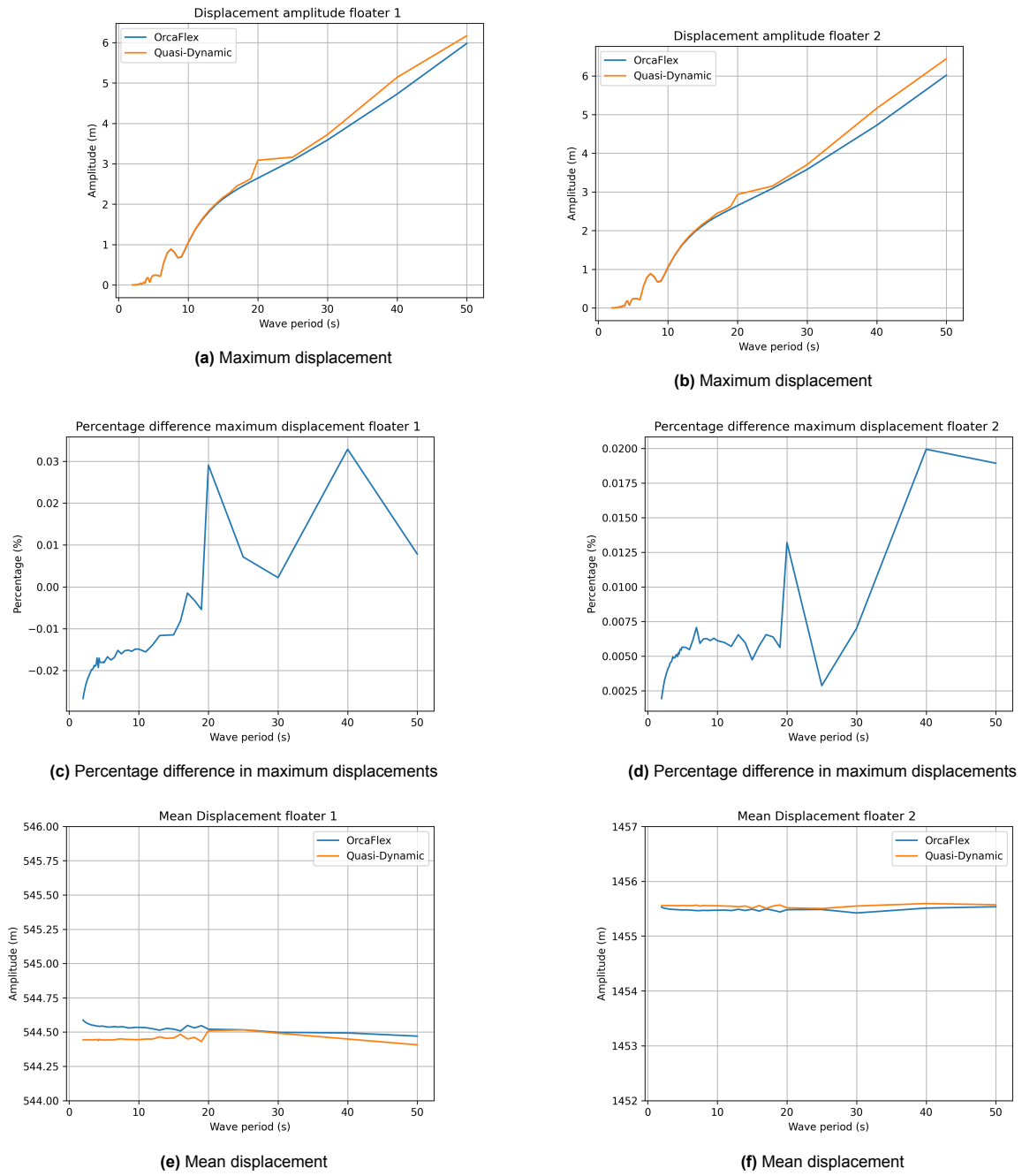


Figure 6.17: Displacements considering only first-order wave loading

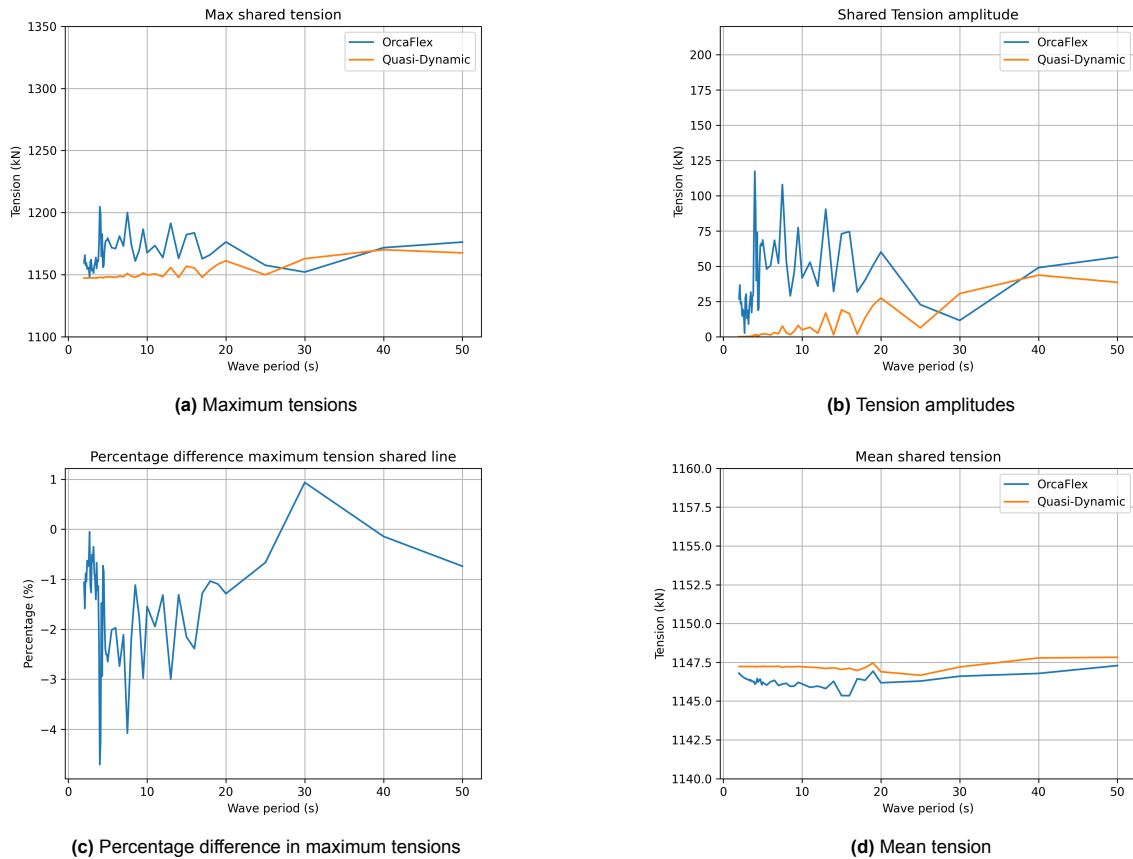


Figure 6.18: Shared line tensions, considering only first-order wave loading

## 6.4. JONSWAP spectrum

To check whether the JONSWAP spectrum was correctly modelled, two checks were done. First, the significant wave height, according to Holthuijsen [33], should be equal to:

$$H_s \cong 4 * \sqrt{m_0} \quad (6.1)$$

Where  $m_0$  is the 0th order spectral moment:

$$m_0 = \int_0^\infty f^0 E(f) df = \int_0^\infty E(f) df \quad (6.2)$$

Which is equal to the total energy of the spectrum contained in the discretized frequencies. This was done for a number of load cases, of which the results can be found below:

Sea state 1	Value	Unit	Sea state 2	Value	Unit	Sea state 3	Value	Unit
Hs	3	m	Hs	9	m	Hs	11	m
Tp	6	s	Tp	7	s	Tp	11	s
m_0	0.562	m	m_0	5.057	m	m_0	7.555	m
Hs_approx	2.999	m	Hs_approx	8.999	m	Hs_approx	10.999	m

Table 6.6: Energy checks of the JONSWAP spectrum

From Table 6.6, the approximate  $H_s$  from Equation 6.1 is in agreement with the original  $H_s$ . Additionally, visual checks on the time wave series were done for multiple sea states, at multiple positions, to see whether the elevations of the waves were correctly modeled. This visual check was possible due to the random phasings being seeded to always get the same time series from the wave spectrum. Below, an example of such a time series is shown in Figure 6.19.

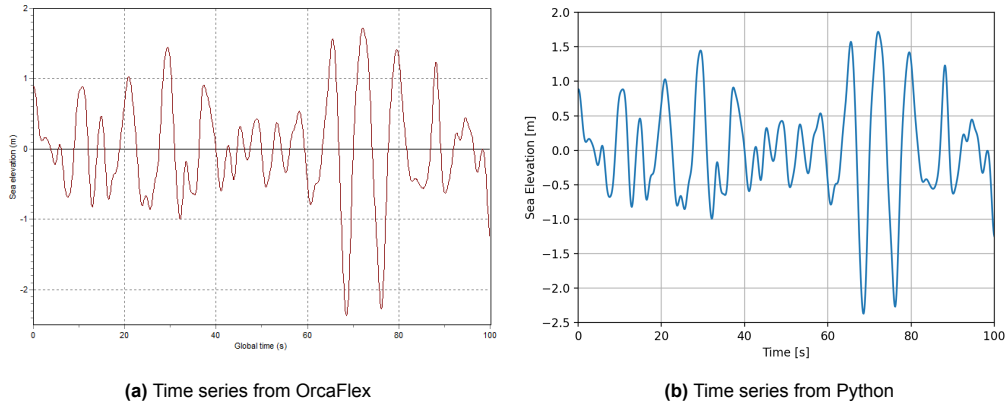


**Figure 6.19:** JONSWAP time series with  $H_s = 3$ ,  $T_p = 8$

From the energy check and visual check of the time-series, it was concluded that the JONSWAP spectrum was corecctly modelled.

## 6.5. Assessment of limitations

For this comparison, multiple simulations of configuration 1 (see Chapter 4) in OrcaFlex were performed. The goal was to determine what the impact on the dynamics would be due to the assumptions of the Quasi-dynamic model using an irregular wave spectrum, defined in Chapter 5. For this environmental loading, the extreme load case, as defined in Chapter 4 was used.

The introduction of irregular waving introduces low-frequency drift forces. Due to limitations in OrcaFlex, the assumption of the mean wave drift force, in comparison with the full QTF, could not be quantified in OrcaFlex itself. However, comparing the limited OrcaFlex simulations with Python would give an indication of the limitation of this assumption. The following constraints were applied to OrcaFlex for the comparison, of which an overview can be found in Table 6.7:

- Constrain all DOFs, except for surge and sway.
- Replace the frequency-dependent hydrodynamic coefficients with the constant added mass and damping values used in the Quasi-dynamic model.
- Simultaneously apply the aforementioned limitations to assess the impact of the slow-varying drift forces.

Description	Simulation
FD	Full Dynamic (FD)
DOF	DOFs constrained (DOF)
DOF+Const.	DOFs constrained +constant hydrodyn. terms (DOF+Const.)
QD	Quasi-dynamic model

**Table 6.7:** Limitations simulated for comparison

The values for the constant added mass and damping matrices were determined based on the frequency yielding the largest load RAO value. This frequency was anticipated to show the most significant responses. The values are provided in Table 6.8-6.9.

Added mass [kg]	Surge	Sway
Surge	13,677,635	0
Sway	0	12,774,446
Damping [kN/(m/s)]	Surge	Sway
Surge	3,814.707	0
Sway	0	3,814.707

Table 6.8: Added mass and damping of the turbine

Added mass [kg]	Surge	Sway
Surge	1,749,172	0
Sway	0	1,751,089
Damping [kN/(m/s)]	Surge	Sway
Surge	3,010.28	0
Sway	0	3,016.46

Table 6.9: Added mass and damping of the Solar array

Note that these values would change for different wave headings, as the values are based on the frequency to which the highest wave loading is coming from. For a different heading, these are expected to change, as different peaks will be present in these RAOs.

### Displacements

From the displacements found in Figure 6.20, it can be concluded that the DOF constraint does not influence the simulation a lot. The limitation of the constant damping and added mass seems to only have a large effect on the maxima, as the mean displacements change little. The Quasi-dynamic model is the least accurate in terms of both mean and maxima. For the mean displacements, this can be explained by the lack of slow varying drift forces, while in the maxima this is complemented by the limitation of constant hydrodynamic terms and the fact that the mooring lines are modelled using the analytic catenary equation.

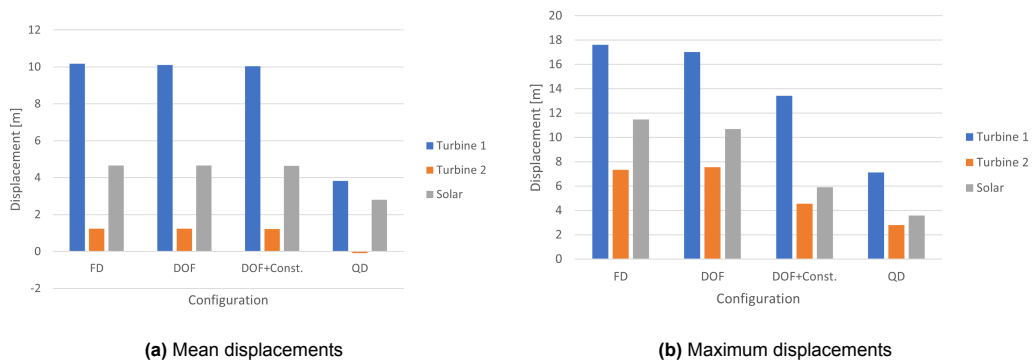


Figure 6.20: Mean and maximum displacements

### Anchored line tensions

In terms of anchor line tensions, the same conclusion can be made on the constrained DOF simulation. Constant damping and added mass however do not influence the anchored tensions a lot. The Quasi-dynamic model shows some interesting behaviour as the mean tensions of the down wave anchored lines are higher than the other simulations. This can be explained due to the different mean positions of the floaters compared to the OrcaFlex simulations, as the down wave anchors will have higher tensions due to the lines being pulled more taut.

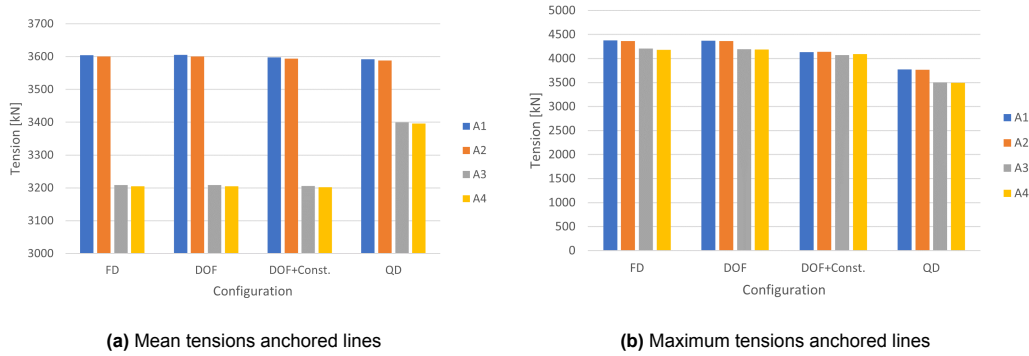


Figure 6.21: Mean and maximum tensions anchored lines

Description	A1		A2		A3		A4	
	Mean	Max	Mean	Max	Mean	Max	Mean	Max
FD	-	-	-	-	-	-	-	-
DOF	0%	0%	0%	0%	0%	0%	0%	0%
DOF+Const.	0%	-5%	0%	-5%	0%	-3%	0%	-2%
QD	0%	-14%	0%	-14%	6%	-17%	6%	-16%

Table 6.10: Percentage differences from full dynamic simulation

Shared line tensions

Regarding the shared line tensions, the mean tensions are reasonably well captured by the Quasi-dynamic model. The large differences become apparent in the maxima, as they are again largely underestimated compared to the OrcaFlex simulations.

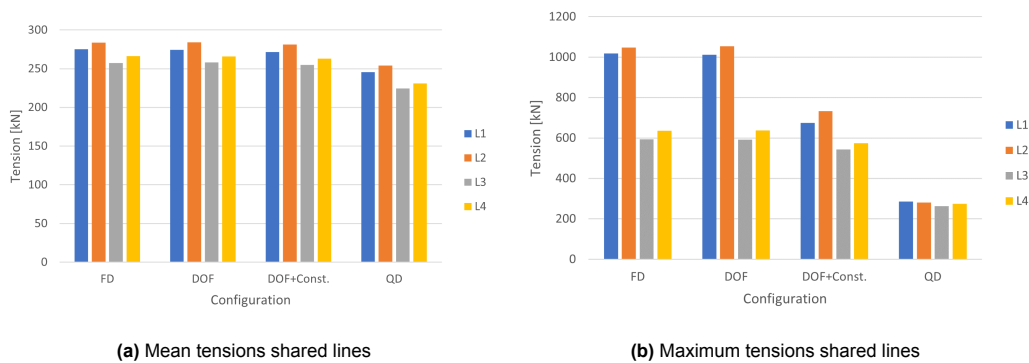


Figure 6.22: Mean and maximum tensions shared lines

Description	T1		L1		L2		L3		L4	
	Mean	Max								
FD	-	-	-	-	-	-	-	-	-	-
DOF	0%	0%	0%	-1%	0%	1%	0%	0%	0%	0%
DOF+Const.	0%	-2%	-1%	-34%	-1%	-30%	-1%	-8%	-1%	-10%
QD	-2%	-22%	-11%	-72%	-10%	-73%	-13%	-56%	-13%	-57%

Table 6.11: Percentage differences from full dynamic simulation

6.6. Conclusions

From the results above, it can be concluded that the Quasi-dynamic model cannot accurately depict the displacements and tensions present in the configurations considered. Based on the comparisons

above, it followed that the largest limitation of the model is the exclusion of the slow-varying drift force. This force contributes significantly to the overall dynamics in all other simulations, both in mean and maxima. Secondly, the utilization of constant hydrodynamic terms has an impact mainly on the maxima, which limits the model's capability of assessing accurate values even further. Thirdly, the fact that the mooring lines neglect the dynamics within the mooring lines limits the model even further. These three factors collectively lead to the observed inaccuracies in the model's predictions when compared to the results obtained from OrcaFlex simulations.

Although the model is not useable for in-depth analysis of the load cases, it can be used to identify critical cases early in the design process. The maximum tensions are not representative, but they do indicate which simulation has the higher tensions. The mean tensions in both the anchored and shared lines can be used as an estimate for the mean tensions, as they have a difference of 13% maximum (see Table 6.10 and Table 6.11). Additionally, the model does follow the trend of the tensions and displacements, indicating which tensions and displacements are the highest for each configuration.

# 7

## Results

This chapter presents the results obtained from the configurations described in Chapter 4, using OrcaFlex and the model described in Chapter 5. First, the static results are presented, stating the initial positions and tensions present in the configurations. Next, the different load cases introduced in Chapter 5 were executed on the configurations using the Quasi-Dynamic model. Since the model could only identify critical cases, these were simulated again in OrcaFlex to obtain the more realistic dynamics. The feasibility of these simulations was assessed using Key Performance Indicators (KPIs), after which the feasible configurations were compared to the base case of a single wind turbine. A full discussion of the results can be found in Chapter 8.

### 7.1. Key Performance Indicators

KPIs were specified to assess the performance of the configurations defined in Chapter 4. Two indicators were used to determine the feasibility of the configurations:

1. Maximum tensions of the lines are below the MBL in the extreme load case.
2. Maximum displacements of the floaters (in surge and sway) are below 25 metres in the operating load case, to accommodate for the limit of the bending radius of the electrical umbilical [25].

The indicators were sorted on importance; KPI 2 was only assessed if:

1. KPI 1 is fulfilled for all simulated wave headings of the configuration considered
2. Maximum displacements of the floaters surpass the 25-metre limit in the extreme load case. The operational load case displacements were found to be lower than the extreme load case (see the displacements from Appendix C). Therefore, the operational load case does not surpass the 25-metre limit if the extreme load case does not do so either.

The flow of the assessment of these KPIs is depicted in Figure 7.1:

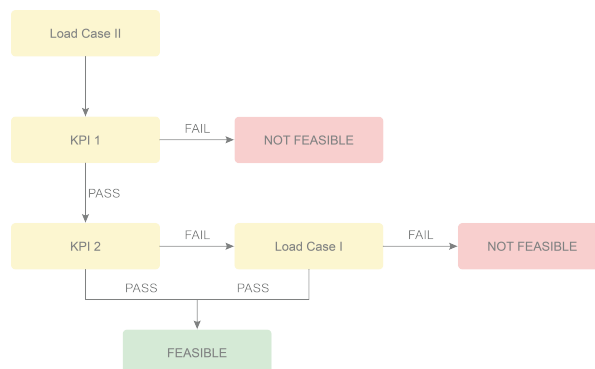


Figure 7.1: Workflow of the assessment of configurations

For KPI 1 to be satisfied across all LCs, The MBLs of the shared lines must remain within limits to consider a configuration feasible. The MBLs defined in Chapter 4 are factorized by safety factors taken from guideline NR493 from Bureau Veritas [3], which can be found in Table 7.1:

Line type	Quasi-Dynamic	Full Dynamic
Line type I	2.2	2.1
Line type II	1.75	1.67

**Table 7.1:** Safety factors defined by Bureau Veritas [3]

Line type I represents lines of systems that are in proximity to other structures and Line type II refers to lines that are far from other structures. As the considered structures are relatively close to one another, Line type I is selected as the safety factor (2.1). The results in the remainder of this chapter are based on the factorized MBL:

$$MBL > SF \cdot T_{max} \quad (7.1)$$

Where  $SF$  is the safety factor and  $T_{max}$  represents the maximum tension in the mooring line considered.

### 7.1.1. Conventions

Before elaborating on the results, some conventions are defined to clarify the obtained results, both in this chapter as in the appendices. For each configuration, the first two floaters (Floater 1 and Floater 2) represent the two wind turbines in each configuration. The solar floaters in between these floaters are referred to as Floater 3, and so on. The fairlead (FL) positions and the lines attached are arranged as shown in Figure 7.2. The lines attached to the fairlead points are numbered from top to bottom, from left to right.

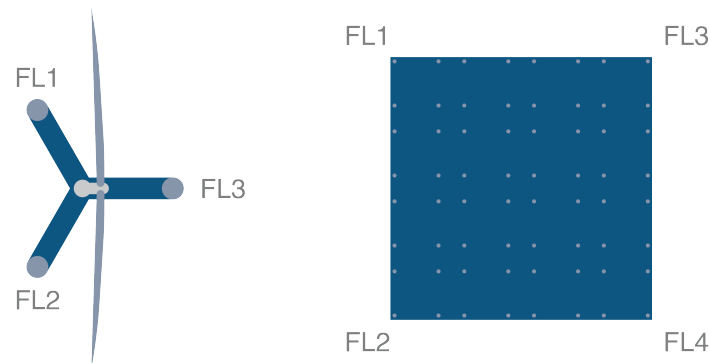


**Figure 7.2:** Conventions used for fairlead positions

## 7.2. Static results

In order to acquire the correct pretensions and initial positions used for the offset calculations, statics were determined by applying no environmental load in the model, resulting in only the restoring forces of the mooring lines applied to the structures. The pretensions of the shared lines were set to be between 10 and 20% of the MBL limit by scaling the line lengths accordingly [42]. The MBLs used can be found in Chapter 4. The lengths, material, and anchor positions of the turbine remained unchanged throughout the analysis. Results of the static analysis, including floater positions and tensions of the mooring lines, can be found in Appendix B. For each configuration, the following line lengths were determined to acquire the required pretension in each line:

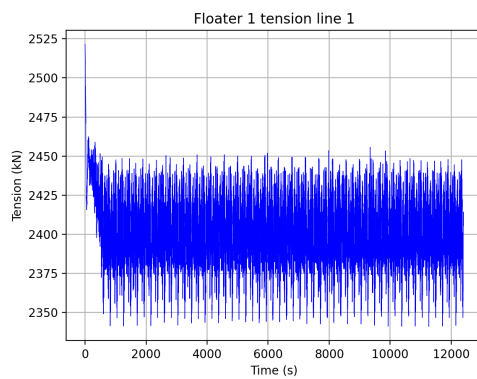
Line lengths	Line type				
	Chain	Rope	Wire	Turbine	Units
Configuration 1	410	390	398	1,020	m
Configuration 2.1	890	800	820	-	m
Configuration 2.2	530	485	498	-	m
Configuration 2.3	348	330	335	-	m
Configuration 2.4	245	237	240	-	m
Configuration 2.5	180	173	176	-	m

Table 7.2: Lengths of the shared mooring lines for each configuration

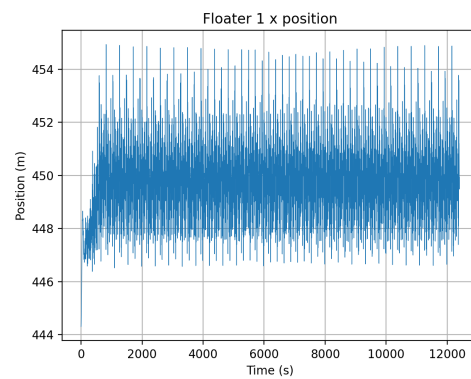
## 7.3. Dynamic Results

### 7.3.1. Simulation parameters

To acquire sufficient data to be statistically certain of acquiring the maximum wave height in the time series, a three-hour sea state is considered to be the standard time period. This allows for approximately 1000 wave cycles to be loaded onto a structure. In order to obtain the dynamics results, the Quasi-dynamic model was used to simulate time series of 14800 seconds, allowing for a 600 seconds wave buildup period and a 3400-second timeframe for transient behaviour to be negligible. The last 10800 seconds (3 hours) were taken to be the steady-state time series used for analysis. An example of a full-time series can be found below:



(a) Example of a time series of tensions in a line



(b) Example of a time series of the position of a floater

Each configuration was executed using two load cases for five wave headings and three mooring line types, as defined in Chapter 4 and 5. The environmental conditions  $H_s = 4$ ,  $T_p = 7$  and  $H_s = 11$ ,  $T_p = 11$  are referred to as Load Case 1 and Load Case 2 respectively. An overview of the conditions simulated is shown in Table 7.3:

Condition	Linetype	Hs	Tp	Heading	Condition	Linetype	Hs	Tp	Heading
0	Chain	11	11	0°	15	Rope	4	7	0°
1	Chain	11	11	15°	16	Rope	4	7	15°
2	Chain	11	11	30°	17	Rope	4	7	30°
3	Chain	11	11	45°	18	Rope	4	7	45°
4	Chain	11	11	90°	19	Rope	4	7	90°
5	Chain	4	7	0°	20	Wire	11	11	0°
6	Chain	4	7	15°	21	Wire	11	11	15°
7	Chain	4	7	30°	22	Wire	11	11	30°
8	Chain	4	7	45°	23	Wire	11	11	45°
9	Chain	4	7	90°	24	Wire	11	11	90°
10	Chain	11	11	0°	25	Wire	4	7	0°
11	Chain	11	11	15°	26	Wire	4	7	15°
12	Chain	11	11	30°	27	Wire	4	7	30°
13	Chain	11	11	45°	28	Wire	4	7	45°
14	Chain	11	11	90°	29	Wire	4	7	90°

Table 7.3: Overview of simulations run for each configuration

## 7.4. Identification of critical cases (Quasi-dynamic Model)

As was concluded from the assessment of the limitations of the model in Chapter 6, the Quasi-dynamic model can not be used to accurately depict the dynamics of the system. It can, however, be used to identify the critical cases in the simulations defined in Table 7.3. As the critical loads were present in the shared lines, the anchored line results are disregarded in this section. In order to show the relative differences between wave headings for Load Case 2, the tensions are normalised to the maximum tension found in all lines in the simulation (Figure 7.4-7.5). The full results of each configuration can be found in Appendix C.

The Load Case 2 results of the Quasi-dynamic simulations showed that the 0°, 30° and 90° wave headings were the critical cases. In terms of tensions, critical cases were found in the 0° and 30° wave headings. In terms of displacements, the 90° heading was most crucial. An explanation for this can be found in Chapter 8. OrcaFlex was used to simulate these specific wave headings, using the more accurate full dynamic approach.

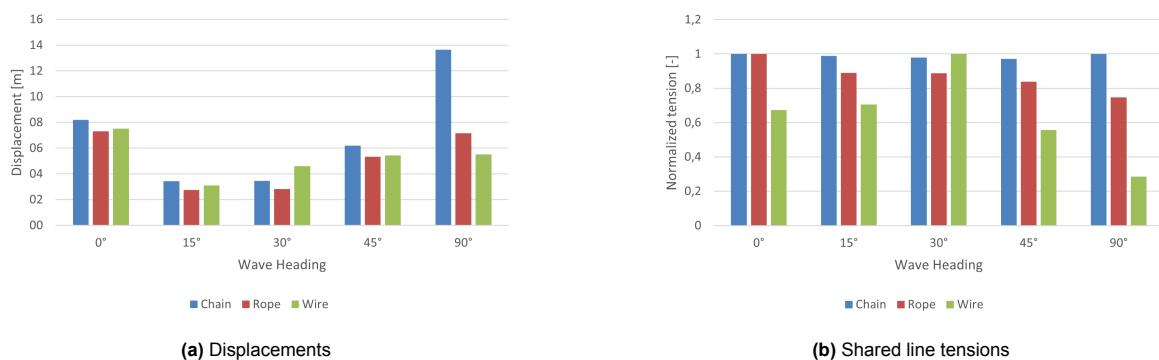


Figure 7.4: Displacements and tensions configuration 1

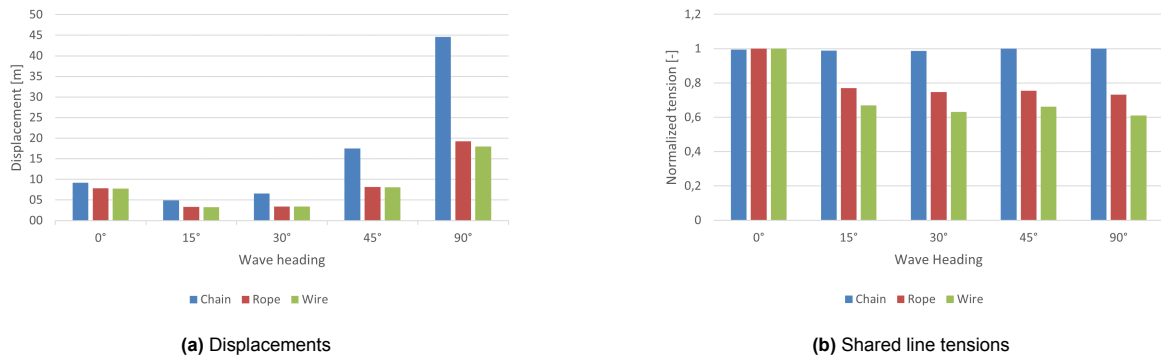


Figure 7.5: Displacements and tensions configuration 2.1

## 7.5. Evaluating the critical cases (OrcaFlex)

The critical cases defined above were simulated again in OrcaFlex to get a more accurate depiction of the dynamics present in the system. For these results, again, only the shared line tensions (utilizations) and displacements of the floaters are given. Total utilization of the tension is based on the ratio of the tension compared to the factorized MBL. From configuration 2.1 onwards, the wire line and chain type simulations are disregarded, as the polyester line showed preferable characteristics. An explanation for this can be found below in subsection 7.5.1.

### 7.5.1. Configuration 1

Regarding configuration 1, both 30° and 0° cases were found to have line failures due to the exceeding of the (factorized) MBL. For demonstrative purposes, the 0° results in Table D.4 are shown below. It was also observed that the 0° wave heading holds the higher tensions. This can be explained by the fact that at 0° wave heading, the displacements act more directly in line with the shared lines. The lines exhibit higher peak loads, due to the higher stiffness in this direction in terms of shared and anchored lines. The 30° and 90° wave heading results can be found in Appendix D.

	Linetype	Mean [kN]	Utilization	Max [kN]	Utilization
<b>T1</b>	Catenary	2,456	46%	3,149	59%
	Rope	2,300	43%	3,078	57%
	Wire	2,163	40%	2,989	<b>56%</b>
<b>L1</b>	Catenary	275	31%	1,018	<b>113%</b>
	Rope	513	28%	1,081	<b>59%</b>
	Wire	720	37%	5,583	<b>289%</b>
<b>L2</b>	Catenary	284	32%	1,048	<b>117%</b>
	Rope	524	29%	1,089	<b>59%</b>
	Wire	712	37%	5,368	<b>278%</b>
<b>L3</b>	Catenary	258	29%	593	66%
	Rope	495	27%	1,090	<b>59%</b>
	Wire	701	36%	5,116	<b>265%</b>
<b>L4</b>	Catenary	266	30%	636	71%
	Rope	506	28%	1,096	<b>60%</b>
	Wire	693	36%	4,978	<b>258%</b>

Table 7.4: Shared line tensions at 0° wave heading

### Polyester line

The results of configuration 1 of the Quasi-dynamic model showed that the polyester line type was found to be preferable in terms of dynamic characteristics, as both maximum displacements and tensions were kept within limits more, as opposed to using chain or wire. It displayed the lowest average maximum tensions while also having reasonable stationkeeping abilities, as can be found in Table D.1. The favourable characteristics of the polyester line can be explained by the fact that the chain and wire

line have higher axial stiffness (see Chapter 4), which results in larger (peak) tensions when pulled more taut, as the elasticity then becomes a more significant part of the restoring force. This can be seen in Equation 3.3 and Equation 3.4 from Chapter 3. With larger horizontal forcing, the elastic (left) part of the catenary equation will take over the equation as it will be significantly larger than the parabolic (right) part.

	Linetype	Surge		Sway	
		Mean [m]	Max [m]	Mean [m]	Max [m]
Turbine 1	Catenary	3.73	10.73	-0.02	-0.06
	Rope	3.25	12.75	-0.01	-0.06
	Wire	6.21	19.82	0.01	5.15
Turbine 2	Catenary	4.20	10.47	-0.02	-0.09
	Rope	3.74	10.95	-0.02	-0.07
	Wire	0.16	11.29	-0.06	6.66
Solar	Catenary	4.60	10.60	-1.39	-2.70
	Rope	3.60	10.10	-0.50	-0.13
	Wire	3.16	17.78	-3.33	32.80

Table 7.5: Displacements configuration 1, 0° heading

### 7.5.2. Configuration 2.1-2.5

As was stated earlier, only the polyester line type was further explored in the process. For this section, only the lines with the highest tensions were chosen to give a clear overview of the KPI checks. As an example, one of the tables used for the assessment of the configurations is shown below, where the utilisation and displacement checks are based on the maximum values in the tables:

Heading	Shared Line	Mean [kN]	Max [kN]	Utilisation [kN]
0	T1	2300	3078	0.57
	L1	513	1081	0.59
	L2	524	1089	0.59
	L3	494	1090	0.59
	L4	506	1096	0.6
30	T1	2298	2727	0.51
	L1	522	990	0.54
	L2	506	981	0.53
	L3	498	1015	0.55
	L4	483	1036	0.56
90	T1	2331	2418	0.45
	L1	549	748	0.41
	L2	455	611	0.33
	L3	531	716	0.39
	L4	435	626	0.34

Figure 7.6: KPI 1 check of configuration 1

Heading	Floater	Mean Surge [m]	Max Surge [m]	Mean Sway [m]	Max Sway [m]	Surge check	Sway check
0	Turbine1	3.2	12.7	-0.02	0.03	0.51	0
	Turbine2	3.69	10.9	-0.02	0.03	0.44	0
	Solar1	3.65	10.1	-0.52	-0.13	0.4	-0.01
30	Turbine1	2.5	10.33	0.71	2.47	0.41	0.1
	Turbine2	2.63	9.01	0.51	1.65	0.36	0.07
	Solar1	2.79	6.13	1.5	4.89	0.25	0.2
90	Turbine1	0.4	1.42	1.5	6.75	0.06	0.27
	Turbine2	0.11	1.05	1.54	6.87	0.04	0.27
	Solar1	0.46	1.29	5.51	15.11	0.05	0.6

Figure 7.7: KPI 2 check of configuration 1

## 7.6. Feasibility of the configurations

KPI 1 was assessed first in order to reach a configuration with a feasible mooring system. Each configuration was evaluated on its maximum tension of all shared lines for the wave directions considered:

Configuration	KPI 1	Heading	MBL	KPI 2	Heading	Max displ. [m]
1	PASS	0	60%	PASS	90	15.11
2.1	PASS	0	38%	FAIL	90	26.68
2.2	PASS	0	46%	FAIL	90	29.48
2.3	PASS	0	92%	FAIL	90	45.64
2.4	FAIL	0	125%	FAIL	90	44.05
2.5	FAIL	0	216%	FAIL	90	46.34

Table 7.6: KPI check

From the OrcaFlex results, of which the full results can be found in Appendix D, configurations 2.4 and 2.5 failed KPI 1. Therefore, it was concluded that these configurations are not feasible. Configurations 2.1-2.3 did not meet KPI 2; these simulations were re-evaluated for the operational load case.

### 7.6.1. Re-evaluation of KPI 2

The configurations which did not pass KPI 2 (see Table 7.6) for the extreme load case were re-evaluated using the results of the operational load case. From Table 7.7 it was found that the re-evaluated configurations had a maximum displacement below 25 metres in this load case (see Table 7.7 ).

Configuration	KPI 2	Max displ. [m]
2.1	PASS	9.94
2.2	PASS	10.43
2.3	PASS	16.48

Table 7.7: Re-evaluation of KPI 2

Concluding, only configurations 2.4 and 2.5 resulted in the failure of mooring lines. These configurations were therefore excluded from the comparison with the base case of a single turbine.

## 7.7. Comparison with the base case

The configurations which met the KPIs were compared to the single turbine base case to assess the behaviour in terms of displacements and anchor tensions. The turbine with the largest anchored tensions, the upwave turbine, was used for this comparison. Only the displacements of the turbine and the tensions of the anchored lines are compared, as the single turbine does not have any shared lines. The full results can be found in Appendix E. The maximum displacements of the upwave turbine can be found in Figure 7.8.

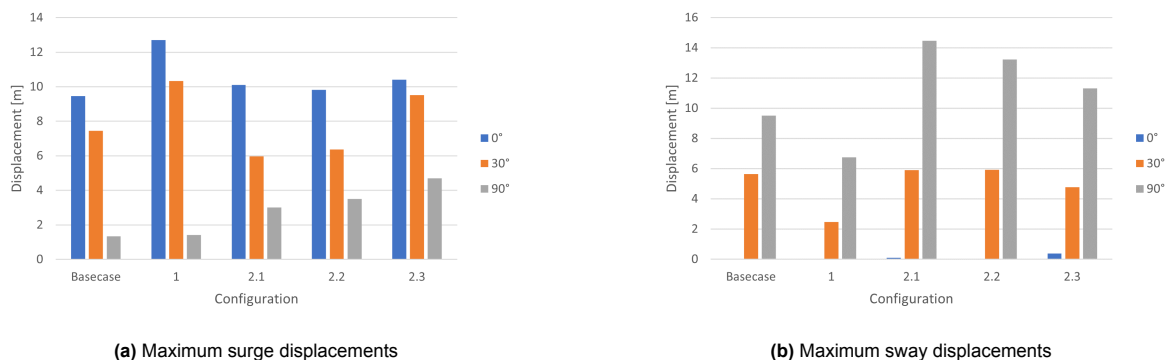
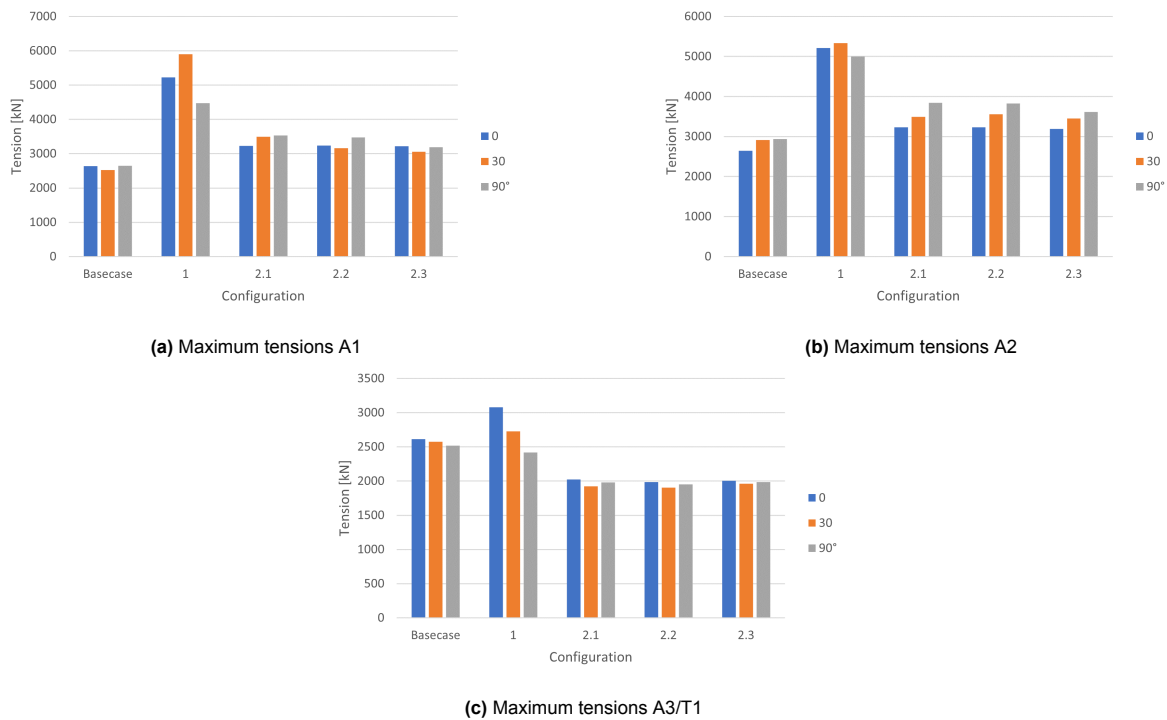


Figure 7.8: Maximum displacements compared to basecase

These results show a clear increase in displacements in terms of surge displacements for the  $0^\circ$  and  $90^\circ$  wave heading. However, for the  $30^\circ$  wave heading, an improved stationkeeping capability can be found in the case of configurations 2.1 and 2.2. The largest differences can be found in configuration 1, which is to be expected, as this configuration has two fewer anchored lines than the other configurations, which mainly provide stiffness in the surge direction.

In terms of sway, configuration 1 performs better in terms of maxima compared to the base case. This can be explained by the overall higher tensions (see Figure 7.9) in the anchored mooring lines, due to the static state of this configuration being different. The higher tensions facilitate the higher stiffness in its mooring stiffness in the sway direction. Regarding the other configurations, the decrease in mooring stiffness in this direction is clearly visible, as in the  $90^\circ$  wave heading, the offsets increase with a minimum of 20%, increasing up to 50%. The maximum sway displacements in configuration 2.2 and 2.3 are however lower than configuration 2.1. This can be explained by the fact that these systems have an overall higher utilisation of the shared lines, increasing the overall mooring stiffness of the solar arrays. This in term brings about less displacement in the turbine.

Figure 7.9 shows the maximum anchored line tensions of turbine 1. In the case of configuration 1, which does not have a third anchored line, the shared line between the two turbines is displayed instead.



**Figure 7.9:** Maximum displacements compared to basecase

Regarding the tensions above, the replacement of the anchored line with a direct shared line in configuration 1 induces larger tensions in the whole system, by up to 134% in the  $30^\circ$  wave heading for Anchor 1. This is due to the fact that this shared line pulls the turbines more towards each other, lifting more anchored line from the seabed. The larger tensions, however, only induce a larger mooring stiffness in the sway direction, as was found in Figure 7.8. Although the MBLs were not reached in this configuration, this does mean that optimisation can be done to a lesser extent than the other configurations which have lower tensions. Regarding the rest of the configurations, the largest differences in anchor tensions are shown below:

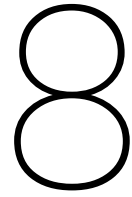
Configuration	A1	A2	A3
1	134%	97%	18%
2.1	39%	31%	-25%
2.2	31%	30%	-26%
2.3	22%	23%	-24%

**Table 7.8:** Largest percentage differences in tensions

From the results of Table 7.8 it can be found that the introduction of one solar array increases the maximum tensions by around 30%. However, adding more than one solar array does not lead to a significant increase in anchored lines. In the  $90^\circ$  wave heading, a decreased opposed to configuration 2.1 and 2.2 is even noted. An explanation for this can be found in Chapter 8.

Looking at the utilization of the tensions of the shared lines (see Table 7.6, these loadings are transferred more towards the shared lines of the system once more solar structures are introduced.

This indicates that the number of solar arrays should be taken into account in the case of an optimization study. The results show that in regard to the utilisation of the lines, configuration 2.3 seems to be the preferred setup, as the shared lines approach their maximum utilisation in the extreme load case while the displacements remained under 25 metres. Additionally, the anchor loads of Anchor 1 and 2 increased the least compared to the other configurations, while Anchor 3 has comparative load reductions. An extensive discussion can be found in Chapter 8.



## Discussion

This chapter provides an evaluation and reflection of the results presented in Chapter 7. Additionally, the limitations of this research are discussed. The results in section 7.6 show that a shared mooring system for a combined renewable array is feasible, as four out of six configurations met the criteria for both the MBL and the displacement assessment defined in section 7.1.

From Chapter 6 it was concluded that the Quasi-dynamic model built in Python could not accurately depict the dynamics present in the systems considered. It was, however, possible to identify the critical cases of the simulations. The identification was used to save computational effort in Orcaflex by disregarding less critical cases. The use of the Quasi-dynamic model resulted in 40% of the simulations being disregarded for the Orcaflex dynamics. In terms of tensions, the  $0^\circ$  and  $30^\circ$  wave heading were identified as critical, as identified in section 7.4. This can be explained by the fact that in the  $0^\circ$  heading, the highest mooring stiffness can be found due to the alignment of the lines and anchors in each configuration. The  $30^\circ$  wave heading also provides a higher mooring stiffness due to the angled alignment of the anchored lines in the configurations relative to other directions. The  $90^\circ$  wave heading was the critical case in terms of displacements, which can be explained by the fact that it provides the lowest mooring stiffness in that direction, counteracting the environmental forces the least. As can be seen from the configurations in section 4.3, no lines are aligned in the sway direction, apart from the anchored lines which provide sway mooring stiffness at an angle of  $60^\circ$ .

Looking at the results from section 7.7, configuration 2.3 was favourable when compared to the anchored line tensions of the base case. The anchored line tensions increased the least of all configurations, by a maximum of 23%, as opposed to the 97%, 31% and 30% in the other shared mooring configurations (Table 7.8). Additionally, the displacements of the floaters stayed within the electrical umbilical limit of 25 metres. The initial increase in anchored line tension when adding a single solar array can be explained by the mean forcing of the shared lines, which stay constant over the addition of more solar arrays (see Appendix D). The fact that the anchored line tensions do not increase after one solar array can be explained by the fact that the dynamic (maximum) shared line tensions connected to the turbines are far out of the eigenfrequency region of the turbines' load response, due to its inertia. The investigation of this phenomenon could be a topic for further research.

An important finding within the results is that the introduction of additional solar arrays next to the one in configuration 2.1 does not appear further to increase the overall anchored line tensions of the turbine. On the contrary, as more solar panels are introduced, tensions can even decrease, as can be seen from Figure 7.9. This phenomenon could be used as an advantage in choosing configurations and in optimisation studies.

When evaluating the shared line utilisations, configuration 2.1 displayed lower tensions, with the highest tension only reaching 38% of its MBL, compared to the 60%, 46% and 92% utilisations of configurations 1, 2.2 and 2.3, respectively. An optimisation of the mooring line dimensions could lead to cost reductions, potentially making this configuration more favourable.

Although the anchored tensions of configurations with more than three solar arrays were found to be within limits, the shared tension limits were exceeded. The exceeding of the limits is due to the cumulative loads on the lines due to the addition of these structures, as effectively each array adds to the drag and inertia forces. Increasing the number of solar arrays results in higher (peak) loads on these shared lines. Considering other line materials could make configurations with more solar arrays feasible, however, this was left out of scope.

Of particular interest is that for both load cases 1 and 2, the maximum displacement difference between configurations 2.1 and 2.2 is not significantly large. Larger displacements appear only when a solar array is solely connected to adjacent solar arrays, which is the case for configuration 2.3-2.5. This could be explained by the fact that more DOFs lead to a lower overall mooring stiffness in the system. This leads to the conclusion that structures that are more indirectly moored to a conventionally (anchored) moored structure perform larger displacements. This conclusion is also supported by Zhang and Liu [49], who observed "Accumulating displacement" in their shared mooring system.

Compared to the base case, the anchor tensions in configuration 1 significantly increase, as the turbine's mooring system itself is less stiff due to two anchored lines missing (Anchors 3 and 4). This in turn increases the displacements of the floaters and the tensions in the other anchored lines. Nevertheless, this configuration remains feasible, as the dynamics stay within their limits.

## 8.1. Limitations of the research

Although the results of this research indicate that a shared mooring system can be a promising innovation, the following limitations of this research should be taken into consideration.

### 8.1.1. Case study

#### Configurations

Regarding the studied configurations, configuration 1 consists of two turbines separated by a distance of 1000 metres (four rotor diameters), while in practice, distances of turbines range between eight to ten rotor diameters. This scenario would therefore probably not be feasible in practice. This configuration would be more realistic when selecting a smaller turbine, such as the OC4 5MW turbine with a rotor diameter of 128 meters as used by [37]. This would, however, introduce different dynamics due to the smaller size of the turbine platform.

For this study, six configurations were analysed for multiple environmental conditions. Although the results have already brought insights into the behaviour of shared mooring systems applied in some configurations, it does not fully answer the main research question. Additional configurations were identified but were not evaluated to stay within the scope of the project in terms of time management. One of these configurations was an extension of configuration 2 and combined multiple arrays into a square array, with varying solar floaters in between turbines. An example of this can be found in Figure 8.1a. This configuration is more representative of an actual farm layout. This configuration is particularly interesting in terms of investigating the scalability of shared mooring systems.

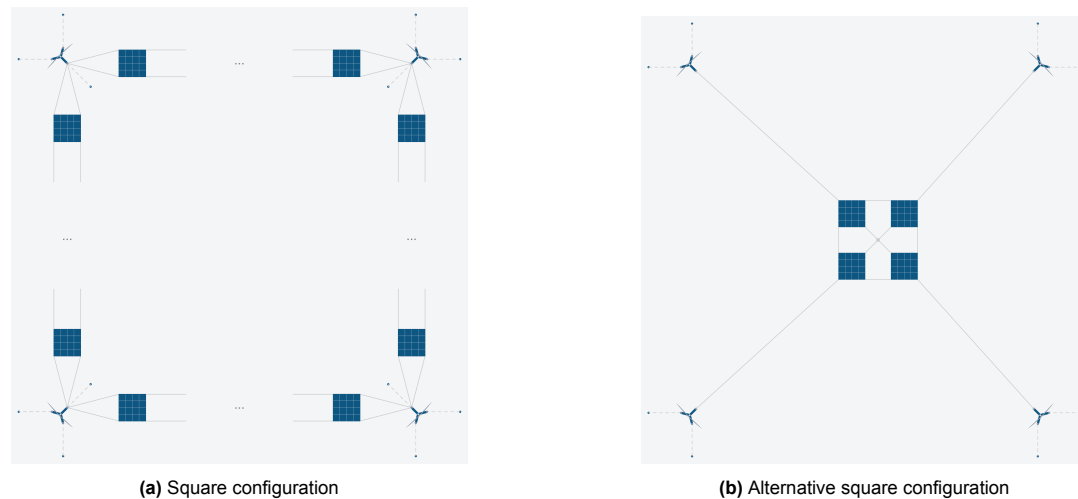


**Figure 8.1:** Alternative configurations

An alternative to the square array would be to place the solar arrays in the middle of the square layout, as depicted in Figure 8.1b. This could potentially improve the dynamics of the solar arrays, as these would now have a more symmetrical mooring stiffness due to the placement of mooring lines. This configuration may also improve the accessibility of the farm, as vessels are not obstructed by mooring lines on the outer edges of the farm, as opposed to the configuration in Figure 8.1a.

#### Solar floaters

As no reference data was available, the Tractebel Seavolt concept was used to design the solar floaters. As the dimensions of this concept were estimated based on rendered pictures, they might not accurately depict the real design. This could cause inaccuracies in the results, as the response of a floater is dependent on its geometry.

Moreover, the solar floaters were scaled to contain 16 floaters in one array, by rigidly connecting the floaters to adjacent floaters. In reality, these connections would be hinging, altering the structures' responses. To stay within scope, a rigid connection was chosen. Although this implies different behaviour, the diffraction analysis was in general considered a conservative way to model the dynamic behaviour, due to the usage of an undisturbed wave field. The selected approach could therefore be considered conservative, as the responses further in the solar array field will be simulated worse than in reality. However, the effect of the rigid connection compared to a flexible connection should be researched, as it could be non-conservative for certain wave periods and situations. The flexibility could introduce other resonance frequencies which could alter the displacement behaviour of the considered arrays. The assessment of the rigid versus flexible effect however was left out of scope.

#### 8.1.2. Quasi-dynamic model

The Quasi-dynamic model used for the identification of the critical cases was verified with Orcaflex to quantify the impact of the limitations on the model.

- Only the mean drift loads (diagonal QTFs) were considered in this model. This shows significant differences with a full QTF calculation in the full dynamic model in irregular waving as was verified in section 6.5. This limitation was identified as the largest contributor in the differences between the Quasi-dynamic model and Orcaflex. In some cases, a 14% difference in anchor tensions, and a 73% difference in shared line tensions was observed, when assessing the total differences between the models. A full independent assessment of the differences between the mean wave drift loads and full QTFs could not be executed.
- Constant added mass and damping were used for irregular waves, which provided another limiting factor in evaluating the dynamics of the system, of around 5% in terms of anchor loads. The full assessment can be found in section 6.5.

- The analytic catenary equation used in the Quasi-dynamic model disregards the dynamic tensions present in mooring lines, which underestimates peak loads compared to a full dynamic model by around 4%, as was assessed in section 6.1.
- The axial stiffness in the polyester mooring lines is assumed constant, based on the average values of the axial stiffness at 10% elongation of the mooring line (see Chapter 5). In reality, polyester lines exhibit nonlinear behaviour, which could significantly influence the results, as the axial stiffness would change based on the elongation of the mooring line. The results are therefore not fully representative for each loading. An assessment of the differences in behaviour was out of scope.
- Wind and current loads are neglected in this model, which can underestimate loading and responses. Also, aerodynamic damping is therefore not taken into account, which is also a significant factor in modelling a wind turbine. To keep the the research within scope and time management, it was chosen to leave these factors out. Wave loading provides a significant heavier loading than current and wind however, so the results are still a valuable addition to knowledge.
- Only 1 simulation of each load case was considered; to acquire more accurate data, at least 5 seeds of simulations should be done to acquire more accurate results, as stated in NR 493 of Bureau Veritas [3].
- Only surge and sway directions were considered in the Quasi-dynamic model. It was found that these degrees of freedom were correctly modelled by comparing them to Orcaflex. The results in Orcaflex are however considering only surge, sway and yaw. Introducing heave, roll and pitch could lead to different results, however, this was not quantified in this research.

# 9

## Conclusions

This research aimed to answer the following research question:

*“What is the feasibility of using a **shared mooring system** within a hybrid renewable farm, combining **floating wind and floating solar**?”*

In short, based on a Quasi-dynamic time domain model and a Full Dynamic model (OrcaFlex), it was concluded that shared mooring systems are feasible for combined floating wind and floating solar. Four out of the six considered configurations passed the KPI considered.

This research considered six configurations (Chapter 4) of the Voltorn US-S reference platform, designed for a 15MW floating wind turbine. The design for the floating solar was based on the Tractebel Seavolt concept. The configurations each consisted of two floating wind turbines with increasing amounts of solar arrays in between the turbines. These solar arrays used shared lines to remain in their intended positions.

To model the hydrodynamic responses of the structures, a Quasi-dynamic time domain model was built in Python to simulate the response of the structures and loadings on the mooring lines (Chapter 5).

Hydrodynamic data of the considered structures was acquired using the diffraction analysis software OrcaWave. In terms of environmental loading, an irregular (JONSWAP) wave spectrum was used to represent wave loading. Drift loads were represented by using the mean wave drift forces. In the case of irregular wave loading, a constant added mass and damping was used to stay within scope. The mooring line restoring forces were modelled using the analytic catenary equation, representing the static mooring force. The analytic catenary equation was chosen as this was regarded as a more computationally efficient approach.

In the verification process (Chapter 6), the mooring restoring forces and first-order wave loading were verified using OrcaFlex. Additionally, the obtained RAOs of the solar arrays were checked for numerical errors. Regarding the Quasi-dynamic model, the mean wave drift loads turned out to be a significant limitation in the case of irregular waving, as the slow-varying drift loads had a substantial impact on the dynamics. Additionally, the constant added mass and damping provided an extra limitation to the results. It was concluded that the Quasi-dynamic model could not be used for a full assessment of the dynamics. However, it was able to identify critical cases. The model was therefore used as a tool to assess the critical cases, from which these cases were re-evaluated using the full dynamic model (OrcaFlex).

The obtained results were evaluated using two KPIs described in Chapter 7:

1. The maximum tensions of the lines should not exceed the MBLs of the mooring lines in the extreme load case.
2. Maximum displacements of the floaters (in surge and sway) should be below 25 metres in the operating load case.

---

Four of the configurations were deemed feasible, after which these were compared to the base case of a single turbine in terms of displacements and anchor loads. One of the observations was that the introduction of solar arrays increased the anchored line tensions, but did not significantly increase when more solar arrays were added. In some cases, a reduction in tensions was even noted.

Based on these results, it is crucial to ensure that the modelling approach used to evaluate the feasibility of these systems is suitable for analysing the behaviour of the structures involved. This is especially important in the case of a shared mooring system, as it introduces more complex dynamics than conventionally moored systems. It was concluded that the slow-varying drift forces have a large influence on the behaviour. Moreover, the damping and added mass cannot be assumed constant in the case of this research.

This research investigated the combination of floating offshore wind and floating solar in a farm layout, using a shared mooring system. This topic had not yet been addressed in the existing literature, and is therefore a valuable addition to knowledge. This research paves the way for more extensive research into this topic, as it has shown that these systems are feasible in terms of loads and displacements. Compared to a conventionally moored single floating turbine, the displacements and loads are within their limits and have a limited effect on the turbines' behaviour. The use of a Quasi-dynamic model decreases computational effort as it identifies critical cases, which can lead to a reduction of cases to assess in later stages. For the final assessment of a mooring design, a fully coupled dynamic model is required, as the dynamic loads on the mooring lines are neglected in the Quasi-dynamic model. The cost-reduction potential due to mooring line and anchor use has not been quantified, and should therefore be done in further research. Additionally, the mooring lines have the potential for optimisation in some configurations, which could make the configurations even more appealing. Further research into the topic of shared mooring, in particularly for combined renewables, is recommended to achieve more insights. Concluding, a first step towards making floating offshore renewables more viable has been made in this research, and paves the way to generate more clean energy in the future.

# 10

## Recommendations

### 10.0.1. Case study

- An extensive economic study has not been performed. This could be valuable to the existing knowledge, as this could provide insights into the LCOE of these renewable farms with shared mooring systems. As line and anchor costs are potentially reduced by the use of shared mooring systems, it is expected to reduce the capital costs of the mooring system.
- Different water depths could lead to a more economic case for the shared mooring setup, as more line length is needed for the conventional mooring method when mooring in deeper waters. However, dynamics will be different and should therefore be evaluated accordingly.
- Only one type of solar PV concept was used for this study. Offshore solar, however, is still in its infancy in terms of design. There has been no convergence towards one particular structure as of yet. It would therefore be interesting to see if other concepts could also be suitable for the use of a shared mooring system within a farm configuration.
- Only a few configurations have been researched. Further research could explore other topologies, of which some are discussed in chapter 8.
- The configurations considered were not optimised in terms of mooring line length and dimensions. In a future study, this should be looked into, as other configurations could exhibit improved characteristics compared to the current scenarios.

### 10.0.2. Modelling

- Implementing a frequency-dependent added mass and damping should be implemented when doing hydrodynamic studies, as this has significant impact on the behaviour of the structures. This can be done by introducing an Impulse Response Function (IRF) which convolutes the wave frequencies over the frequency-dependent damping and added mass each timestep. This is expected to increase the accuracy of the model for irregular wave loading.
- Using irregular waves, the full QTF should be evaluated to take into account the full dynamics. This can be done by implementing the Newman's approach, which extrapolates the diagonal terms to the off-diagonal entries in the QTF matrix.
- A study on flexible connections for diffraction analysis could be done. Multibody diffraction analysis could provide a solution, however, this was considered out of scope for this research.
- Implementing wind and current loading will give a more accurate representation of reality, and should therefore be taken into account. Current loading could be implemented by using the Morrison equation. Wind loading could be implemented by using a constant thrust, or by using Blade Element Method (BEM) theory on a wind turbine.
- Taking into account more DOFs can improve the accuracy of the model, as these could significantly affect the behaviour of a system. It does however come at the cost of computational effort.
- Implementing nonlinear axial stiffness of the polyester mooring lines would improve the accuracy of the modelling.

### 10.0.3. Results

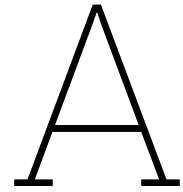
- Transient effects are ignored, as this is a steady-state dynamic model. Transient effects can however introduce significant loading. In future research, this could be taken into account for certain cases, such as in the event of a line failure, which introduces significant transient effects. It should be noted, however, that a Quasi-Dynamic approach would not be sufficient due to the increase in dynamic loading in the lines.
- The results were checked on displacements and ultimate tensions. However, mooring lines are subjected to dynamic and thus cyclic loading, which causes fatigue. Fatigue is one of the largest contributors to the lifetime of mooring lines, so this should be taken into account in future research.
- One of the believed benefits of shared mooring is the savings on installation time. Future research could explore this by providing a novel installation method incorporating shared mooring systems, which could provide insight into the actual savings using this novel technology.
- Although configuration 2.3 seems to have the best properties in this research, with an optimization study this could shift to another favourable configuration. Moreover, introducing economics in the research could also have a significant influence on the steps towards a preferred layout.

# Bibliography

- [1] A world's first: offshore floating solar farm installed at the Dutch North Sea - Oceans of Energy. URL <https://oceansofenergy.blue/2019/12/11/a-worlds-first-offshore-floating-solar-farm-installed-at-the-dutch-north-sea/>.
- [2] Acteon. URL <https://acteon.com/blog/how-do-suction-piles-work/>.
- [3] Bureau Veritas NR493. URL [https://erules.veristar.com/dy/data/bv/pdf/493-NR\\_2021-07.pdf](https://erules.veristar.com/dy/data/bv/pdf/493-NR_2021-07.pdf).
- [4] Corewind Review of the state of the art of mooring and anchoring designs 2.
- [5] *DNV-RP-C205 Environmental conditions and environmental loads - DNV*.
- [6] Driven pile design, fabrication & installation - Acteon. URL <https://acteon.com/products-services/driven-pile-design-fabrication-installation/>.
- [7] EcoTLP. URL <https://ecotlp.com/>.
- [8] Extra pakket maatregelen dicht gat tot klimaatdoel 2030 | Nieuwsbericht | Rijksoverheid.nl. URL <https://www.rijksoverheid.nl/actueel/nieuws/2023/04/26/extra-pakket-maatregelen-dicht-gat-tot-klimaatdoel-2030>.
- [9] Floating Offshore Wind: Virtual classroom. URL <https://www.rwe.com/en/research-and-development/wind-power/floating-offshore-wind/floating-wind-education/>.
- [10] Gmsh: a three-dimensional finite element mesh generator with built-in pre- and post-processing facilities. URL <https://gmsh.info/>.
- [11] Hywind Scotland - the world's first floating wind farm - Equinor. URL <https://www.equinor.com/energy/hywind-scotland>.
- [12] Kincardine offshore windfarm project construction method statement.
- [13] NR493 Classification of mooring systems for permanent and mobile offshore units | Marine & Offshore. URL <https://marine-offshore.bureauveritas.com/nr493-classification-mooring-systems-permanent-and-mobile-offshore-units>.
- [14] North Sea Energy Outlook DNV. URL <https://www.dnv.nl/Publications/north-sea-energy-outlook-192287>.
- [15] Offshore wind farm in North Sea to host 5 MW floating PV plant, . URL <https://www.pv-magazine.com/2022/11/14/offshore-wind-farm-in-north-sea-to-host-5-mw-floating-pv-plant/>.
- [16] Offshore Mooring Systems - Turrets, Spreads & Yokes - SOFEC, . URL <https://www.sofec.com/mooring-systems/>.
- [17] Orcaflex Dynamic analysis: Quasi-dynamic analysis. URL <https://www.orcina.com/webhelp/OrcaFlex/Content/html/Dynamicanalysis,Quasi-dynamicanalysis.htm>.
- [18] Rhino - Rhinoceros 3D. URL <https://www.rhino3d.com/>.
- [19] Rope/wire: Axial and bending stiffness. URL <https://www.orcina.com/webhelp/OrcaFlex/Content/html/Ropewire,Axialandbendingstiffness.htm>.
- [20] Runge-Kutta-Fehlberg Method (RK45).

- [21] Stevpris@MK6 - Delmar Systems. URL <https://delmarsystems.com/products/anchors/stevpris-mk6/>.
- [22] SeaVolt. URL <https://www.seavolt.be/>.
- [23] Suction piles. URL <https://mct-eng.com/suction-piles>.
- [24] Windfloat Atlantic. URL <https://www.lankhorstoffsore.com/about-us/news-events/windfloat-atlantic-floating-wind-turbine-moorings>.
- [25] C. Allen, A. Viselli, H. Dagher Andrew Goupee, E. Gaertner, N. Abbas, M. Hall, and G. Barter. Definition of the UMaine VoltumUS-S Reference Platform Developed for the IEA Wind 15-Megawatt Offshore Reference Wind Turbine Technical Report. 2020. URL [www.nrel.gov/publications](http://www.nrel.gov/publications).
- [26] P. Connolly and M. Hall. Comparison of pilot-scale floating offshore wind farms with shared moorings. *Ocean Engineering*, 171:172–180, 1 2019. ISSN 00298018. doi: 10.1016/j.oceaneng.2018.08.040.
- [27] X. Costoya, M. Decastro, D. Carvalho, B. Arguilé-Pérez, and M. Gómez-Gesteira. Combining offshore wind and solar photovoltaic energy to stabilize energy supply under climate change scenarios: A case study on the western Iberian Peninsula. 2022. doi: 10.1016/j.rser.2021.112037. URL <http://creativecommons.org/licenses/by/4.0/>.
- [28] J. Davidson and J. V. Ringwood. Mathematical modelling of mooring systems for wave energy converters - A review. *Energies*, 10(5), 5 2017. ISSN 19961073. doi: 10.3390/EN10050666. URL [https://www.researchgate.net/publication/316622047\\_Mathematical\\_Modelling\\_of\\_Mooring\\_Systems\\_for\\_Wave\\_Energy\\_Converters-A\\_Review](https://www.researchgate.net/publication/316622047_Mathematical_Modelling_of_Mooring_Systems_for_Wave_Energy_Converters-A_Review).
- [29] H. Díaz, J. Serna, J. Nieto, and C. Guedes Soares. Market Needs, Opportunities and Barriers for the Floating Wind Industry, 7 2022. ISSN 20771312.
- [30] I. Energy Agency. Offshore Wind Outlook 2019: World Energy Outlook Special Report. URL [www.iea.org/t&c/](http://www.iea.org/t&c/).
- [31] M. Goldschmidt and M. Muskulus. Coupled mooring systems for floating wind farms. In *Energy Procedia*, volume 80, pages 255–262. Elsevier Ltd, 2015. doi: 10.1016/j.egypro.2015.11.429.
- [32] M. Hall, E. Lozon, S. Housner, and S. Srinivas. Design and analysis of a ten-turbine floating wind farm with shared mooring lines. *Journal of Physics: Conference Series*, 2362(1):012016, 11 2022. ISSN 1742-6588. doi: 10.1088/1742-6596/2362/1/012016. URL <https://iopscience.iop.org/article/10.1088/1742-6596/2362/1/012016>.
- [33] L. H. Holthuijsen. Waves in oceanic and coastal waters. *Waves in Oceanic and Coastal Waters*, 9780521860284:1–387, 1 2007. doi: 10.1017/CBO9780511618536.
- [34] R. M. Isherwood. A revised parameterisation of the Jonswap spectrum. *Applied Ocean Research*, 9(1):47–50, 1 1987. ISSN 0141-1187. doi: 10.1016/0141-1187(87)90030-7.
- [35] R. James and M. C. Ros. Floating Offshore Wind: Market and Technology Review.
- [36] X. Jiang, H. Ren, M. Wang, Y. Qu, X. Jiang, H. Ren, M. Wang, and Y. Qu. Simulation of Mooring Line Operation in Ship Mooring. *JIEIC*, 102(2):439–446, 4 2021. ISSN 22500553. doi: 10.1007/S40032-020-00647-7. URL <https://ui.adsabs.harvard.edu/abs/2021JIEIC.102..439J/abstract>.
- [37] J. Jonkman, S. Butterfield, W. Musial, and G. Scott. Definition of a 5-MW Reference Wind Turbine for Offshore System Development. 2009. URL <http://www.osti.gov/bridge>.
- [38] J. M. J. Journée and W. W. Massie. Offshore Hydromechanics: First Edition. 2001.

- [39] I. Lehmann. Deepwater Mooring Systems Design and Analysis – A Practical Overview of Various Calculation Methods. *World Maritime Technology Conference, San Francisco, California, USA, 17-20 October 2003, Delft University of Technology, Ship Hydromechanics Laboratory, Department of Maritime Technology*, 2003. URL <https://repository.tudelft.nl/islandora/object/uuid%3Ac8a61e43-bec3-477a-a310-ecb9fa97fff9>.
- [40] L. Li, Z. Gao, and T. Moan. Joint environmental data at five european offshore sites for design of combined wind and wave energy devices. 2013.
- [41] M. López, N. Rodríguez, and G. Iglesias. Combined Floating Offshore Wind and Solar PV. *Journal of Marine Science and Engineering* 2020, Vol. 8, Page 576, 8(8):576, 7 2020. ISSN 2077-1312. doi: 10.3390/JMSE8080576. URL <https://www.mdpi.com/2077-1312/8/8/576/html><https://www.mdpi.com/2077-1312/8/8/576>.
- [42] K. T. Ma, Y. Luo, T. Kwan, and Y. Wu. Mooring system engineering for offshore structures. *Mooring System Engineering for Offshore Structures*, pages 1–350, 1 2019. doi: 10.1016/C2018-0-02217-3. URL <http://www.sciencedirect.com:5070/book/9780128185513/mooring-system-engineering-for-offshore-structures>.
- [43] J. N. Newman. The Drift Force and Moment on Ships in Waves. *Journal of Ship Research*, 11(01): 51–60, 3 1967. ISSN 0022-4502. doi: 10.5957/JSR.1967.11.1.51. URL <https://dx.doi.org/10.5957/jsr.1967.11.1.51>.
- [44] J. A. Pinkster, G. Van Oortmetsseh, N. Ship, and M. Basin. Computation of the first and second order wave forces on oscillating bodies in regular waves. *Proceedings of the 2nd International Conference on Numerical Ship Hydrodynamics, Berkeley, California, USA, 1978*. URL <https://repository.tudelft.nl/islandora/object/uuid%3Ac494f1f5-c021-49f1-8f66-f2486f6119b0>.
- [45] R. C. Ramachandran, C. Desmond, F. Judge, J.-J. Serraris, and J. Murphy. Floating wind turbines: Marine operations challenges and opportunities. Technical report.
- [46] Vryhof. The guide to anchoring: Vryhof Manual. 1984.
- [47] S. D. Weller, L. Johanning, P. Davies, and S. J. Banfield. Synthetic mooring ropes for marine renewable energy applications. *Renewable Energy*, 83:1268–1278, 11 2015. ISSN 0960-1481. doi: 10.1016/J.RENENE.2015.03.058.
- [48] S. Wilson, M. Hall, S. Housner, and S. Srinivas. Linearized modeling and optimization of shared mooring systems. *Ocean Engineering*, 241, 12 2021. ISSN 00298018. doi: 10.1016/j.oceaneng.2021.110009.
- [49] Y. Zhang and H. Liu. Coupled dynamic analysis on floating wind farms with shared mooring under complex conditions. *Ocean Engineering*, 267:113323, 1 2023. ISSN 0029-8018. doi: 10.1016/J.OCEANENG.2022.113323.



# Sanity checks

## Two floaters, first order wave loading

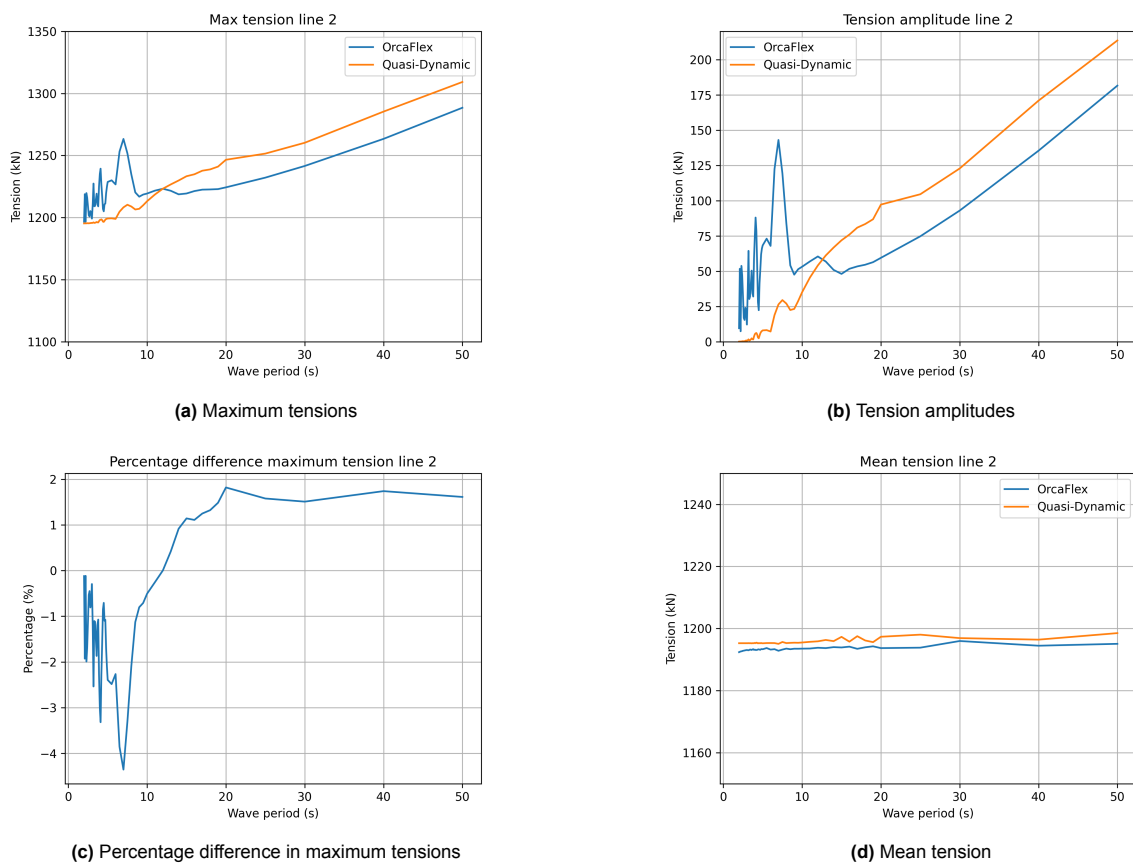
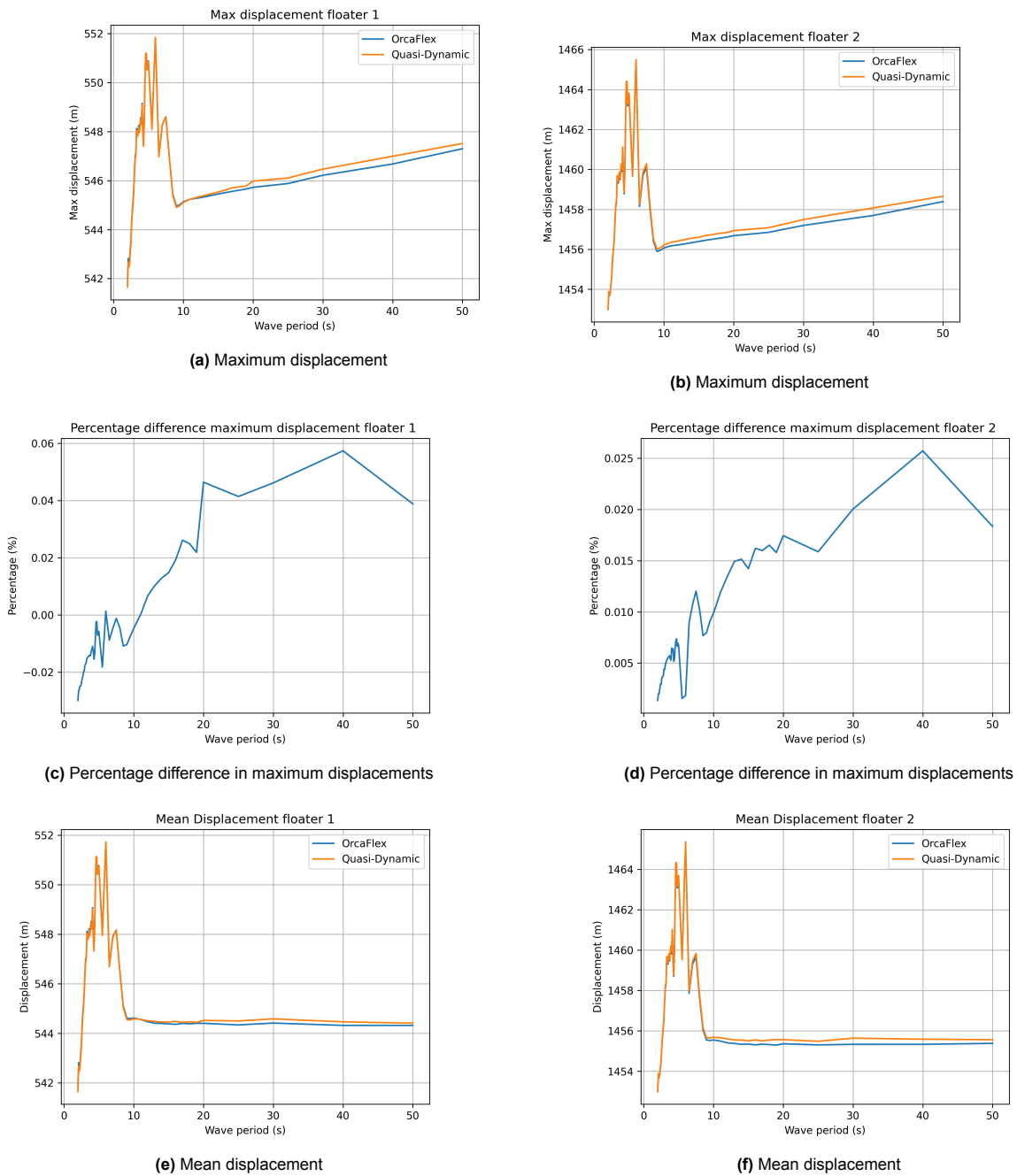
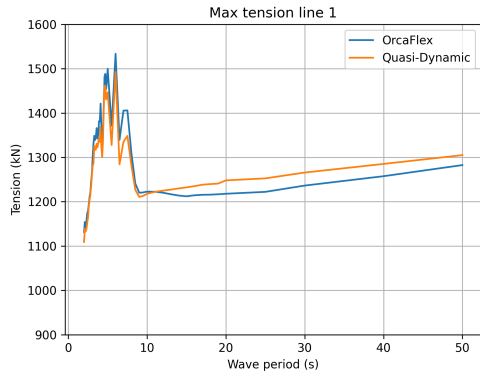


Figure A.1: Line 2 tensions, considering only first order wave loading

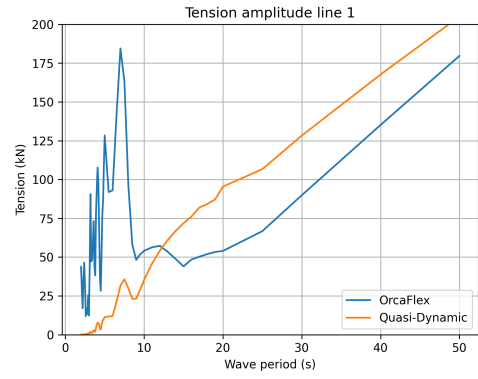
## Two floaters, including wave drift



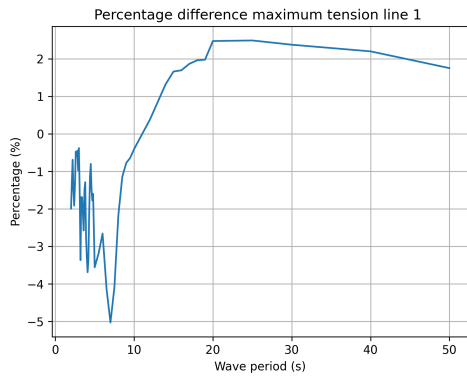
**Figure A.2:** Displacements including drift



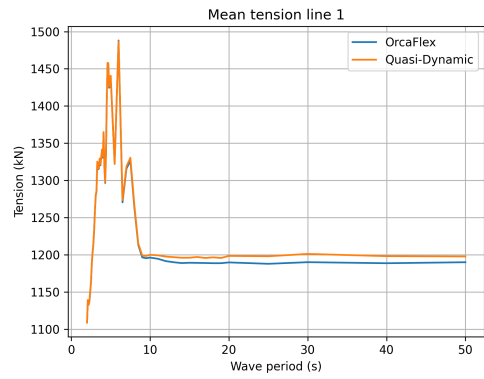
(a) Maximum tensions



(b) Tension amplitudes

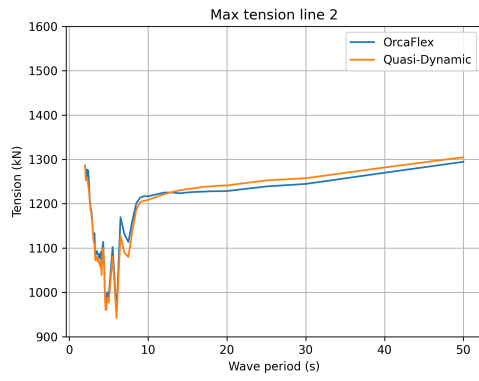


(c) Percentage difference in maximum tensions

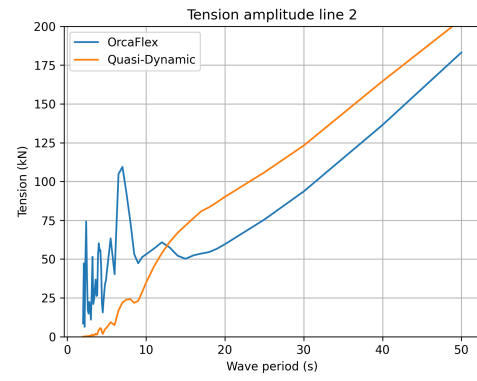


(d) Mean tension

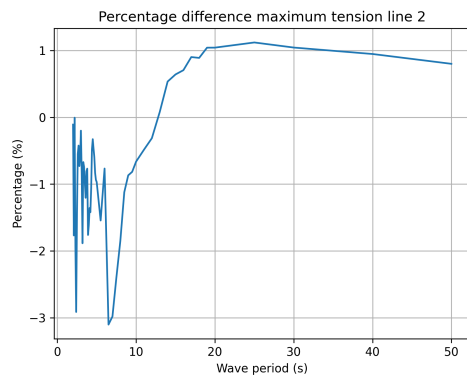
Figure A.3: Line 1 tensions including drift



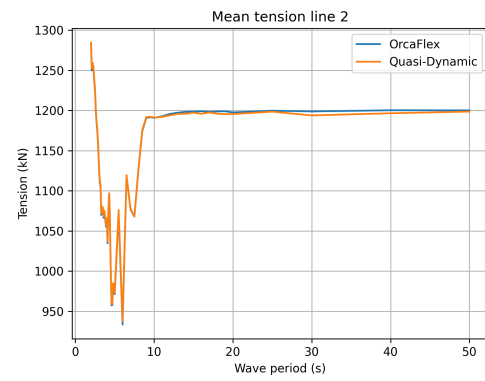
(a) Maximum tensions



(b) Tension amplitudes

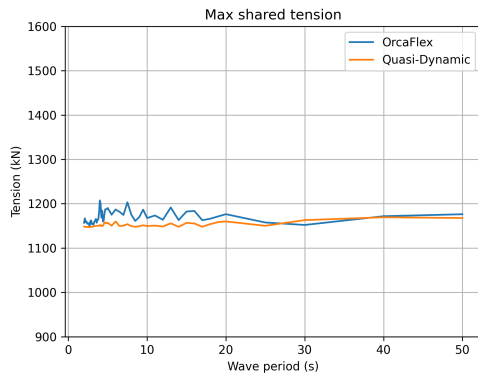


(c) Percentage difference in maximum tensions

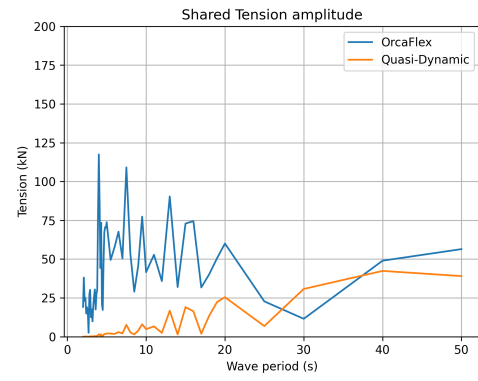


(d) Mean tension

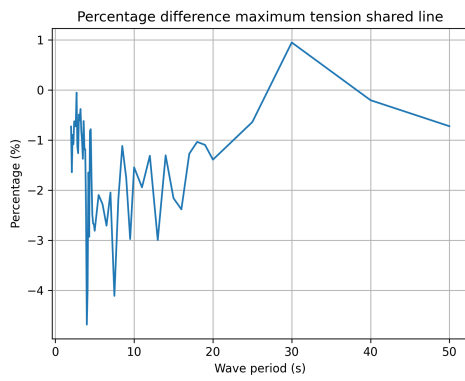
Figure A.4: Line 2 tensions including drift



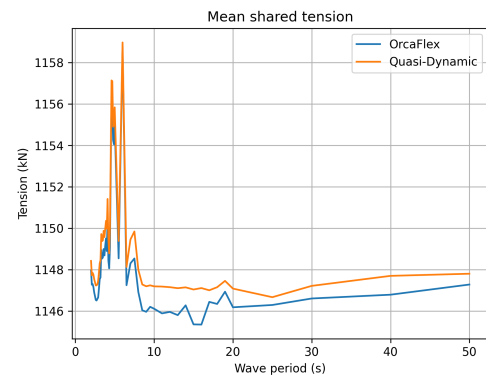
(a) Maximum tensions



(b) Tension amplitudes



(c) Percentage difference in maximum tensions



(d) Mean tension

**Figure A.5:** Shared line tensions including drift

# B

## Static results

### Configuration 1

Configuration 1	Static positions					
Linetype	x1	y1	x2	y2	x3	y3
Catenary	447,27	0,00	1505,53	0,00	976,40	0,00
Rope	452,75	0,00	1500,05	0,00	976,40	0,00
Wire	452,38	0,00	1500,42	0,00	976,40	0,00

Table B.1: Static positions configuration 1

Configuration 1	Anchored line pretensions [%]			
Linetype	Anchor 1	Anchor 2	Anchor 3	Anchor 4
Catenary	15,23%	15,23%	15,23%	15,23%
Rope	16,52%	16,52%	16,52%	16,52%
Wire	16,42%	16,42%	16,42%	16,42%

Table B.2: Anchored line pretensions configuration 1

Configuration 1	Shared line pretensions [%]				
Linetype	Turbine line	Solar line 1	Solar line 2	Solar line 3	Solar line 4
Catenary	21,71%	13,95%	13,95%	13,95%	13,95%
Rope	20,67%	12,80%	12,80%	12,80%	12,80%
Wire	20,73%	11,80%	11,80%	11,80%	11,80%

Table B.3: Shared line pretensions configuration 1

### Configuration 2.1

Configuration 2.1	Static positions					
Linetype	x1	y1	x2	y2	x3	y3
Catenary	425,80	0,00	2331,80	0,00	1378,80	0,00
Rope	433,48	0,00	2324,12	0,00	1378,80	0,00
Wire	432,75	0,00	2324,85	0,00	1378,80	0,00

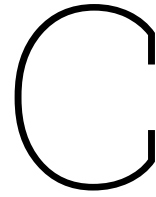
Table B.4: Static positions configuration 2.1

<b>Configuration 2.1</b>	<b>Anchored line pretensions [%]</b>					
<b>Linetype</b>	<b>Anchor 1</b>	<b>Anchor 2</b>	<b>Anchor 3</b>	<b>Anchor 4</b>	<b>Anchor 5</b>	<b>Anchor 6</b>
Catenary	11,70%	11,70%	9,63%	9,63%	11,70%	11,70%
Rope	12,74%	12,74%	8,58%	8,58%	12,74%	12,74%
Wire	12,63%	12,63%	8,67%	8,67%	12,63%	12,63%

**Table B.5:** Anchored line pretensions configuration 2.1

<b>Configuration 2.1</b>	<b>Shared line pretensions [%]</b>			
<b>Linetype</b>	<b>Solar line 1</b>	<b>Solar line 2</b>	<b>Solar line 3</b>	<b>Solar line 4</b>
Catenary	16,01%	16,01%	16,01%	16,01%
Rope	12,73%	12,73%	12,73%	12,73%
Wire	11,72%	11,72%	11,72%	11,72%

**Table B.6:** Shared line pretensions configuration 2.1



# Quasi-Dynamic model results

## Configuration 1 C.0.1. Displacements

Simulation	Displacements												
	x1	y1	x2	y2	x3	y3	Simulation	x1	y1	x2	y2	x3	y3
0	8,2	0,0	3,3	0,0	3,9	-1,3	15	1,5	0,0	0,4	0,0	0,9	-0,2
1	3,4	1,0	0,8	1,0	1,5	0,6	16	1,0	0,3	0,1	0,2	0,4	0,5
2	3,5	2,1	0,2	2,0	1,3	2,6	17	0,9	0,5	0,1	0,5	0,4	1,0
3	5,5	5,4	1,7	3,9	2,5	6,2	18	0,8	0,8	0,1	0,9	0,4	1,6
4	1,5	5,8	1,4	5,6	1,6	13,6	19	0,2	1,1	0,2	1,1	0,2	3,6
5	2,0	0,0	0,1	0,0	1,4	-0,4	20	7,5	0,0	3,9	0,0	3,3	-0,2
6	1,4	0,3	-0,3	0,3	0,8	1,2	21	3,1	1,0	2,1	1,0	2,6	0,6
7	1,3	0,6	-0,2	0,6	0,7	2,2	22	3,4	2,0	0,4	1,9	4,6	1,3
8	1,0	0,9	-0,1	1,0	0,7	3,8	23	4,9	5,4	2,1	3,7	2,0	2,5
9	0,3	1,2	0,2	1,2	0,3	8,1	24	1,5	5,5	1,3	5,2	1,1	4,8
10	7,3	0,0	3,9	0,0	3,1	-0,5	25	1,2	0,0	0,7	0,0	0,9	-0,1
11	2,8	1,0	1,4	1,0	1,4	0,5	26	0,8	0,3	0,3	0,2	0,4	0,3
12	2,8	2,0	1,1	2,0	1,3	1,6	27	0,7	0,5	0,3	0,5	0,3	0,6
13	5,1	5,3	2,4	3,7	1,9	3,3	28	0,6	0,8	0,3	0,9	0,3	1,0
14	1,4	5,5	1,3	5,2	1,1	7,1	29	0,2	1,1	0,2	1,1	0,2	1,9

Figure C.1: Displacements of configuration 1

## C.0.2. Tensions

Simulation	Shared lines						Average	Simulation	Shared lines						Average
	T1	L1	L2	L3	L4				T1	L1	L2	L3	L4		
0	2451	500	556	377	410	481	15	2326	705	709	661	665	685		
1	2462	322	314	276	280	298	16	2327	505	496	483	477	490		
2	2456	341	304	268	268	295	17	2326	511	492	490	479	493		
3	2461	348	282	277	264	293	18	2326	560	513	507	499	520		
4	2454	373	259	327	247	301	19	2330	551	483	542	480	514		
5	2451	307	312	276	279	293	20	2326	1783	1831	1596	1645	1713		
6	2462	276	268	252	247	261	21	2327	2001	1827	1606	1766	1800		
7	2456	272	259	256	247	259	22	2326	2705	2584	2421	2485	2549		
8	2461	300	267	265	250	271	23	2326	1766	1101	1305	1503	1419		
9	2454	298	250	290	246	271	24	2330	884	561	754	711	728		
10	2451	743	754	719	730	736	25	2326	2326	2339	1270	1285	1805		
11	2462	694	676	616	632	655	26	2327	604	578	530	524	559		
12	2456	718	664	605	630	654	27	2326	617	563	619	628	607		
13	2461	665	569	604	632	618	28	2326	687	559	544	547	584		
14	2454	611	502	585	503	550	29	2330	750	504	645	511	602		

Figure C.2: Shared line tensions configuration 1

## Configuration 2.1

Simulation	Displacements													
	x1	y1	x2	y2	x3	y3	Simulation	x1	y1	x2	y2	x3	y3	
0	9,2	0,0	2,8	0,0	8,4	-2,1	15	1,9	0,0	0,1	0,0	1,0	-0,5	
1	4,5	1,3	-0,1	1,3	4,9	0,7	16	1,4	0,4	-0,1	0,4	0,5	1,6	
2	4,6	2,5	-0,7	2,3	5,9	6,6	17	1,2	0,7	-0,2	0,7	0,5	3,0	
3	6,2	5,9	1,2	4,7	7,1	17,5	18	1,0	1,1	-0,1	1,2	0,5	5,1	
4	1,2	7,4	1,6	7,4	4,9	44,6	19	0,2	1,5	0,2	1,6	0,2	11,5	
5	2,6	0,0	-0,6	0,0	4,8	-0,7	20	7,8	0,1	4,4	0,0	3,4	-1,5	
6	2,0	0,4	-0,8	0,4	3,5	3,7	21	3,2	1,2	1,0	1,2	1,3	0,7	
7	1,7	0,8	-0,8	0,8	3,7	7,3	22	3,3	2,4	0,5	2,2	0,9	3,4	
8	1,4	1,2	-0,5	1,3	3,2	12,4	23	5,5	5,7	2,0	4,4	1,8	8,1	
9	0,2	1,7	0,2	1,8	1,6	28,8	24	1,5	6,8	1,4	6,8	1,2	18,0	
10	7,9	0,0	4,3	0,0	3,4	-1,5	25	1,8	0,0	0,2	0,0	1,0	-0,5	
11	3,3	0,9	1,2	1,4	0,7	0,7	26	1,3	0,4	-0,1	0,4	0,5	1,5	
12	3,4	2,4	0,4	2,2	1,0	3,3	27	1,1	0,7	-0,2	0,7	0,4	3,0	
13	5,5	5,7	1,9	4,4	1,9	8,1	28	0,9	1,1	0,0	1,2	0,4	5,0	
14	1,3	6,8	1,4	6,7	1,2	19,3	29	0,2	1,5	0,1	1,6	0,2	10,7	

Figure C.3: Displacements of configuration 2.1

Simulation	Shared lines					Simulation	Shared lines				
	L1	L2	L3	L4	Average		L1	L2	L3	L4	Average
0	314	316	294	295	305	15	584	588	577	581	583
1	310	310	296	296	303	16	490	483	477	471	480
2	314	312	293	292	303	17	498	484	486	474	485
3	321	315	297	294	307	18	532	502	504	486	506
4	320	308	304	295	307	19	528	476	522	470	499
5	310	310	296	296	303	20	1003	1056	661	699	855
6	306	305	296	295	301	21	592	586	550	557	572
7	308	305	296	294	301	22	599	557	505	496	539
8	310	307	298	296	303	23	641	545	548	526	565
9	310	303	305	298	304	24	600	461	557	467	521
10	675	684	730	742	708	25	556	563	518	524	540
11	556	553	534	537	545	26	476	467	462	455	465
12	563	544	506	502	529	27	487	468	473	458	471
13	574	528	527	512	535	28	541	492	500	475	502
14	564	486	543	483	519	29	528	458	518	453	489

Figure C.4: Shared line tensions configuration 2.1

## Configuration 2.2

Simulation	x1	y1	x2	y2	x3	y3	x4	y4
0	9.53	-0.02	3.17	-0.02	10.90	-2.18	9.78	-2.24
1	4.70	1.29	0.13	1.30	6.66	0.69	5.46	0.65
2	4.93	2.58	-0.38	2.35	8.10	8.58	7.14	9.24
3	6.56	6.07	1.49	4.86	9.08	22.91	8.76	25.44
4	1.64	7.79	1.73	7.77	5.50	56.15	7.17	60.68
5	2.89	-0.01	-0.37	-0.01	6.36	-0.74	5.76	-0.75
6	2.16	0.46	-0.57	0.44	4.77	5.03	4.18	5.32
7	1.92	0.86	-0.56	0.83	4.90	10.09	4.55	10.79
8	1.64	1.37	-0.35	1.43	4.26	17.10	3.99	18.13
9	0.38	2.00	0.28	2.04	1.91	39.19	2.65	40.36
10	8.20	-0.04	4.79	-0.02	4.28	-1.29	3.42	-1.31
11	3.47	1.14	1.20	1.20	1.97	0.67	1.20	0.64
12	3.68	2.37	0.86	2.23	2.15	2.98	1.33	2.82
13	5.92	5.78	2.34	4.45	2.72	6.93	2.17	7.08
14	1.62	6.98	1.71	6.94	1.44	16.32	1.71	16.50
15	2.15	-0.02	0.42	-0.02	1.57	-0.42	1.20	-0.42
16	1.53	0.39	0.09	0.38	0.95	1.31	0.67	1.29
17	1.38	0.73	0.01	0.72	0.88	2.49	0.65	2.51
18	1.16	1.15	0.11	1.24	0.79	4.21	0.61	4.26
19	0.30	1.68	0.28	1.73	0.25	9.47	0.47	9.54
20	8.30	0.96	5.01	0.04	4.11	-1.11	3.62	-1.26
21	3.39	1.19	1.12	1.23	2.08	0.62	1.36	0.75
22	3.94	2.44	0.57	2.26	2.94	2.32	1.03	2.57
23	6.12	5.96	2.51	4.59	2.63	5.71	2.07	6.71
24	1.96	7.25	1.46	7.22	1.44	12.60	1.45	13.53
25	1.90	-0.02	0.68	-0.02	1.48	-0.35	1.06	-0.38
26	1.29	0.41	0.33	0.40	0.88	1.09	0.53	1.13
27	1.17	0.78	0.21	0.76	0.79	2.01	0.49	2.16
28	1.00	1.23	0.27	1.31	0.72	3.36	0.45	3.60
29	0.42	1.78	0.17	1.83	0.28	7.00	0.32	7.25

Figure C.5: Displacements of configuration 2.2

Simulation	L1	L2	L3	L4	L5	L6	Average
0	234	243	208	208	193	195	214
1	228	228	206	206	197	198	211
2	245	232	209	209	192	188	213
3	255	229	209	209	198	189	215
4	274	216	215	215	227	192	223
5	222	225	206	206	193	193	208
6	220	217	204	204	196	194	206
7	225	215	205	205	198	191	206
8	228	214	207	207	203	194	209
9	238	207	209	209	224	197	214
10	632	656	553	553	624	649	611
11	631	624	558	558	626	638	606
12	708	657	619	619	578	575	626
13	655	553	554	554	586	556	576
14	660	482	517	517	605	476	543
15	533	540	543	543	503	511	529
16	527	512	497	497	501	488	504
17	540	508	498	498	503	476	504
18	551	496	509	509	519	476	510
19	585	475	508	508	572	463	518
20	970	1069	694	694	933	1127	914
21	976	936	647	647	842	920	828
22	1231	953	1162	1162	768	731	1001
23	945	543	600	600	700	586	662
24	756	344	433	433	576	357	483
25	493	512	519	519	405	419	478
26	442	414	395	395	409	387	407
27	470	409	406	406	408	369	412
28	473	381	442	442	433	366	423
29	535	347	409	409	505	338	424

Figure C.6: Shared line tensions configuration 2.2

## Configuration 2.3

Simulation	x1	y1	x2	y2	x3	y3	x4	y4	x5	y5
0	9.84	-0.05	3.70	-0.03	8.13	-1.69	8.32	-2.41	6.13	-2.02
1	4.75	1.28	0.53	1.30	4.75	0.73	4.71	0.64	2.81	0.68
2	5.14	2.61	0.06	2.38	5.37	5.20	5.55	8.95	3.64	6.95
3	7.04	6.22	1.85	4.96	6.26	13.06	6.68	24.21	5.33	18.80
4	2.54	8.07	1.88	8.03	2.92	30.45	4.16	53.73	5.19	38.28
5	3.05	-0.02	-0.02	-0.01	4.26	-0.57	4.50	-0.81	3.14	-0.66
6	2.27	0.49	-0.28	0.46	3.13	3.01	3.25	5.29	2.10	3.71
7	2.09	0.91	-0.29	0.88	3.05	5.78	3.37	10.43	2.33	7.35
8	1.81	1.45	-0.11	1.51	2.65	9.86	2.92	17.58	2.15	12.17
9	0.78	2.21	0.30	2.23	0.87	22.12	1.38	37.79	2.00	24.41
10	8.61	-0.07	5.30	-0.05	4.76	-0.88	4.31	-1.77	3.31	-0.90
11	3.64	1.16	1.49	1.22	2.57	0.71	1.98	0.61	1.16	0.68
12	3.96	2.44	1.27	2.29	2.94	2.58	2.43	3.78	1.93	2.31
13	6.28	5.95	2.80	4.65	3.66	5.58	2.81	9.36	2.42	5.78
14	1.92	7.37	1.99	7.39	1.93	12.69	1.94	21.96	1.93	13.09
15	2.37	-0.03	0.73	-0.03	2.09	-0.29	1.72	-0.57	1.26	-0.29
16	1.70	0.42	0.33	0.41	1.38	1.01	1.08	1.80	0.72	0.98
17	1.57	0.80	0.27	0.78	1.33	1.88	1.07	3.49	0.72	1.89
18	1.34	1.26	0.33	1.36	1.17	3.16	0.97	5.93	0.68	3.21
19	0.41	1.91	0.37	1.97	0.51	7.01	0.48	13.31	0.49	7.06
20	8.64	-0.05	5.93	-0.07	4.37	-0.34	4.17	-1.41	4.43	-0.43
21	3.76	1.13	1.48	1.18	2.25	0.62	1.74	0.72	1.92	0.90
22	6.27	2.37	-0.78	2.27	7.11	1.94	6.14	2.90	4.86	1.67
23	6.10	6.07	2.91	4.58	3.32	3.44	2.75	7.22	3.01	4.33
24	2.15	7.25	1.75	7.20	1.80	6.78	1.62	15.26	1.68	7.62
25	1.95	-0.03	1.27	-0.03	1.67	-0.10	1.45	-0.44	1.39	-0.11
26	1.23	0.41	0.77	0.41	0.94	0.52	0.81	1.26	0.78	0.51
27	1.17	0.78	0.67	0.77	0.96	0.92	0.84	2.43	0.87	0.96
28	0.99	1.23	0.66	1.33	0.80	1.51	0.71	4.09	0.74	1.63
29	0.46	1.85	0.32	1.92	0.40	3.03	0.35	8.73	0.42	3.13

Figure C.7: Displacements of configuration 2.3

Simulation	L1	L2	L3	L4	L5	L6	L7	L8	Average
0	270	319	214	214	189	189	180	196	221
1	277	270	216	216	194	194	184	187	217
2	356	261	227	227	197	197	184	171	228
3	400	233	220	220	193	193	204	168	229
4	436	194	237	237	218	218	295	166	250
5	224	232	202	202	187	187	173	177	198
6	228	214	197	197	185	185	183	175	196
7	240	204	200	200	186	186	188	166	196
8	251	202	201	201	191	191	202	172	201
9	292	185	212	212	206	206	262	172	218
10	623	656	504	504	497	497	666	701	581
11	683	665	569	569	539	539	590	612	596
12	758	667	624	624	659	659	619	641	656
13	706	549	528	528	494	494	572	564	554
14	675	423	472	472	453	453	595	424	496
15	500	511	462	462	464	464	450	461	472
16	499	476	442	442	432	432	452	435	451
17	508	461	450	450	432	432	454	419	451
18	517	442	446	446	438	438	473	416	452
19	571	407	455	455	448	448	545	391	465
20	1784	1888	1580	1580	1789	1789	2445	2584	1930
21	2028	1899	1519	1519	1454	1454	1636	1783	1661
22	3032	2863	3181	3181	3460	3460	2590	2598	3045
23	1956	1282	1156	1156	1248	1248	1402	1588	1379
24	1221	567	608	608	550	550	892	747	718
25	823	846	793	793	1018	1018	720	744	844
26	743	683	589	589	548	548	643	622	621
27	759	640	589	589	560	560	624	581	613
28	707	540	539	539	541	541	608	559	572
29	718	448	520	520	517	517	671	450	545

Figure C.8: Shared line tensions configuration 2.3

# Configuration 2.4

Simulation	x1	y1	x2	y2	x3	y3	x4	y4	x5	y5	x6	y6
0	10.18	0.36	4.53	0.04	6.47	-0.57	6.18	-2.13	5.77	-2.31	4.12	-1.30
1	4.66	1.24	0.91	1.29	3.47	0.65	3.25	0.51	2.56	0.58	1.50	0.83
2	5.18	2.62	0.68	2.41	4.02	2.32	3.65	6.08	2.89	6.90	1.58	3.61
3	7.55	6.40	2.34	5.06	5.22	4.99	4.52	16.44	4.15	18.75	3.33	9.31
4	3.30	8.25	1.89	8.27	2.85	11.64	2.56	35.67	3.19	38.44	2.95	16.49
5	3.01	-0.03	0.56	-0.03	3.07	-0.22	3.10	-0.77	2.71	-0.77	1.83	-0.38
6	2.20	0.50	0.20	0.48	2.20	1.11	2.09	3.67	1.79	3.93	1.06	1.52
7	2.08	0.95	0.15	0.92	2.12	2.01	2.09	7.10	1.84	7.65	1.18	2.94
8	1.84	1.50	0.24	1.59	1.86	3.38	1.82	11.92	1.63	12.72	1.08	4.79
9	1.06	2.36	0.27	2.40	0.80	7.33	0.73	25.13	1.03	25.89	0.85	8.64
10	9.00	-0.09	5.77	-0.10	5.45	-0.93	5.10	-1.82	4.55	-1.86	3.84	-0.54
11	3.81	1.17	1.72	1.23	2.79	0.75	2.45	0.53	1.84	0.51	1.27	0.70
12	4.27	2.50	1.68	2.35	3.40	2.29	3.18	4.37	2.66	4.42	2.73	1.98
13	6.66	6.15	3.21	4.82	4.29	4.69	3.45	10.55	3.17	10.89	2.66	4.83
14	2.33	7.76	2.24	7.80	2.49	10.02	2.23	24.23	2.33	24.87	2.18	10.19
15	2.61	-0.03	1.05	-0.04	2.46	-0.18	2.29	-0.58	1.96	-0.66	1.54	-0.18
16	1.87	0.45	0.57	0.45	1.79	0.78	1.46	2.07	1.23	2.10	0.89	0.74
17	1.77	0.86	0.52	0.85	1.65	1.42	1.45	4.00	1.23	4.07	0.92	1.41
18	1.52	1.36	0.55	1.47	1.48	2.36	1.29	6.78	1.09	6.89	0.84	2.40
19	0.58	2.14	0.45	2.21	0.78	5.06	0.58	15.14	0.61	15.26	0.55	5.09
20	9.58	-0.05	6.18	-0.10	5.25	-0.20	5.09	-1.58	4.64	-1.64	5.03	-0.26
21	4.07	1.12	1.56	1.19	2.52	0.66	2.34	0.69	1.81	0.81	1.67	1.07
22	7.29	2.43	-0.89	2.33	7.89	1.83	7.43	3.21	7.75	3.40	7.09	2.31
23	6.89	6.42	2.73	4.05	3.41	3.38	3.54	8.55	2.92	9.21	2.95	4.52
24	2.66	7.65	1.87	7.62	2.13	6.45	2.11	18.78	1.89	19.42	1.93	7.01
25	2.30	-0.04	1.64	-0.04	2.05	-0.06	2.15	-0.51	1.85	-0.52	1.88	-0.07
26	1.37	0.45	1.04	0.44	1.13	0.48	1.27	1.65	1.01	1.67	1.05	0.45
27	1.35	0.84	0.94	0.83	1.15	0.82	1.40	3.16	1.02	3.23	1.21	0.88
28	1.16	1.33	0.91	1.44	0.90	1.32	1.15	5.36	0.83	5.48	0.95	1.45
29	0.61	2.08	0.42	2.15	0.49	2.55	0.65	11.46	0.41	11.60	0.49	2.66

Figure C.9: Displacements of configuration 2.4

Simulation	L1	L2	L3	L4	L5	L6	L7	L8	L9	L10	Average
0	827	1188	390	390	277	277	220	220	319	627	479
1	935	792	351	351	318	318	269	269	292	353	425
2	1335	537	541	541	969	969	292	292	354	326	495
3	1215	347	374	374	266	266	221	221	307	208	380
4	949	218	321	321	270	270	258	258	586	169	362
5	288	307	251	251	223	223	198	198	192	203	233
6	288	256	228	228	211	211	198	198	211	194	222
7	313	239	228	228	217	217	200	200	216	176	229
8	320	223	235	235	218	218	204	204	242	180	228
9	400	191	249	249	240	240	235	235	348	173	256
10	693	730	537	537	467	467	491	491	725	761	590
11	736	703	581	581	583	583	558	558	633	687	621
12	814	669	615	615	650	650	721	721	706	775	693
13	746	527	518	518	472	472	445	445	566	626	534
14	724	431	444	444	417	417	408	408	604	426	472
15	486	498	447	447	426	426	398	398	410	422	436
16	476	448	409	409	392	392	378	378	414	397	409
17	492	432	405	405	404	404	378	378	409	375	408
18	493	406	415	415	396	396	380	380	432	379	409
19	552	370	412	412	403	403	399	399	518	353	422
20	2535	2612	2346	2346	1542	1542	1799	1799	3123	3260	2291
21	2707	2541	1819	1819	1774	1774	1713	1713	1920	2238	2002
22	4488	4001	5037	5037	5476	5476	4931	4931	6546	6148	5269
23	2245	1466	1293	1293	1310	1310	1229	1229	1677	2179	1523
24	1664	936	711	711	605	605	574	574	1237	1062	870
25	1051	1073	1101	1101	968	968	835	835	866	891	969
26	848	767	657	657	678	678	580	580	693	697	683
27	894	756	714	714	654	654	676	676	702	686	713
28	783	554	551	551	537	537	527	527	618	655	584
29	789	488	506	506	491	491	485	485	694	490	542

Figure C.10: Shared line tensions configuration 2.4

# Configuration 2.5

Simulation	x1	y1	x2	y2	x3	y3	x4	y4	x5	y5	x6	y6	x7	y7
0	10.94	-0.06	4.90	0.69	6.55	-0.21	6.13	-1.92	5.98	-2.38	5.24	-2.17	4.46	-0.38
1	5.09	1.27	1.06	1.30	3.74	0.72	3.52	0.45	2.86	0.49	2.32	0.66	1.96	1.08
2	6.49	2.68	0.48	2.46	5.34	1.89	6.19	5.31	6.33	7.39	6.90	6.76	4.44	3.52
3	8.30	6.76	2.54	3.19	5.33	3.19	4.53	15.10	9.59	20.89	3.61	16.64	2.76	6.25
4	4.12	8.58	2.01	8.61	3.81	7.76	2.60	31.94	2.76	41.88	3.06	35.29	2.69	10.06
5	3.15	-0.04	0.97	-0.03	3.06	-0.09	3.06	-0.65	2.85	-0.80	2.50	-0.72	1.79	-0.20
6	2.25	0.54	0.55	0.51	2.14	0.49	2.07	3.58	1.92	4.76	1.60	3.98	1.03	0.91
7	2.19	1.00	0.48	0.98	2.10	1.22	2.06	6.90	1.55	9.26	1.68	7.77	3.10	1.73
8	1.98	1.59	0.53	1.68	1.93	1.99	1.79	11.50	1.72	15.33	1.50	12.72	0.99	2.80
9	1.39	2.57	0.36	2.62	1.42	3.96	0.71	23.31	0.81	30.32	0.94	24.34	0.64	4.59
10	9.32	-0.11	6.31	-0.12	5.93	-0.34	5.63	-1.56	5.43	-1.96	4.77	-1.64	4.19	-0.34
11	3.97	1.13	1.99	1.20	3.05	0.78	2.85	0.58	2.55	0.53	2.13	0.54	2.02	0.89
12	4.57	2.47	2.69	2.34	3.62	2.04	3.81	3.86	3.39	4.57	3.10	3.97	3.72	1.95
13	7.03	6.26	3.69	4.81	4.82	4.16	4.16	9.13	3.87	11.23	3.65	9.59	2.88	4.07
14	2.68	7.77	2.50	7.80	2.77	8.02	2.58	20.86	2.67	25.53	2.67	21.54	2.41	8.27
15	2.85	-0.04	1.37	-0.04	2.73	-0.11	2.67	0.51	2.46	0.64	2.21	0.58	1.81	-0.11
16	2.04	0.45	0.82	0.49	1.86	0.61	1.79	1.77	1.61	2.17	1.39	1.79	1.06	0.54
17	1.96	0.86	0.78	0.86	1.80	1.08	1.79	3.39	1.67	4.23	1.45	3.49	1.14	1.08
18	1.70	1.36	0.77	1.49	1.61	1.78	1.59	5.75	1.48	7.18	1.27	5.91	0.99	1.83
19	0.71	2.21	0.53	2.29	0.64	3.72	0.73	12.87	0.76	16.00	0.75	13.05	0.61	3.74
20	10.54	-0.07	4.49	-0.08	5.94	-0.13	5.30	-1.43	5.33	-1.96	5.45	-1.83	6.10	-0.14
21	4.05	1.10	2.22	1.16	3.00	0.62	2.29	0.61	2.12	0.70	2.25	0.78	2.40	1.08
22	7.11	2.47	-0.37	2.37	7.35	2.16	7.22	2.98	6.88	3.52	6.82	3.01	7.09	4.44
23	7.65	6.67	3.28	4.65	4.10	3.40	3.44	7.93	3.19	10.14	3.05	8.89	2.97	4.44
24	3.37	7.82	1.39	7.80	2.99	6.45	2.99	16.09	2.28	22.63	2.35	18.98	2.19	6.20
25	2.81	-0.04	2.21	-0.04	2.70	-0.08	2.61	-0.66	2.52	-0.60	2.44	-0.68	2.29	-0.04
26	1.54	0.45	1.25	0.45	1.31	0.45	1.37	1.59	1.24	2.00	1.27	1.62	1.19	0.43
27	1.58	0.86	1.18	0.86	1.59	0.77	1.52	3.04	1.45	3.87	1.41	3.15	1.35	0.82
28	1.37	1.37	1.10	1.48	1.23	1.26	1.29	5.21	1.20	6.64	1.16	5.38	1.06	1.37
29	0.88	2.19	0.47	2.28	0.74	2.36	0.65	11.11	0.58	14.12	0.62	11.31	0.45	2.44

Figure C.11: Displacements of configuration 2.5

Simulations	L1	L2	L3	L4	L5	L6	L7	L8	L9	L10	L11	L12	Average
0	1710	1832	1260	1260	806	806	344	344	241	241	753	1864	958
1	1400	1203	713	713	594	594	368	368	313	313	632	1092	692
2	2178	1596	2469	2469	1978	1978	3004	3004	2723	2723	1901	2228	2354
3	2077	607	1153	1153	473	473	373	373	297	297	381	334	666
4	1651	457	503	503	338	338	291	291	316	316	1167	203	331
5	435	478	285	285	254	254	209	209	187	187	195	213	266
6	355	294	225	225	208	208	190	190	179	179	214	192	209
7	386	257	243	243	226	226	195	195	180	180	207	165	225
8	406	232	230	230	212	212	201	201	185	185	235	173	225
9	481	200	259	259	243	243	234	234	237	237	407	171	267
10	880	914	696	696	633	633	597	597	586	586	962	995	731
11	938	861	705	705	647	647	626	626	639	639	806	907	729
12	1038	810	797	797	755	755	770	770	977	977	970	1136	894
13	1042	706	750	750	652	652	610	610	582	582	675	850	705
14	955	657	549	549	516	516	495	495	491	491	787	635	595
15	629	640	559	559	527	527	511	511	497	497	545	555	546
16	611	579	499	499	487	487	470	470	462	462	539	532	508
17	623	555	511	511	495	495	474	474	460	460	514	493	506
18	631	527	496	496	486	486	471	471	457	457	530	500	501
19	674	495	501	501	491	491	484	484	481	481	635	478	516
20	2987	3087	2819	2819	2177	2177	2361	2361	3049	3049	3709	3860	2871
21	3301	3076	2325	2325	2186	2186	2258	2258	2324	2324	2516	3014	2508
22	5257	4120	7819	7819	5351	5351	4702	4702	6748	6748	4677	4803	5679
23	3142	2074	1612	1612	1583	1583	1631	1631	1522	1522	2017	3084	1918
24	2651	1891	982	982	832	832	788	788	860	860	2097	2074	1393
25	1395	1413	1330	1330	1518	1518	1206	1206	1356	1356	1319	1338	1357
26	1074	983	856	856	807	807	729	729	822	822	970	1038	875
27	1229	1108	984	984	1072	1072	1117	1117	955	955	911	919	1035
28	1048	735	744	744	876	876	670	670	742	742	658	894	787
29	996	671	592	592	578	578	578	578	565	565	868	822	663

Figure C.12: Shared line tensions configuration 2.5

# D

## Orcaflex results

### Configuration 1 D.0.1. Displacements

	Linetype	Surge		Sway	
		Mean [m]	Max [m]	Mean [m]	Max [m]
<b>Turbine 1</b>	Catenary	3.73	10.73	-0.02	-0.06
	Rope	3.25	12.75	-0.01	-0.06
	Wire	6.21	19.82	0.01	5.15
<b>Turbine 2</b>	Catenary	4.20	10.47	-0.02	-0.09
	Rope	3.74	10.95	-0.02	-0.07
	Wire	0.16	11.29	-0.06	6.66
<b>Solar</b>	Catenary	4.60	10.60	-1.39	-2.70
	Rope	3.60	10.10	-0.50	-0.13
	Wire	3.16	17.78	-3.33	32.80

**Table D.1:** Displacements configuration 1, 0° heading

	Linetype	Surge		Sway	
		Mean [m]	Max [m]	Mean [m]	Max [m]
<b>Turbine 1</b>	Catenary	3,34	8,23	0,76	2,48
	Rope	2,55	10,38	0,71	2,47
	Wire	3,96	10,02	0,65	2,69
<b>Turbine 2</b>	Catenary	2,99	7,45	0,61	2,15
	Rope	2,68	9,06	0,51	1,65
	Wire	1,50	6,64	0,48	2,11
<b>Solar</b>	Catenary	3,83	7,16	2,49	6,72
	Rope	2,79	6,13	1,50	4,89
	Wire	2,65	9,03	1,23	7,06

**Table D.2:** Displacements configuration 1, 30° heading

	Linetype	Surge		Sway	
		Mean [m]	Max [m]	Mean [m]	Max [m]
<b>Turbine 1</b>	Catenary	0,54	0,54	1,63	6,90
	Rope	0,47	1,47	1,49	6,75
	Wire	0,40	1,17	1,43	6,82
<b>Turbine 2</b>	Catenary	0,10	1,78	1,65	7,00
	Rope	0,16	1,10	1,54	6,87
	Wire	0,62	1,29	1,45	6,86
<b>Solar</b>	Catenary	0,82	1,90	9,90	15,10
	Rope	0,46	1,29	5,50	15,11
	Wire	0,34	0,86	2,39	8,37

Table D.3: Displacements configuration 1, 90° heading

## D.0.2. Shared line tensions

	Linetype	Mean [kN]	Utilization	Max [kN]	Utilization
<b>T1</b>	Catenary	2,456	46%	3,149	59%
	Rope	2,300	43%	3,078	57%
	Wire	2,163	40%	2,989	<b>56%</b>
<b>L1</b>	Catenary	275	31%	1,018	<b>113%</b>
	Rope	513	28%	1,081	<b>59%</b>
	Wire	720	37%	5,583	<b>289%</b>
<b>L2</b>	Catenary	284	32%	1,048	<b>117%</b>
	Rope	524	29%	1,089	<b>59%</b>
	Wire	712	37%	5,368	<b>278%</b>
<b>L3</b>	Catenary	258	29%	593	66%
	Rope	495	27%	1,090	<b>59%</b>
	Wire	701	36%	5,116	<b>265%</b>
<b>L4</b>	Catenary	266	30%	636	71%
	Rope	506	28%	1,096	<b>60%</b>
	Wire	693	36%	4,978	<b>258%</b>

Table D.4: Shared line tensions at 0° wave heading

	Linetype	Mean [kN]	Utilization	Max [kN]	Utilization
<b>T1</b>	Catenary	2447	46%	2860	53%
	Rope	2295	43%	2727	51%
	Wire	2273	42%	2729	51%
<b>L1</b>	Catenary	280	31%	623	69%
	Rope	523	28%	991	<b>54%</b>
	Wire	576	30%	3313	<b>172%</b>
<b>L2</b>	Catenary	272	30%	634	71%
	Rope	506	28%	982	<b>54%</b>
	Wire	558	29%	3124	<b>162%</b>
<b>L3</b>	Catenary	257	29%	427	<b>48%</b>
	Rope	499	27%	1015	55%
	Wire	551	29%	3565	<b>185%</b>
<b>L4</b>	Catenary	250	28%	548	61%
	Rope	484	26%	1036	<b>56%</b>
	Wire	536	28%	3478	<b>180%</b>

Table D.5: Shared line tensions at 30° wave heading

	Linetype	Mean [kN]	Utilization	Max [kN]	Utilization
<b>T1</b>	Catenary	2447	46%	2550	48%
	Rope	2332	43%	2418	<b>45%</b>
	Wire	2340	44%	2424	45%
<b>L1</b>	Catenary	301	34%	478	53%
	Rope	550	30%	749	<b>41%</b>
	Wire	535	28%	1018	53%
<b>L2</b>	Catenary	250	28%	403	45%
	Rope	455	25%	612	<b>33%</b>
	Wire	436	23%	1120	58%
<b>L3</b>	Catenary	284	32%	443	49%
	Rope	532	29%	717	<b>39%</b>
	Wire	517	27%	1033	54%
<b>L4</b>	Catenary	232	26%	338	38%
	Rope	436	24%	626	<b>34%</b>
	Wire	417	22%	1096	57%

Table D.6: Shared line tensions at 90° wave heading

## Configuration 2.1

Heading	Structure	Mean Surge [m]	Max Surge [m]	Mean Sway [m]	Max Sway [m]	Surge check	Sway check
0	Turbine1	3.6	10.1	-0.04	0.09	0.4	0
	Turbine2	3.52	7.92	-0.04	0.08	0.32	0
	Solar1	3.88	8.2	-2.02	-1.57	0.33	-0.06
30	Turbine1	2.91	5.97	0.97	5.9	0.24	0.24
	Turbine2	2.58	6.34	0.79	2.69	0.25	0.11
	Solar1	3.13	6.12	3.2	4.24	0.24	0.17
90	Turbine1	0.15	3.01	2.57	14.46	0.12	0.58
	Turbine2	0.43	3.07	2.59	14.68	0.12	0.59
	Solar1	0.59	1.43	20.55	26.68	0.06	1.07

Figure D.1: Displacement check configuration 2.1

Heading	Shared Line	Mean [kN]	Max [kN]	MBL check
0	L1	492	687	0.37
	L2	502	702	0.38
	L3	473	651	0.35
	L4	484	664	0.36
30	L1	503	668	0.36
	L2	490	638	0.35
	L3	479	628	0.34
	L4	468	598	0.33
90	L1	562	630	0.34
	L2	463	592	0.32
	L3	545	613	0.33
	L4	445	564	0.31

Figure D.2: Tension check configuration 2.1

## Configuration 2.2

Heading	Structure	Mean Surge [m]	Max Surge [m]	Mean Sway [m]	Max Sway [m]	Surge check	Sway check
0	Turbine1	3.92	9.81	-0.07	0.01	0.39	0
	Turbine2	3.77	7.65	-0.07	0.06	0.31	0
	Solar1	4.08	9.33	-2.19	-1.82	0.37	-0.07
	Solar2	4.37	9.08	-2.15	-1.78	0.36	-0.07
30	Turbine1	3.35	6.36	0.99	5.91	0.25	0.24
	Turbine2	2.91	5.95	0.85	3.12	0.24	0.12
	Solar1	3.5	5.59	3.51	6.25	0.22	0.25
	Solar2	3.69	6.81	3.49	4.99	0.27	0.2
90	Turbine1	0.69	3.5	2.8	13.22	0.14	0.53
	Turbine2	0.5	3.03	2.84	13.95	0.12	0.56
	Solar1	0.73	3.45	21.82	28.93	0.14	1.16
	Solar2	1.23	3.77	21.97	29.48	0.15	1.18

Figure D.3: Displacement check configuration 2.2

Heading	Shared Line	Mean [kN]	Max [kN]	MBL check
0	L1	518	778	0.42
	L2	536	799	0.44
	L3	492	710	0.39
	L4	513	732	0.4
	L5	480	740	0.4
	L6	499	758	0.41
30	L1	540	814	0.44
	L2	518	793	0.43
	L3	513	824	0.45
	L4	487	814	0.44
	L5	493	685	0.37
	L6	472	724	0.39
90	L1	630	848	0.46
	L2	461	711	0.39
	L3	622	796	0.43
	L4	419	639	0.35
	L5	595	796	0.43
	L6	423	704	0.38

Figure D.4: Tension check configuration 2.2

## Configuration 2.3

Heading	Structure	Mean Surge [m]	Max Surge [m]	Mean Sway [m]	Max Sway [m]	Surge check	Sway check
0	Turbine1	4.24	10.4	-0.1	0.37	0.42	0.01
	Turbine2	3.98	8.97	-0.1	0.49	0.36	0.02
	Solar1	4.52	13.01	-2.2	-1.44	0.52	-0.06
	Solar2	4.63	13.47	-3.64	-2.23	0.54	-0.09
	Solar3	4.52	12.68	-2.11	-0.59	0.51	-0.02
30	Turbine1	4.49	9.52	1.12	4.76	0.38	0.19
	Turbine2	2.56	7.96	1.03	3.99	0.32	0.16
	Solar1	4.71	14.82	6.24	15.22	0.59	0.61
	Solar2	4.4	12.21	7.68	13.38	0.49	0.54
	Solar3	3.44	15.29	4.92	14	0.61	0.56
90	Turbine1	1.47	4.7	3.06	11.32	0.19	0.45
	Turbine2	0.26	4.07	3.13	11.44	0.16	0.46
	Solar1	1.49	9.47	20.2	33.45	0.38	1.34
	Solar2	1.37	9.4	33.55	45.64	0.38	1.83
	Solar3	1.03	9.92	20.14	31.01	0.4	1.24

Figure D.5: Displacement check configuration 2.3

Heading	Shared Line	Mean [kN]	Max [kN]	MBL check
0	L1	475	1049	0.57
	L2	497	1059	0.58
	L3	441	1210	0.66
	L4	471	1212	0.66
	L5	423	1183	0.64
	L6	453	1234	0.67
	L7	443	1030	0.56
	L8	419	1033	0.56
30	L1	525	1387	0.76
	L2	500	1622	0.88
	L3	494	1546	0.84
	L4	459	1458	0.79
	L5	476	1685	0.92
	L6	432	1506	0.82
	L7	424	1512	0.82
	L8	460	1535	0.84
90	L1	611	1332	0.73
	L2	411	1052	0.57
	L3	612	1035	0.56
	L4	347	757	0.41
	L5	594	996	0.54
	L6	328	689	0.38
	L7	353	1129	0.62
	L8	556	1209	0.66

Figure D.6: Tension check configuration 2.3

## Configuration 2.4

Heading	Structure	Mean Surge [m]	Max Surge [m]	Mean Sway [m]	Max Sway [m]	Surge check	Sway check
0	Turbine1	5.82	25.12	-0.18	2.74	1	0.11
	Turbine2	2.82	16.34	-0.14	2.67	0.65	0.11
	Solar1	6.01	23.96	-3.01	13.72	0.96	0.55
	Solar2	5.33	23.44	-5.34	4.83	0.94	0.19
	Solar3	4.69	22.47	-5.26	8.19	0.9	0.33
30	Solar4	3.79	18.71	-3.13	7.79	0.75	0.31
	Turbine1	4.98	12.17	1.21	6.66	0.49	0.27
	Turbine2	2.61	9.93	1.04	4.11	0.4	0.16
	Solar1	5.42	16.87	4.61	12.03	0.67	0.48
	Solar2	4.97	16.13	7.91	16.5	0.65	0.66
90	Solar3	4.37	17.51	7.8	15.96	0.7	0.64
	Solar4	3.66	17.94	4.79	15.05	0.72	0.6
	Turbine1	1.81	4.33	3.32	10.41	0.17	0.42
	Turbine2	0.31	3.89	3.44	9.72	0.16	0.39
	Solar1	2.16	6.1	17.85	28.26	0.24	1.13
90	Solar2	1.63	5.69	37.21	43.88	0.23	1.76
	Solar3	1.75	6.88	37.55	44.05	0.28	1.76
	Solar4	0.96	6.5	17.52	27.96	0.26	1.12

Figure D.7: Displacement check configuration 2.4

Heading	Shared Line	Mean [kN]	Max [kN]	MBL check
0	L1	493	1902	1.04
	L2	512	2012	1.1
	L3	446	2031	1.11
	L4	474	1911	1.04
	L5	426	2294	1.25
	L6	457	2110	1.15
	L7	436	2021	1.1
	L8	416	1972	1.07
	L9	438	2282	1.24
	L10	410	2286	1.25
30	L1	512	2279	1.24
	L2	480	2152	1.17
	L3	470	2046	1.12
	L4	425	2105	1.15
	L5	449	2093	1.14
	L6	400	2145	1.17
	L7	383	1890	1.03
	L8	413	1752	0.95
	L9	379	1881	1.03
	L10	423	1821	0.99
90	L1	591	1167	0.64
	L2	377	873	0.48
	L3	597	1051	0.57
	L4	286	681	0.37
	L5	595	1150	0.63
	L6	250	787	0.43
	L7	298	890	0.49
	L8	517	1182	0.64
	L9	249	621	0.34
	L10	562	937	0.51

Figure D.8: Tension check configuration 2.4

## Configuration 2.5

Heading	Structure	Mean Surge [m]	Max Surge [m]	Mean Sway [m]	Max Sway [m]	Surge check	Sway check
0	Turbine1	8.99	32.74	-0.18	3.95	1.31	0.16
	Turbine2	0.13	16.48	-0.19	7.95	0.66	0.32
	Solar1	8.21	36.6	-2.41	24.54	1.46	0.98
	Solar2	6.78	41.2	-4.98	19.28	1.65	0.77
	Solar3	5.44	41.2	-5.84	22.24	1.65	0.89
	Solar4	4.27	31.51	-5.03	18.74	1.26	0.75
30	Turbine1	2.46	29.81	-2.57	24.56	1.19	0.98
	Turbine2	6.58	15.84	1.09	5.95	0.63	0.24
	Turbine2	1.93	8.67	1.02	5.31	0.35	0.21
	Solar1	6.71	23.19	4.21	16.07	0.93	0.64
	Solar2	6.16	20.82	7.81	19.34	0.83	0.77
	Solar3	5.37	23.93	9.28	22.67	0.96	0.91
90	Solar4	4.31	23.96	8.1	21.79	0.96	0.87
	Solar5	3.17	22.49	4.07	17.52	0.9	0.7
	Turbine1	2.13	4.67	3.27	11.17	0.19	0.45
	Turbine2	0.79	4.34	3.48	11.5	0.17	0.46
	Solar1	2.46	5.84	13.79	22.35	0.23	0.89
	Solar2	2.19	5.11	30.36	35.48	0.2	1.42
90	Solar3	2.19	6.01	36.79	46.34	0.24	1.85
	Solar4	2.09	5.74	31.08	35.12	0.23	1.4
	Solar5	1.27	5.61	13.69	22.52	0.22	0.9

Figure D.9: Displacement check configuration 2.5

Heading	Shared Line	Mean [kN]	Max [kN]	MBL check
0	L1	730	3740	2.04
	L2	743	3637	1.98
	L3	643	3969	2.16
	L4	663	3433	1.87
	L5	623	3354	1.83
	L6	647	3645	1.99
	L7	609	3617	1.97
	L8	587	3710	2.02
	L9	629	3722	2.03
	L10	604	3391	1.85
	L11	629	3702	2.02
	L12	644	3804	2.07
30	L1	675	3098	1.69
	L2	650	3141	1.71
	L3	594	2809	1.53
	L4	558	2779	1.51
	L5	574	2647	1.44
	L6	532	2824	1.54
	L7	488	2809	1.53
	L8	525	2610	1.42
	L9	508	2510	1.37
	L10	551	2846	1.55
	L11	545	2494	1.36
	L12	521	2880	1.57
90	L1	701	1460	0.8
	L2	515	1177	0.64
	L3	682	1401	0.76
	L4	383	934	0.51
	L5	694	1351	0.74
	L6	332	802	0.44
	L7	326	851	0.46
	L8	630	1310	0.71
	L9	314	948	0.52
	L10	677	1361	0.74
	L11	604	1410	0.77
	L12	413	1160	0.63

Figure D.10: Tension check configuration 2.5

## Re-simulated configurations with load case 1

### D.0.3. Configuration 2.1

Heading	Structure	Mean Surge [m]	Max Surge [m]	Mean Sway [m]	Max Sway [m]	Surge check	Sway check
90	Turbine1	0.24	0.32	1.15	1.56	0.01	0.06
	Turbine2	-0.04	0.03	1.15	1.57	0	0.06
	Solar1	0.21	0.45	9.25	9.94	0.02	0.4

Figure D.11: Displacement check configuration 2.1

Heading	Shared Line	Mean [kN]	Max [kN]	MBL check
90	L1	511	521	0.28
	L2	466	478	0.26
	L3	505	514	0.28
	L4	460	472	0.26

Figure D.12: Tension check configuration 2.1

## D.0.4. Configuration 2.3

Heading	Structure	Mean Surge [m]	Max Surge [m]	Mean Sway [m]	Max Sway [m]	Surge check	Sway check
90	Turbine1	0.46	0.64	1.46	1.86	0.03	0.07
	Turbine2	0.16	0.33	1.48	1.87	0.01	0.07
	Solar1	0.44	1.08	9.64	10.32	0.04	0.41
	Solar2	0.49	1.39	15.79	16.48	0.06	0.66
	Solar3	0.45	1.07	9.6	10.28	0.04	0.41

Figure D.13: Displacement check configuration 2.3

Heading	Shared Line	Mean [kN]	Max [kN]	MBL check
90	L1	515	582	0.32
	L2	414	487	0.27
	L3	512	544	0.3
	L4	380	410	0.22
	L5	506	531	0.29
	L6	374	406	0.22
	L7	394	463	0.25
	L8	496	561	0.31

Figure D.14: Tension check configuration 2.3

# E

## Basecase comparisons

Heading	Configuration	Mean Surge [m]	Max Surge [m]	Mean Sway [m]	Max Sway [m]
0°	Basecase	2.8	9.46	0	0
	1	3.2	12.7	-0.02	0.03
	2.1	3.6	10.1	-0.04	0.09
	2.2	3.92	9.81	-0.07	0.01
	2.3	4.24	10.4	-0.1	0.37
30°	Basecase	2.32	7.45	1.23	5.64
	1	2.5	10.33	0.71	2.47
	2.1	2.91	5.97	0.97	5.9
	2.2	3.35	6.36	0.99	5.91
	2.3	4.49	9.52	1.12	4.76
90°	Basecase	-0.13	1.34	2.66	9.5
	1	0.4	1.42	1.5	6.75
	2.1	0.15	3.01	2.57	14.46
	2.2	0.69	3.5	2.8	13.22
	2.3	1.47	4.7	3.06	11.32

Figure E.1: Turbine displacements

		A1			
Heading	Configuration	Mean [kN]	perc	Max [kN]	perc
0°	Basecase	2479	0%	2641	0%
	1	3880	57%	5228	98%
	2.1	2939	19%	3226	22%
	2.2	2969	20%	3240	23%
	2.3	2918	18%	3215	22%
30°	Basecase	2418	0%	2520	0%
	1	3782	56%	5898	134%
	2.1	2979	23%	3493	39%
	2.2	2894	20%	3165	26%
	2.3	2859	18%	3057	21%
90°	Basecase	2314	0%	2646	0%
	1	3567	54%	4477	69%
	2.1	2742	18%	3529	33%
	2.2	2751	19%	3474	31%
	2.3	2682	16%	3192	21%

Figure E.2: Anchor 1 tensions

		A2			
Heading	Configuration	Mean [kN]	perc	Max [kN]	perc
0°	Basecase	2479	0%	2641	0%
	1	3876	56%	5214	97%
	2.1	2935	18%	3229	22%
	2.2	2962	19%	3234	22%
	2.3	2906	17%	3191	21%
30°	Basecase	2526	0%	2911	0%
	1	3898	54%	5332	83%
	2.1	2979	18%	3493	20%
	2.2	3013	19%	3555	22%
	2.3	2990	18%	3449	18%
90°	Basecase	2528	0%	2934	0%
	1	3836	52%	5002	70%
	2.1	3010	19%	3840	31%
	2.2	3054	21%	3823	30%
	2.3	3011	19%	3616	23%

Figure E.3: Anchor 2 tensions

		A3			
Heading	Configuration	Mean [kN]	perc	Max [kN]	perc
0°	Basecase	2294	0%	2612	0%
	1	2300	0%	3078	18%
	2.1	1816	-21%	2024	-23%
	2.2	1797	-22%	1984	-24%
	2.3	1830	-20%	2005	-23%
30°	Basecase	2314	0%	2574	0%
	1	2298	-1%	2727	6%
	2.1	1830	-21%	1924	-25%
	2.2	1808	-22%	1903	-26%
	2.3	1824	-21%	1960	-24%
90°	Basecase	2419	0%	2516	0%
	1	2331	-4%	2418	-7%
	2.1	1902	-21%	1982	-24%
	2.2	1875	-22%	1952	-25%
	2.3	1900	-21%	1987	-24%

Figure E.4: Anchor 3 tensions